UNIVERSIDADE FEDERAL DO CEARÁ
CENTRO DE TECNOLOGIA
DEPARTAMENTO DE ENGENHARIA QUÍMICA
PROGRAMA DE PÓS-GRADUAÇÃO EM ENGENHARIA QUÍMICA

KLÉVER SANTIAGO SÁNCHEZ ZAMBRANO

MICROCALORIMETRIC STUDY OF FUNCTIONALIZED MESOPOROUS SILICAS FOR CO_2 CAPTURE UNDER DRY CONDITIONS

FORTALEZA
2018

KLÉVER SANTIAGO SÁNCHEZ ZAMBRANO

MICROCALORIMETRIC STUDY OF FUNCTIONALIZED MESOPOROUS SILICAS FOR CO_2 CAPTURE UNDER DRY CONDITIONS

Dissertação apresentada ao Programa de Pós-Graduação em Engenharia Química da Universidade Federal do Ceará, como requisito parcial à obtenção do título de Mestre em Engenharia Química Área de concentração: Processos de separação químicos e bioquímicos.
Orientadora: Profª. Diana Cristina Silva de Azevedo
Coorientadora: Drª. Débora Aline Soares Maia
Coorientador: Dr. Enrique Vilarrasa Garcia

FORTALEZA
2018

Dados Internacionais de Catalogação na Publicação
Universidade Federal do Ceará
Biblioteca Universitária
Gerada automaticamente pelo módulo Catalog, mediante os dados fornecidos pelo(a) autor(a)

S193m Sánchez Zambrano, Kléver Santiago.
Microcalorimetric study of functionalized mesoporous silicas for CO2 capture under dry conditions / Kléver Santiago Sánchez Zambrano. – 2018.
101 f. : il. color.

Dissertação (mestrado) – Universidade Federal do Ceará, Centro de Tecnologia, Programa de Pós-Graduação em Engenharia Química, Fortaleza, 2018.
Orientação: Profa. Dra. Diana Cristina Silva de Azevedo.
Coorientação: Prof. Dr. Enrique Vilarrasa Garcia/ Débora Aline Soares Maia.

1. Sílica funcionalizada. 2. Adsorção de CO2. 3. Microcalorimetria. 4. Pós-combustão. I. Título.
CDD 660

KLÉVER SANTIAGO SÁNCHEZ ZAMBRANO

MICROCALORIMETRIC STUDY OF FUNCTIONALIZED MESOPOROUS SILICAS FOR CO_2 CAPTURE UNDER DRY CONDITIONS

Dissertation submitted to Universidade Federal do Ceará as a requirement to obtain the Master's Degree in Chemical Engineering.
Concentration area: Chemical and biological separation processes.

Approved on 23 February 2018

_____
Profª. Dra. Diana Cristina Silva de Azevedo
Universidade Federal do Ceará

_____
Prof. Dr. Célio Loureiro Calvacante Júnior
Universidade Federal do Ceará

_____
Prof. Dr. Vaeudo Valdimiro de Oliveira
Universidade Federal do Piauí

ACKNOWLEDGMENTS

A mi familia y amigos en Ecuador, en especial para mi madre que siempre me apoyo en la decisión de viajar a Brasil y fue fuerte para afrontar momentos difíciles.

A la Organización de Estados Americanos (OEA) y al Conselho Nacional de Desenvolvimiento Científico e Tecnológico (CNPq), por la concesión de la beca otorgada que me permitió desenvolver este trabajo de conclusión de maestrado.

A la Universidad Federal de Ceará de manera especial al programa de post graduación en Ingeniería Química, a sus profesores por la formación en estos dos años de adquisición de nuevos conocimientos y habilidades para desarrollar este trabajo.

A la Profesora Dra. Diana Cristina Silva de Azevedo excelente académica de reconocimiento internacional por la gran confianza depositada y por su apoyo desde el inicio de este trabajo de grado como orientadora.

A los profesores Moisés y Eurico por su disposición ante dudas presentadas en el desarrollo de este trabajo.

A mis Co-orientadores Doctores Débora Soares y Enrique Vilarrasa además de a la Post doctoranda Karine Moura por toda las guías prestadas en la realización experimental y en la discusión de resultados.

A todos mis compañeros del Grupo de Pesquisa em Separações por Adsorção (GPSA) por la ayuda desde el momento que comencé, en especial para Enrique Vilarrasa que asumió mi Co-orientación de manera desinteresada y se portó como amigo brindándome ayuda y consejos cuando los necesite.

A la Universidad de Málaga y a la Universidad Estatal de Campinas por la ayuda en la realización de algunos experimentos valiosos para este trabajo.

A todas las personas que directa o indirectamente han ayudado en la realización de este trabajo.

“So now you'd better stop and rebuild all your ruins. For peace and trust can win the day despite of all your losing”

Jimmy Page and Robert Plant

RESUMO

A adsorção de CO_2 em sílica mesoporosa funcionalizada foi estudada usando microcalorimetria, a fim de investigar a influência do aumento da densidade de amina ancorada e do tipo de funcionalização no mecanismo de captura de CO_2. Um microcalorímetro Tian-Calvet acoplado a um sistema manométrico foi utilizado para avaliar a distribuição de sítios energéticos de adsorção e calcular o parâmetro termocinético a partir das curvas de entalpia diferencial de adsorção. As isotermas de equilíbrio de adsorção de CO_2 até 1 bar também foram medidas a 25 °C para todas as amostras conhecendo qual material funcionalizado tem a maior capacidade de adsorção de CO_2 e comparando com uma amostra duplo funcionalizada no cenário pós-combustão. Além disso, ciclos de adsorção-dessorção foram realizados a 25 e 50 ° C e isotermas de mistura de CO_2 / N_2 a 50 e 75 ° C até 10 bar. O estudo microcalorimétrico sugere uma mudança na distribuição de sítios ativos à medida que aumenta a densidade de aminas ancorada. O parâmetro termocinético máximo foi calculado para as amostras; 471 segundos para a sílica pura em 30,7 $kJmol^{-1}$sugere que fisissorção é o mecanismo dominante. Um comportamento diferente foi observado para as amostras ancoradas, que apresentaram valores de entalpia de adsorção maiores, correspondentes à formação de produtos intermédiários (CO_2 quimissorvido), que dependem da densidade de amina ancorada e dos grupos silanóis disponíveis. Os resultados mostraram que a amostra MSG60, escolhida entre as amostras enxertadas, poderia ser regenerado com sucesso a 120 °C, mantendo uma capacidade de adsorção constante para 3 ciclos de adsorção-dessorção usando vácuo molecular a 50 °C. A amostra dupla funcionalizada apresentou as mesmas boas características e também apresentou o parâmetro API para o processo pós-combustão superior a amostra MSG60; portanto, esse tipo de funcionalização provavelmente seria mais apropriado para esse processo em condições de CO_2 seca.

Palavras-chave: Sílica funcionalizada; Adsorção de CO_2; Microcalorimetria; Pós-combustão.

ABSTRACT

CO_2 adsorption on functionalized mesoporous silica was studied by microcalorimetry in order to investigate the influence of increasing the density of grafted amine and the type of functionalization on the CO_2 capture mechanism. A Tian-Calvet microcalorimeter coupled to a manometric setup was used to evaluate the energy distribution of adsorption sites and calculate the thermokinetic parameters from the differential adsorption enthalpy curves. CO_2 equilibrium adsorption isotherms were also measured at 25 °C for all samples up to 1 bar in order to know which grafted material has the highest CO_2 adsorption capacity at 25°C contrasting it with a sample double functionalized in post-combustion scenario. Besides that, adsorption-desorption cycles were performed at 25 and 50°C and binary CO_2/N_2 isotherms at 50 and 75°C up to 10 bar. The adsorption calorimetric study suggests a change in active sites distribution as the density of grafted amines increases. The maximum thermokinetic parameter was calculated for the samples; 471 seconds for the pure silica at 30.7 $kJmol^{-1}$suggests that physisorption is the dominant binding mechanism. A different behavior occurs with the grafted samples, which have considerably higher enthalpy values corresponding to the formation of intermediate products (chemisorbed CO_2), which depend on grafted amine density and available free surface silanols. The MSG60, chosen among the grafted samples, could be successfully regenerated at 120 °C, maintaining a constant adsorption capacity for 3 adsorption–desorption cycles using molecular vacuum at 50°C. The sample double functionalized presented these same good characteristics and also presented the API parameter for post-combustion process higher than MSG60; therefore, this type of functionalization probably would be more appropriate for this process under dry condition.

Keywords: Functionalized silica; CO_2 adsorption; microcalorimetry; post-combustion.

LIST OF FIGURES

LIST OF TABLES

LIST OF ABREVIATIONS AND ACRONYMS

API	Adsorbent performance indicator
APTES	(3-Aminopropyl) triethoxysilane
BET	Brunauer-Emmett-Teller method
BJH	Barrett, Joyner and Halenda method
DR	Dubinin-Radushkevich method
DSL	Dual site Langmuir model
DTGA	Derivative temperature gravimetric analysis
GHC	Greenhouse gases
HCl	Chlorhydric acid
IEA	International Energy Agency
IR	Infrared
LM	Langmuir model
MAS NMR	Magic-Angle Spinning Nuclear Magnetic resonance
MOF	Metal-organic framework
MREL	Multi region extended Lagmuir
MTAC	Maximum theoretical adsorption capacity by chemisorption
PD	4-amino-2-hydroxy-6-methylpyrimidine
PEI	Propyl Ethyl imine
PSA	Pressure swing adsorption
PSD	Pore size distribution
PZ	Piperazine
P123	Pluronic 123
TEOS	Tetraethylorthosilicate
TEPA	Tetraethylenepentamine
TSA	Temperature swing adsorption
VSA	Vacuum swing adsorption
WC	Working Capacity
XPS	X-ray photoelectron spectroscopy

SUMMARY

1. INTRODUCTION

In recent years, the concern for climate change has grown. Several factors like global warming and natural disasters have led governments to discuss this issue.

The causes of these changes have been extensively studied, mainly the so-called greenhouse effect. Kiehl and Trenberth[1] studied the impact of all greenhouse gases in the atmosphere, and found that CO_2 was the second gas with the highest impact in radiation force, only surpassed by water vapor.

The high share of fossil fuels in the world energy matrix has intensified the concentration of carbon dioxide in the atmosphere. The production of CO_2 is one of the topics of most concern in the scientific community in the environmental field, especially in the production of energy, where alternative sources have had a significant development. According to the IEA (International Energy Agency), the 2015 report, entitled "CO_2 Emissions from fuel combustion", showed that the energy production is responsible for 68% of the total production of anthropogenic gases. CO_2 accounts for 90% of this percentage as shown in the Figure 1

Figure 1 Shares of global anthropogenic GHG, 2010.

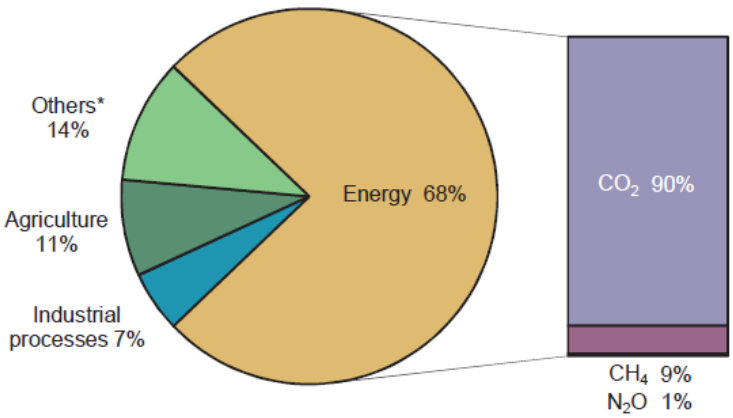

Source: IEA estimates for CO_2 from fuel combustion, 2015[2].

In this context, it is necessary to study and develop efficient technologies to capture CO_2. Thus adsorption has been widely considered for this purpose for its low operating cost contrasting with other processes[3]. Different adsorbents have been investigated for CO_2 capture, including activated carbons, mesoporous silicas, zeolites, metal oxides, mixed hydroxides and metal-organic frameworks[4–7]. In this group, mesoporous silicas may be

used as adsorbents due to their high specific surface area. Moreover, it is possible to add specific functional groups without hindering CO_2 diffusion and with high mechanic and thermal stability. Recently, these materials have been functionalized with amine groups, attracting the attention of scientists, due to enhanced CO_2 adsorption capacity, lower heat capacity in contrast with amine liquids, as well as less equipment corrosion[8]. It means less energy required to outgas CO_2. Thus, functionalized materials have gained attention in adsorption research.

Lately, adsorption microcalorimetry has been used to study catalysts surface and its adsorption properties, as well as the interaction mechanism between several solids and gases[9–12]. Adsorption microcalorimetry is a very helpful tool to evaluate the type and amount of available active sites and understand the process mechanism under dry or moist conditions.

Moreover, it is necessary to study the adsorption stability of these materials under post-combustion conditions. It means successive cycles of work, at temperatures around 50-80°C and under the pressures range of 0−1 bar. The results would aim to contrast between different strategies of functionalization to improve the synthesis and obtain better adsorption efficiency.

These studies have been complemented with Si ^{29}NMR (Nuclear Magnetic Resonance), which allows us to determine the distribution of Si-OH groups on the solid surface. Such data provides important insights into the mechanisms involved during CO_2 adsorption.

The results of this work may be used as a guide to synthesize more efficient adsorbents, while the collected data provides new understandings of the mechanism and kinetics of CO_2 adsorption process at medium and high amine surface loadings.

1.1 Objectives

The main objective of this work is to evaluate mesoporous silica samples under different strategies of functionalization leading different densities of nitrogen surface groups and compare the two most promising materials for CO_2 capture in a post-combustion scenario. Therefore, the specific objectives are:

a) Synthesize mesoporous silica and functionalize them with different loadings of amine groups, using APTES for grafting and PEI for impregnation;
b) Characterize all samples to investigate their textural properties, surface chemistry and thermal stability, using N_2 adsorption, X-ray diffraction, elemental analysis, ^{29}Si RMN and TGA techniques;

c) Use adsorption microcalorimetry to evaluate the improvement of the functionalized materials respect to CO_2 adsorption as compared to the pure sample and thus obtain information about the equilibrium, kinetics and adsorption mechanisms. From this point, select the two samples with better performance regarding the aforementioned properties;
d) Verify the reversibility in adsorption cycles with and without increase in temperature and estimate the energy consumption in post-combustion conditions for the two materials with highest CO_2 uptakes;
e) Measure high pressure adsorption equilibrium data for pure components CO_2 and N_2 at 50 and 75 °C and for gas mixture consisting of CO_2/ N_2 (15/85 v/v) for the two previously selected materials;
f) Calculate the working capacity, selectivity and adsorbent performance indicator in post combustion scenario and select the most appropriate functionalization method to be applied in this process.

2. LITERATURE REVIEW

2.1. Fundaments of adsorption of gases

Adsorption is a natural and exothermic phenomenon which takes place when molecules of a fluid are electrostatically attracted and retained on the surface of a solid when they are in contact. This phenomenon creates a film of molecules on the surface that are capable of generating force fields and attract molecules on its environs.

This phenomenon occurs whenever a solid surface is in contact with a fluid, and it is defined as the enrichment of material or increase in the density of the fluid in the zone of an interface[13]. Under certain conditions, there is a remarkable enhancement in the concentration of a particular component and the overall effect is then dependent on the extent of the interfacial area[13]. According to the nature of the forces that govern the phenomenon, we can classify it as physical (physisorption) or chemical (chemisorption). In physisorption the intermolecular forces involved are similar to the energy leading to the non-ideal behavior of gases and the condensation of vapors. In addition to the attractive dispersion forces and the short range repulsive forces, usually occur as a result of particular geometric and electronic properties of the fluid and solid[14]. In chemisorption, the intermolecular forces involved in the process lead to the formation of chemical bonds.

Currently, adsorption has been applied as a technological process of great importance. Thus, some adsorbents are commonly used as catalysts or catalyst supports, desiccants; others are used for the separation of light gases- in cases where adsorption has advantages over distillation[15], in the purification of pollution industrial discharge and even in stages of biological mechanisms like enzymatic immobilization[16].

Gas adsorption is now a widely used procedure for determining the surface area and pore size distribution of a diverse range of porous materials[17]. These data are determinant for the selection of type, size and number of adsorption columns at given gas feed, product specifications and environmental conditions, among others.

Adsorbent is the solid phase with external and internal surfaces (pores), exposed to the molecules of a gas or liquid. Different types of adsorbents are known in industry applications, for example, activated carbons and silica gels materials that have pore structure not well defined –therefore commonly known as amorphous-. Zeolites, on the contrary, have a surface and pore size within a defined range, and are thus part of a group denominated crystalline solid.

Figure 2 Adsorption system components

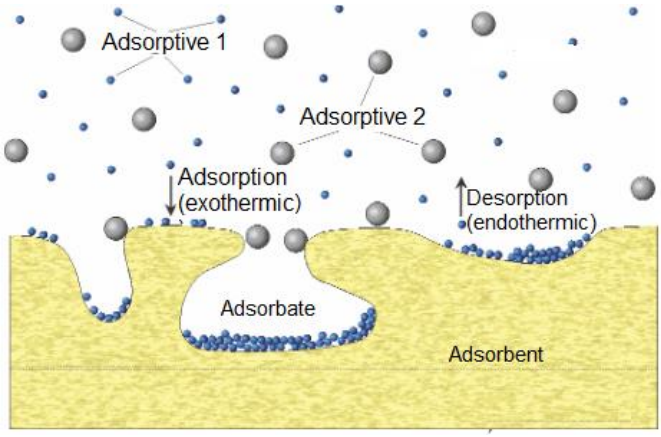

Source: Modified Keller and Staudt, 2005.[18]

Adsorptive is the fluid; gas or liquid which some molecules interact with the surface of the adsorbent without these being retained on the solid surface. Figure 2 shows an illustration of the adsorption phenomena on a porous solid in contact with a mixture of two adsorptive gases. The fluid is called adsorbate when its molecules are adsorbed on the surface of an (often porous) solid material[18].

Porous solids possess various surface groups and irregularities (surface heterogeneity), as well as fine pores of different sizes and shapes (structural heterogeneity). Thus pores are classified according their width, which represents either the diameter of a cylindrical pore, or the distance between the sides of a slit-shaped pore. The International Union of Pure and Applied Chemistry (IUPAC) proposed the following classification: pores with widths exceeding about 50 nm (500 Å) are called macropores, pores of widths between 2 nm and 50 nm are called mesopores and pores with widths less than 2 nm are called micropores[14].

In the procedures for synthesizing porous solids it is necessary to control the various process variables involved, such as carbonization, temperature, type and concentration of functional groups, these activation parameters determinant of the chemical and physical properties of adsorbents. Many research groups around the world like Bastos-Neto *et al.*[19] Prauchner *et al.*[20] Castrillon *et al.*[21] have been concerned in enhance of materials porous due to several applications that these may have.

Nature of surface groups, hydrophobic or hydrophilic character and acidic or basic behavior are some of the relevant physicochemical properties of the adsorbents for the adsorption process and they determine the application and performance of these; surface area,

pore diameter, pore size distribution, heats of adsorption are necessary to precisely determine the parameters that characterize these materials[22].

Adsorption is described through isotherms, functions connecting the amount of adsorbate taken up by the adsorbent (or the change of any other physical parameter related to the adsorption of matter) with the adsorptive equilibrium pressure, the temperature and all parameters being constant[23]. It is like the fingerprint of the solid in interaction with the fluid in equilibrium. The result of this test is known as adsorption isotherm, and it represents the adsorption equilibrium which can be measured by different methods.

A novel classification of the adsorption isotherms was presented by Thommes *et al*,[14] with new characteristic types of isotherms identified and found to be closely related to particular pore structures, compared to the last classification showed in 1985[17]. For more details of this topic, the reader could consult this work.

2.2. Adsorption microcalorimetry

Adsorption microcalorimetry has its origin with Pierre Antoine Favre in 1854. He development a calorimeter to measure for first time adsorption heats of gases on solids. Nowadays, it has been applied to the study of adsorption and catalysis[11,24].

The determination of heat of adsorption is essential in the description of gas solid energy interactions. The term *"heat of adsorption"* is discouraged since it does not correspond to any well-defined thermodynamic change of state, but several authors give that name to this energetic property, being commonly used the term *"adsorption enthalpy"* in the scientific community.

With this data one can get a better understanding of the behavior of the gas- solid interaction, and adsorption microcalorimetry is the technique that studies these thermal effects that can be simplified as heat.

The measurement of the heat of adsorption by a suitable calorimeter is the most reliable method for evaluating the strength of adsorption (either physical or chemical).[23] Tian Cavet heat-flow microcalorimeters are an example of high sensibility apparatus which are suitably adapted to the study of gas-solid interactions when connected to sensitive volumetric systems[25,26]. However, due to the nontrivial nature of the measurements and the strict experimental conditions required to obtain good results, calorimetry has remained the specialty of a relatively small number of research groups in these subfields[27].

The energetic information obtained provides supplementary resolution with respect to manometry adsorption and is complementary to other structural and/or diffusion studies[28]. It is a readily accepted fact that surface heterogeneity leads to a heterogeneous population of active sites on the surface of a solid adsorbent previously functionalized or a catalyst. Thanks to the improved sensitivity of calorimeters and to the development of refined data analysis techniques, adsorption calorimetry can make a significant contribution to the characterization of a solid surface.[29] It is very often discussed but very seldom taken into account in practical cases, simply because there are very few tools with which to study the heterogeneity if active sites in solid.

The adsorption of at least one reactant is the first step of the mechanism of any catalytic reaction. This step is followed by surface interactions between adsorbed species or between a gaseous reactant and adsorbed species. In many cases, these interactions may be detected by the successive adsorptions of the reactants in different sequences. Heat-flow microcalorimetry can be used with profit for such studies.[30]

However the technique also has some limitations, it is often difficult to determine the nature of the adsorbed species, or even to distinguish between the different kinds of products formed for chemisorption from the calorimeter data. In many cases this technique fails to distinguish between cations and protonic sites due to the insufficient selectivity of the adsorption. For example in catalysis can make it difficult in some cases to discriminate Lewis and Brönsted sites solely by adsorption microcalorimetry because the different enthalpies of NH_3 adsorption on these sites are relatively close to each other. Because no exact information can be obtained regarding the nature of the acid centers from calorimetry measurements, suitable IR, MAS NMR and/or XPS investigations are necessary to identify these sites.[31]

2.2.1. Energy of Adsorption

If we assume that the adsorption systems are well characterized and that the experimental measurements are made under carefully controlled conditions, energy of adsorption data can provide valuable information concerning the process mechanism whatever the nature of the interactions is: strong surface interactions (physisorption) or chemical interactions (chemisorption).

When a polar molecule is adsorbed on an ionic or polar surface various types of specific interactions may contribute to the adsorption energy. A useful general expression for

the adsorption energy was proposed by Barrer [32], at very low surface coverage in the form of the sum shown in Equation 1.

$$E_0 = E_D + E_R + E_P + E_{F\mu} + E_{FQ} \quad (1)$$

In which: E_D represents the dispersion energy characterized by London[33] and E_R represents the repulsion energy, both contributions known as non-specific and various type of additional specific interactions can contribute to the adsorption energy such as the polarization energy E_P that takes place for every adsorbate/adsorbent system as a result of the proximity from electric field between adsorbent and the adsorbate -the dipole field $E_{F\mu}$- and the energy quadrupole gradient field E_{FQ}[32]and the adsorption energy is the sum of these energy terms taking place between all atoms of both adsorbate and adsorbent. There are a few adsorbents which give rise to essentially non-specific interactions with a wide range of different adsorptive in which polarity and specific contributions have a minimum effect. One of the most popular is the graphitized carbon black which is a non-porous adsorbent and its uniform state has a surface structure composed almost entirely of the graphitic basal planes. Several studies show a strong impact of the non-specific contributions. Already in 1990 results was obtained for Ludwing and Schmidt[34], therefore there is evidence to confirm the essentially non-specific nature of the interactions between the surface of graphitized carbon and all types of gas molecules.

The scenario is different when a polar molecule is adsorbed on an ionic or a polar adsorbent surface. Studies with n-hexane and benzene demonstrated the effects of the specific contributions on the interaction energy at low surfaces for the benzene with ionic or polar surfaces, as did Kiselev[35] evidencing it with hydroxylated silica and Belyakova *et al.* [36] with barium sulphate as adsorbent materials; hence, the adsorption energy is directly dependent on the nature of the adsorbent/adsorbate system. Thus, to avoid confusion, we can rewrite as is shown in Equation 2 so that

$$E_0 = E_{SC} + E_{NSC} \quad (2)$$

where E_{SC} represents the specific contributions and E_{NSC} the non-specific ones.

For an increase in coverage, an additional (self-potential) term E_{aa} must be added to E_0 according to the principle of addition of the pairwise interactions[11]. The last statement

suggests that the differential enthalpy changes significantly with an increase in the surface coverage, whereas in other cases the change can be much smaller. In fact, the increase in the differential enthalpy of adsorption, usually observed for an energetically homogeneous adsorbent surface. It is likely due to the attractive interactions between adsorbed molecules which become more relevant when the population in the monolayer increases or when micropore filling approaches completion. According to the ideal Langmuir model the heat of adsorption should be independent of coverage, but this requirement is seldom fulfilled in real systems because the effects of surface heterogeneity and adsorbate-adsorbate interactions are generally significant[15]. The progressive decrease in the differential enthalpy is generally expected if the adsorbent surface is energetically heterogeneous as was studied by Furlong *et al.*[37] and Grillet *et al.*[38] with rutile and graphitized carbon respectively. A quasi plane profile for the differential enthalpy is often related to the interactions between the adsorbate and a mildly energetically heterogeneous adsorbent surface, the significant decrease in the adsorbent–adsorbate interactions being almost exactly balanced by an increase in the lateral adsorbate–adsorbate interactions[13].

Adsorption is a spontaneous and exothermic process. The adsorption Gibbs energy and the adsorption enthalpy are then negative. As the molecules are adsorbed in micropores and bond to the solid by physical or chemical interactions, they lose degrees freedom. The adsorbate forms a phase, which is more ordered compared to the gas phase. Therefore the adsorption entropy is negative too. Thus the sign of the Gibbs energy depends on the enthalpic term which is always negative and the entropic term which is positive according Equation 3:

$$\Delta_r G^a = \Delta_r H^a - T\Delta_r S^a \qquad ((4))$$

where $\Delta_r G^a$ is the energy Gibbs in adsorption, $\Delta_r H^a$ is the adsorption enthalpy and $\Delta_r S^a$ the entropy adsorption to constant temperature T.

One of particularities of the adsorption process is that the adsorption enthalpy and entropy depend on the adsorbed amount and, sometimes, the composition of gas mixture. The knowledge of these two thermodynamics values, as a function of the adsorbed amount, is then of a relevant interest for the understanding of adsorption mechanism.[23]

Complementary studies of the energetics of physisorption can be explored using considerations in molecular simulations that, with the aid of fast computing facilities, are nowadays intensively employed as numerical experiments to clarify, together with the microcalorimetric profile, the forecasts of the adsorption mechanism at the microscopic scale or the adsorption properties of a wide range of solids. The latter point is very helpful for narrowing down the choices of promising adsorbents for some adsorption/separation applications, which will need further experimental investigations.

2.2.2 Computation of enthalpy adsorption

In this section we present the thermodynamic models[39] that help us process and interpret the calorimetric data. The isosteric method, in which the adsorption enthalpies are calculated from information, obtained of at least three adsorption isotherms at different temperatures, so that this is an indirect method. Furthermore, there are the direct methods that make use of a manometric system adapted to a calorimeter to measure the generated heat in a continuous or discontinuous procedure. The latter is the principal calculation method currently used at adsorption calorimetry[20].

Discontinuous Procedure

Currently, the most common calorimetric procedure is the discontinuous one where the adsorptive is introduced in successive steps. The calorimetric cell with its contents (adsorbent and adsorptive) is considered an open system as can be seen in the Figure 3:

Figure 3 Schematic diagram of an adsorption microcalorimeter.

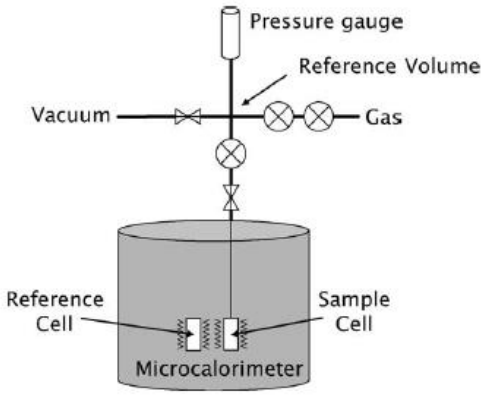

Source: Llewellyn and Maurin, 2005.[40]

To calculate the differential enthalpy of adsorption via the point by point procedure, one must introduce quantities *dn* small enough for a given pressure increase *dp*.

Under these conditions, and taking into account the internal energy contribution by the gaseous adsorptive, we can write as Equation 4[13]:

$$dU = dQ_{rev} + dW_{rev} + u_T^g dn \quad (4)$$

where dQ_{rev} is the reversible heat exchange with the surroundings at *T* temperature, dW_{rev} is the reversible work done by the gas against the external pressure, u_T^g is the molar internal energy of the adsorbable gas at temperature T and dn is the amount of adsorbable gas introduced during a given gas injection.

The calculation of dW_{rev} can easily be done if one notionally splits the volume of the whole adsorption system into two parts[13]; VA external to the calorimetric cell, but in contact with the thermostat and V_C located within the calorimetric cell. If we assume a reversible compression of an ideal gas by reduction of volume V_A, the whole system exchanges work with the surroundings according to Equation 5:

$$dW_{rev}(A + C) = RTdn^{\sigma} + (VA + VC)dp \quad (5)$$

where dn^{σ}represents the amount adsorbed during the compression of the gas. The work received for the calorimetric cell is presented in Equation 6:

$$dW_{rev}(C) = RTdn^{\sigma} + (VC)dp \quad (6)$$

Combining the last equations it gets the expression in Equation 7:

$$d(n^g u^g + n^{\sigma} u^{\sigma})_{T,V,A} = dQ_{rev} + RTdn^{\sigma} + V_C dp + u^g(dn^g + dn^{\sigma}) \quad (7)$$

And reorganizing, the Equation 8 is found

$$\left(\frac{dQ_{rev}}{dn^{\sigma}}\right)_{T,A} + V_C\left(\frac{dp}{dn^{\sigma}}\right)_{T,A} = \left[\left(\frac{dU^{\sigma}}{dn^{\sigma}}\right) - u^g - RT\right] = \Delta h_{ads,T,n} \quad (8)$$

where, V_C in this equation is the dead space volume of the sample cell within the calorimeter itself (thermopile). The term $VCdp$ can be obtained via blank experiments, a process that will be later explained.

2.2.3. Classification of calorimetric curves.

The nature of the interaction between adsorbate-adsorbent and adsorbate-adsorbate affects the shape of the interaction energy curve relative to the coverage of the adsorbent. Filling mechanism and phase transitions of several adsorbates can be distinguish aside from structural changes of the adsorbent. Llewellyn[28] proposed in the Handbook of thermal analysis and calorimetry the following classification:

Figure 4 Classification of calorimetric curves.

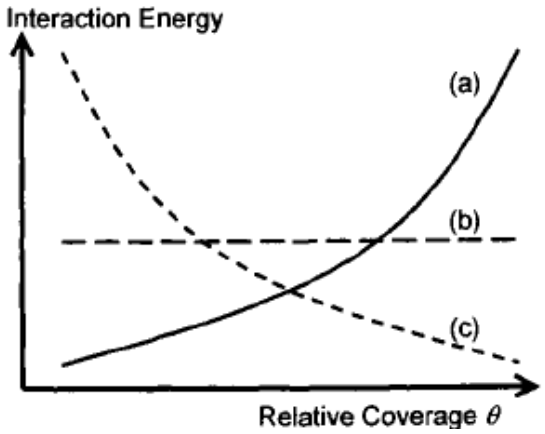

Source: Modified from Llewellyn, 2000.[28]

Figure 4, shows the three different hypothetical breakdowns of calorimetric curves due to various interactions during the adsorption of simple gases; (a) interactions between adsorbate molecules, (b) adsorbate-homogeneous adsorbent and finally (c) adsorbate–heterogeneous adsorbent

The curve (c) shows that for adsorbents that are *energetically heterogeneous* due to a pore size distribution and/or a varying surface chemistry (defects, functionalization, cations, etc), exhibit a decrease in heat of adsorption with gas loading due to its characteristic of highly heterogeneous adsorbents, with a wide distribution of gas-solid interaction energies.[41]

In the adsorption process the amount of adsorbate increases on a sample, thus the interactions between the adsorbate molecules increase too, as can be seen in Figure 4 curve (a). The curve (b) takes place when the surface of the solid is homogeneous; this results in a

constant plateau. In such cases, to describe the change in the adsorption heats with coverage, another approach is to plot ***energy site distribution***: assuming that the variation in the adsorption enthalpies coincides with energy distributions, one may wish to measure the number of sites with the same energy, i.e. sites that give rise to the same differential heat. This is achieved upon plotting $-\mathrm{d}n/\mathrm{d}\Delta H_{\mathrm{diff}}$ as a function of ΔH_{diff}. The area below the curve included between ΔH_{diff} and $\Delta H_{\mathrm{diff}} + \mathrm{d}\Delta H_{\mathrm{diff}}$ represents the population of sites of identical strength estimated via ΔH_{diff}. The validity of energy distributions derived from heats of adsorption has been examined in the literature[42] and it has been commonly used in the study of heterogeneous on catalyst. Thus for example, Bennici *et al.*[43] studied by calorimetry two series of binary oxide catalysts (CuGa/SA and CuSn/SA) containing CuO coupled with Ga_2O3 or SnO_2 were prepared by dispersing the metal phases onto a high surface area acidic silica-alumina (SA) support by an adsorption method. They found that the acid strength of the surfaces, moderate acidity was associated with the Cu sites ($100\ \mathrm{kJ.mol^{-1}} < q_{\mathrm{diff}} < 150\mathrm{kJ.mol^{-1}}$) whereas the most acidic fraction of the sites ($q_{\mathrm{diff}} < 150\mathrm{kJ.mol^{-1}}$) increased with the presence of Ga and Sn. Auroux[44] studied the effect of proton exchange level, or sodium content on strong acid sites of zeolites by calorimetry. The energy site distribution clearly showed that, at low exchange levels, most of the acid sites are rather weak. While this population of stronger sites remained almost constant with the exchange level, the population of stronger sites increased progressively up to the point where, for extensively exchange samples, the strongest sites became predominant.

2.2.4. ***Tian-Calvet microcalorimeter***

A Tian-Calvet heat-flux microcalorimeter is used for measurement of heats of adsorption and reaction on solid surfaces. Heat-flux signals are measured in transducer assemblies consisting of several hundred Seebeck-effect (production of differential voltage caused by temperature difference), thermo elements connected in series and arranged in a thimble configuration. These transducers surround calorimeter cells connected to a high-vacuum manometric adsorption system. The sensitivity of the microcalorimeter can be calibrated with a Joule-effect device[45] or by measurement of heats of adsorption for known processes. Measurement of the heat flux is possible for a mean ΔT smaller than 10^{-6} K.

This calorimeter was developed by professors Tian and Calvet in France, in the mid 20th century, was first applied by Tian in 1923 and improved by Calvet and Prat[46] who

also introduced the differential assembly. Since then this has become a tool for different applications.

Figure 5. Tian- Calvet calorimeter cell representation

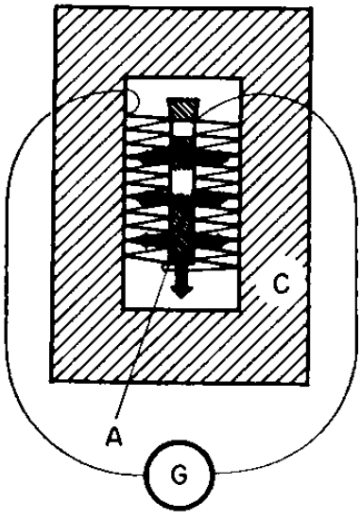

Source: Modified of Calvet and Prat, 1963 [46]

In Figure 5 most of the heat produced in A is conducted to the external jacket C by the bank of thermocouples surrounding the calorimeter container. The electromotive force produced in the thermoelectric pile or in the bank of thermocouples is proportional to the calorific power transferred.[46]

If the main way of heat transfer is conduction, the thermal characteristics necessary for constructing a useful core unit are straightforward, to deliver the unknown sample heat signal as efficiently and rapidly as possible to the heat-flux transducers and insure that the transducer elements deliver this heat flow to a sinking element held in perfectly isothermal conditions.[45] The main characteristic of this device is the presence of two calorimetric cells, as a twin arrangement[46]. In this, one of the twin elements acts as reference-element, and is thoroughly maintained at the thermostat temperature, whilst in the second or measurement-element. The heat of the process under investigation is internally compensated by Peltier cooling or by Joule heating.

After the value of the voltage signal returns to the initial point, the system reaches the equilibrium, and the measurement of the next point in the thermogram begins. This point is known as base line and it can have fluctuations generated by air convection or thermal fluctuations usually known as noise.[47] The noise level can affect the measurement of the heat,

so that it is important to keep it low in order to have trustworthy results and to be able to reproduce the experiment. In this work the noise level is approximately 1μW, represented in Figure 6.

Figure 6 Thermogram with the representation of the noise level and base line

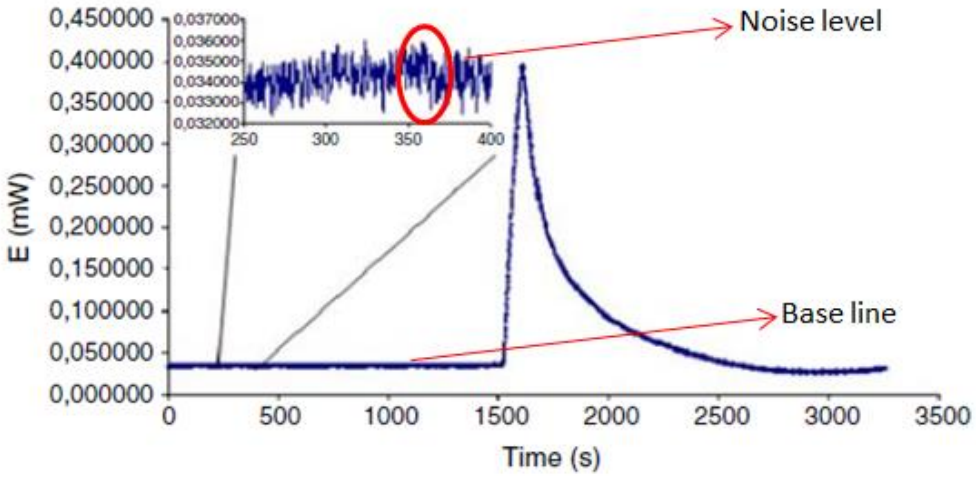

Source: García-Cuello *et al.* [48]

The result of the measurement is usually represented as a curve named thermogram. This is a graphic representation of the change of an energetic property at relation with the time or the temperature. Its analysis can produce not only thermodynamic, but also kinetic data. The kinetics of heat release during adsorption can be monitored by the change in the ***thermokinetic parameter*** τ[49,50].This thermokinetic parameter is indeed not constant and varies with coverage. Measurement of the thermokinetic parameter gives an indication of the rate at which various processes take place during adsorption. The minimum adsorption rate appears as a maximum in a plot of the thermokinetic parameter as a function of the surface coverage, indicative of a change from irreversible to reversible adsorption[51]. Thus, for example Ferino *et al.*[52]found by thermokinetic parameter calculation that the time needed to stablish equilibrium after the addition of doses of pyridine on zeolites increases with increasing coverage. This due to the fast adsorption rate because the molecules are bonded irreversibility to the strongest acid sites. The curve then passes through a maximum as the adsorption rate decreases because a smaller number of strong sites are available and the molecules must diffuse over greater distances on the surface. They suggested that this coverage should correspond to the filling of the acid sites of intermediate strength. Finally they mentioned the fact that only exchange between pyridine among the weaker sites occurs.

This is a fast process resulting in decrease of equilibrium time, which reaches a value close to the time constant of the calorimeter. In this way they can difference between strong and weak adsorption can be done.

2.3. Ordered mesoporous silicas

The development of mesoporous materials as adsorbent solids began 25 years ago with researches presented by Beck *et al.*[53] and Kresge *et al.*[54], leading to an extensive amount of works related to this kind of solids. Ordered mesoporous materials where first developed when studying the hexagonally arranged MCM-41 and subsequently the cubic MCM- 48 and layered MCM-50, collectively known as the M41S family. Other works that followed exhibit the possibility to prepare materials using non-ionic surfactants with notably materials such as well-known members SBA-15 (hexagonal) and SBA-16 (cubic) [55,56].

The adsorption on these mesoporous materials can be physical or chemical in relation to the capture of CO_2, depending on the synthesis condition and its functionalization with organic molecules incorporated on their porous walls, as it is explained below.

2.3.1 SBA-15 family

SBA-15 consists of a 2D hexagonal mesopore structure (P6mn space group) (Zhao et al., 1998 a[9],b[10]). The pore size can vary depending of the use of block co-polymers of different sizes. The pore geometry is an arrangement of cylinders and it can be considered as a model to understand capillary condensation[13] phenomena much like MCM-41. However, depending on the synthesis conditions -especially the temperature-, there is a possibility of the block copolymer chains to be occluded in the silica walls, which, when it was removed, leads to the possibility of materials having a certain degree of microporosity[55–58]. It is also possible to influence on the degree of microporosity and the formation of several silanols types by varying the calcination temperature[59].

These species of silanols were classified by Sindorf and Maciel[60] who worked with silica-gel sample by ^{29}Si NMR can be technical classified for their intensity, at low intensity peak at 91 ppm in mesoporous samples corresponds to silicon atoms bonded to two siloxane bonds –Si–O–Si– (Q^2) and two geminal silanol groups. Similarly, the resonance peak at 100 ppm is attributed to silicon atoms with three siloxane bonds (Q^3) and one silanol. Finally, the resonance peak a 109 ppm is related to silicon atoms with four siloxane bonds (Q^4).

Due to the reactivity existing between carbon dioxide and amino groups,[61,62] it has focused on the functionalization of mesostructured materials with amino-containing molecules in order to obtain highly selective adsorbents.

Grafting process, based on the chemical reaction between surface silanol groups and organo - alkoxy molecules[63], has been employed to incorporate amine organo silanes into a wide range of silica supports.

The CO_2/N ratio for these materials is usually close to 0.50 mol CO_2/ mol N, which is the maximum value for CO_2 capture under dry conditions, taking into account the reaction stoichiometry as seen in Figure 7.

Figure 7 Reaction scheme between CO_2 and grafted amino groups

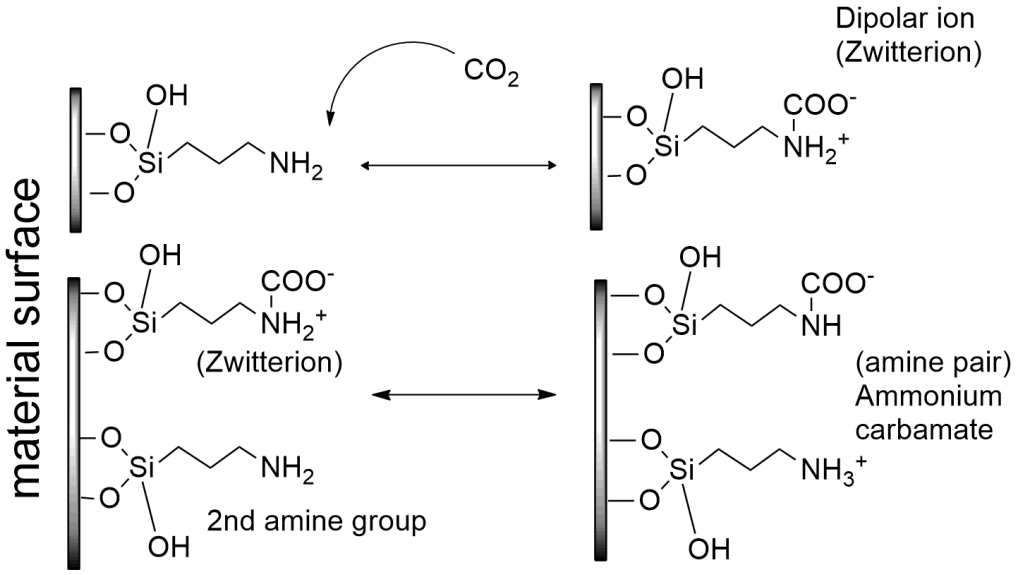

Source: Our authorship

Chang *et al.*[64] examined the adsorption of CO_2 on amine-grafted mesoporous silica. MCM-41, SBA-15 and pore-expanded MCM-41 were modified by mono-, di- and tri-aminosilanes to make hybrid adsorbents for CO_2 capture. SBA-15 was found to be a better support than MCM- 41 or pore-expanded SBA-15 for grafting amine moieties for the adsorption of CO_2. The tri-amine-grafted SBA-15 exhibited a CO_2 adsorption capacity of 2.4 mmol/g_{ads} at 60°C under anhydrous gas flow.

A new sustainable route to functionalize silica SBA-15 with APTES in supercritical CO_2 ($scCO_2$) was proposed in the work presented by Sánchez-Vicente *et al.*[65] The functionalization process in $scCO_2$ was compared to the conventional method using

toluene. The performance of the materials for CO_2 sorption at low and high-pressure was evaluated. The amine functionalized silica SBA-15 exhibited good CO_2 adsorption capacity: 0.7– 1.5 mmol g^{-1} at ambient pressure and 8–12 mmol g^{-1} at 40bar. These values indicate the great potential of the amine functionalized silica obtained in $scCO_2$ for carbon capture technology.

The reuse and recycling of amine-silica materials as CO_2 adsorbents were investigated for understanding their industrial viability in a novel study presented by Sanz-Pérez *et al.*[66] CO_2 adsorbents were obtained by grafting of diethylenetriamine (DT) or impregnation of polyethyleneimine (PEI) onto SBA-15 silica. The results showed for the grafting materials adsorbed 1.90 mmol g^{-1} at 45°C at 1 bar and for the impregnating material 1.72 mmol g^{-1} at the same temperature-pressure conditions, moreover CO_2 desorption conditions were evaluated, optimizing the time and temperature to reduce energy costs. In all cases, conditions as mild as 90°C and 90 min were enough to completely remove all CO_2 adsorbed.

The total nitrogen content incorporated into the support is restricted by the amount of silanol groups present in the surface. In order to overcome the limitation previously mentioned and to incorporate a higher quantity of amino groups, the impregnation method is used. This procedure consists of the physical incorporation of organic molecules into the porous structure (Figure 8), so that the whole pore volume can be filled with no restrictions apart from the organic molecule size relative to the pore entrance space. Impregnation leads to the incorporation of high amounts of large molecules providing a noticeable amount of amino groups in the resulting adsorbent.[8]

Sanz *et al.*[63]development a functionalization method based on the impregnation of previously grafted pore-expanded SBA-15. The combination of tethered and mobile amino groups has led to a synergic effect, yielding samples with CO_2 uptakes up to 5.34 mmol CO_2 g^{-1} at 45°C and 0.15 bar CO_2 and high adsorption efficiencies showing the advantages of this method of functionalization.

In a novel study Choi *et al.*[67] studied amine impregnated materials for CO_2 capture, in this work, two new amine-tethered solid adsorbents were prepared using preformed PEI stabilized with silane and titaniu um based additives, specifically APTES and titanium(IV), by using a novel, one-step synthesis. These new sorbents, A-PEI/silica and T-PEI/silica, respectively, were characterized alongside a standard amino silica adsorbent

prepared by impregnating PEI in the same commercial silica support, to give PEI/silica. The adsorption experiments showed that these new adsorbents offered both high adsorption capacity and improved adsorption kinetics compared to the conventional PEI/silica adsorbent. The modified PEI samples, A-PEI/silica and T-PEI/silica, also presented higher decomposition temperatures compared to the standard PEI/silica, resulting in hybrid adsorbents with enhanced thermal stability over multiple temperature swing cycles. The adsorption capacity at 25°C shown values of 2.26 mmol g^{-1} for A-PEI/silica, 2.19 mmol g^{-1} for T-PEI/silica and 2.36 mmol g^{-1} for PEI/silica CO_2 g^{-1} in atmospheric pressure.

Figure 8 Schematic of primary, secondary, and tertiary amino-silane compounds impregnated on SBA-15 and their nomenclature

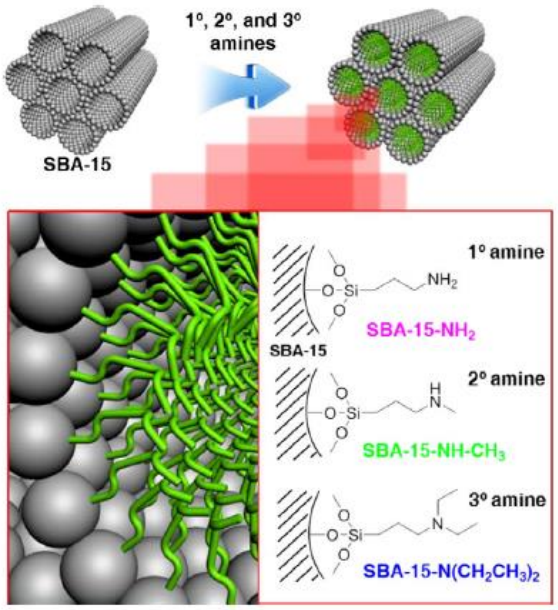

Source: Modified of Ko *et al.*[68]

Son *et al.*[69] impregnated PEI onto different types of mesoporous silica support materials and compared their performance for CO_2 capture. The CO_2 adsorption capacities of the materials decreased according to the following sequence: KIT-6>SBA-16≈SBA-15>MCM-48>MCM-41, as dictated by the mean pore diameter of the support material. However nowadays, novel studies with other start silica have been published per example in 2016, Ojeda *et al.*[70] worked with a mesostructured named KIL-2 this silica material was synthesized and functionalized by impregnation with two different amino sources, polyethylenimine (PEI) and Tetraethylenepentamine (TEPA). The adsorption capacity for these materials at 25°C and 1 bar, were of 2.19 mmol g^{-1} with PEI and 3.37 mmol g^{-1} with TEPA, at 90°C and 1 bar the capacity was higher 3.60 for PEI and 4.32 for TEPA. Finally

they concluded that CO_2 capture capacity, which seems to be strongly dependent on the size of the amino-precursors, can be further enhanced at higher temperatures for this kind of materials. Sanz-Pérez *et al.* [71] used a series of representative amines to impregnate on SBA-15. Ethylenediamine, 1,6-diaminohexane, hexamethyleneimine, tetraethylenepentamine (TEPA), branched polyethyleneimine (PEI), piperazine (PZ), and 4-amino-2-hydroxy-6-methylpyrimidine (PD) were used as impregnating agents. PEI, TEPA and PZ were selected as the best molecules for impregnation. PEI, TEPA and PZ were impregnated in SBA-AP support, a sample previously modified by grafting SBA-15 with AP. In all cases, obtained adsorbents showed higher CO2 uptake, amine efficiency and cyclic stability. SBA- AP–TEPA was found as the best adsorbent, with a pure CO_2 uptake of 2.36 mmol CO_2/g_{ads} (45°C, 1 bar).

3 EXPERIMENTAL

3.1. Materials

3.1.1. Gases

The gases used as adsorbates during the adsorption capacity and microcalorimetric studies were helium, carbon dioxide and nitrogen (*White Martins Praxair, Inc., Brazil*). Nitrogen was also used to determine the textural properties from isotherms at -196 °C. Helium was used for calibration procedures. The specifications of the gases are presented in Table 1:

Table 1 Characteristics of the gases used as adsorbates

Gases	Concentration (%)	Impurities
Helium	99.999	THC*<0.5 ppm, CO_2, O_2<1 ppm, N_2<5 ppm
Carbon dioxide	99.800	-
Nitrogen	99.999	THC*<0.5 ppm, CO_2, O_2<1 ppm, H_2O<2 ppm

* THC: Total hydrocarbon content

Source: White Martins Praxair, Inc., Brazil.

3.1.2. Adsorbents

3.1.2.1.Synthesis of mesoporous silica

The synthesis of pure mesoporous silica (MSS) was performed using a hydrothermal route as described by Fulvio *et al*[72], with some minor modifications attempting to obtain SBA-15. So, 5.7 g of P123 *(Sigma Aldrich, Brazil)* was used as structure-directing agent and 0.065 g of NH_4F *(Sigma Aldrich, Brazil)* as a swelling agent to reduce the length of the channels[73] moreover is known that this substance changes the molecular arrangement of a conventional sba-15, making it more suitable for the grafting step. They were mixed in 200 mL HCl solution (1.3 M) *(Labsynth, Brazil)* and stirred at room temperature until the complete dissolution of the surfactant. Then, 12.2 g of TEOS *(Sigma Aldrich, Brazil)* was added as a silica source under stirring for 24h at room temperature. The solution was then transferred to a teflon lined reactor and heated at 100 °C for 48 h.

After that, the solids were filtered, washed and dried at 100 °C for 24 h. The dried solids were then calcined at 550 °C at a heating rate of 3 °C min^{-1} for 5 h. A process flowchart is presented in the Figure 9.

Figure 9 Synthesis MSS flowchart

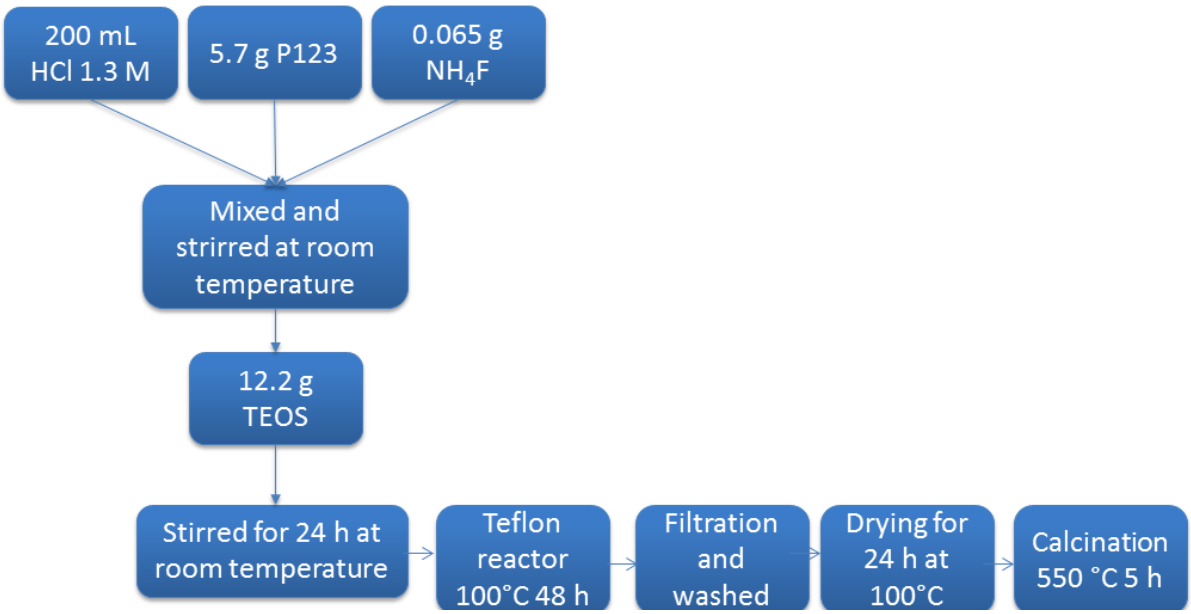

Source: Own authorship

3.1.2.2. Grafting with APTES

APTES grafting on pure mesoporous silica (MSS) was carried out following the methodology described by Hiyoshi *et al.*[74] . The pure mesoporous silica (2.0g), previously dried at 110 °C, was introduced into a three neck flask and soaked with 10%, 20%, 40% and 60% v/v APTES *(Sigma Aldrich, Brazil)* solution in dry toluene. The solution was heated overnight under reflux at 110 °C under N_2 atmosphere. The different grafted silicas were filtered, washed with pure toluene *(Labsynth, Brazil)* and dried at 100 °C. The samples were named as MSG10, MSG20, MSG40 and MSG60. The numbers in these labels represent the different volume/volume ratios of APTES to toluene in the grafting step (see Figure 10).

3.1.2.3.Impregnation with poly ethyl imine (PEI)

In this step, the grafting and impregnation methods were combined to obtain a higher nitrogen incorporation (as compared to MSG materials) and a higher mobility of amino groups.[63]

MSG20 was chosen as starting material because the previous result of parameter thermokinetic is lower in contrast with the other grafting materials, it would let a lower impact for diffusional CO_2 resistances. Following the wet impregnation method used by Xu *et al.*, 2002[75], 0.40 g of PEI 50% m/v in water (*Fluka Analytical, Switzerland*) were stirred with

3.6 g of methanol *(Labsynth, Brazil)* for about 15 min. Then 0.45 g of MSG20 was added to the solution, maintaining a proportion of 8 g of methanol per gram of MSG20 sample.

The resultant slurry was continuously stirred for about 30 min and the solid was dried at room temperature overnight.[71]

The as-prepared adsorbent was denoted as MSG20I30, where "30" represents the loading of PEI as weight percentage of the sample. A process flowchart is presented in the Figure 10.

Figure 10 Grafting and Impregnation process flowchart

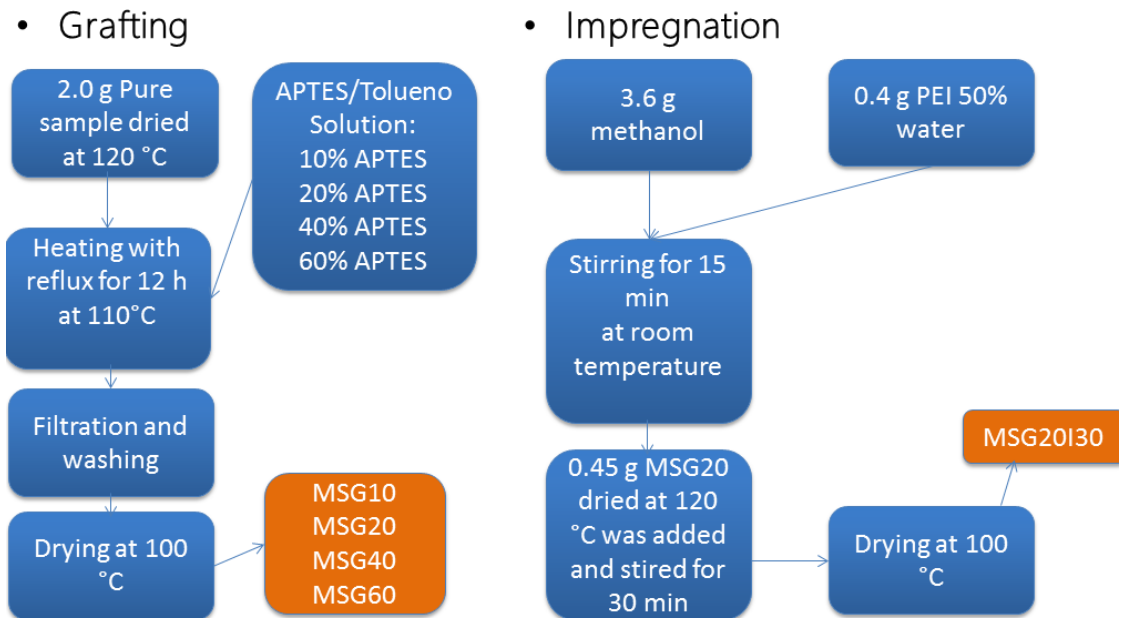

Source: Own authorship.

3.2.Methods

3.2.1. Adsorbents characterization

All samples were characterized using the methods and techniques presented in the following sections.

3.2.1.1. Textural Characterization

N_2 adsorption/desorption isotherms at -196 °C were used to calculate the textural properties of silica samples. The isotherms were measured in an Autosorb-iQ *(Quantachrome Instruments, USA)*. The MSS and functionalized samples were outgassed at 120 °C under

vacuum (10^{-6} bar) during 4 hours before the beginning of the experiment in order to ensure a clean solid surface for the test.

SPECIFIC SURFACE AREA:

The specific surface area of all materials was calculated using the Brunauer-Emmett-Teller (BET) [76] equation. The model equation is generally applied in a linearized form as in Equation 9.

$$\frac{{}^{P}/_{P_O}}{n\left(1-{}^{P}/_{P_o}\right)} = \frac{1}{n_m C} + \frac{C-1}{n_m}\left(\frac{P}{P_O}\right) \quad (9)$$

By plotting $\frac{{}^{P}/_{P_O}}{n\left(1-{}^{P}/_{P_o}\right)}$ vs. ${}^{P}/_{P_O}$ in a relative pressure range from 0.05 to 0.35, a straight line is expected with slope $(C-1)/n_m$ and an intercept equal to $1/n_m C$. Since n_m is the number of moles required to cover a monolayer, and the cross section of the nitrogen molecule (σ) is a known value[13] equal to 0.162 nm^2.

It is possible to estimate the surface area (A_{BET}) using Equation 10, where the Avogadro Number (A_N) equals to $6.023 \cdot 10^{23}\ mol^{-1}$.

$$A_{BET} = n_m A_N \sigma \quad (10)$$

TOTAL PORE VOLUME

The total pore volume was estimated using Equation 10, where n_m is the amount adsorbed at a relative pressure of 0.985. For this relative pressure, it is assumed that all pores are filled with liquid adsorbate[14].

$$V_p = n_m \frac{MM}{\rho N_2} \quad (3)$$

where, MM and ρN_2 are the molar mass and the density of liquid N_2, respectively.

MICROPORE VOLUME

The micropore volume was calculated using the Dubinin-Radushkevich (DR) equation[13], which is based on the potential theory of Polanyi[13].The essential parameter (Polanyi adsorption parameter) A is defined by Equation 11, which is related to the affinity of adsorption.

$$A = RTln\frac{P_o}{P} \tag{4}$$

where R is the gas constant and T is temperature.

The characteristic curve is Usually expressed as shown in Equation 12.

$$\frac{V}{V_o} = e^{\left(-A/E\right)^2} \tag{5}$$

where V is the volume that can be adsorbed in a given relative pressure value, V_o is the maximum volume that can be adsorbed and E is a characteristic energy of the system.

By combining equations 11 and 12, one can obtain the DR equation shown as Equation 13.

$$log\left(\frac{V}{V_o}\right) = -Dlog_{10}^2\left(\frac{P_o}{P}\right) \tag{6}$$

where D is the DR (Dubinin–Radushkevich) constant.

Equation 13 can be written in terms of adsorbed moles, thus it is rewritten as in Equation 14:

$$log\left(n_{(po)}\right) = log_{10}\left(n_{(po)(mic)}\right) - Dlog_{10}^2\left(\frac{P_o}{P}\right) \tag{7}$$

where $n_{(po)}$ are the adsorbed moles for a given relative pressure value, and $n_{(po)(mic)}$ is the amount of moles that can be adsorbed in the micropores.

$n_{(po)(mic)}$ may then be estimated from the intercept of the straight line obtained by plotting $log_{10}(n_{(po)})$ vs $log_{10}^2\left(\frac{P_o}{P}\right)$ for a relative pressure range of 10^{-5} to 0.4. Finally, Equation 15 was used to obtain the micropores volume.

$$\hat{V}_{po(mic)} = n_{(po)(mic)} \frac{MM}{\rho N_2} \quad (8)$$

PORE SIZE DISTRIBUTION

The pore size distribution (PSD) of each sample was obtained using the BJH method from the nitrogen isotherms at -196.15°C applied to the desorption branch. This method was developed by Barrett, Joyner and Halenda.[77] They used the concepts of capillary condensation and formation of superficial layer in mesoporous solids. The PSD is one of the main properties of a solid adsorbent for gas separation/purification and storage, and it is necessary for molecular simulation and development of new materials.

3.2.1.2.X-ray diffraction (XRD)

In this work, an automatic diffractometer model X'Pert Pro MPD (*PANalytical , Netherlands*) was used, with a X'Celerator detector operating under continuous scan conditions. The measurements were obtained for 2θ between 1 and 10°. This technique was used to identify the possible semi-crystalline phases of the mesoporous silica materials in low angle and compare them to the typical structural arrangement of SBA-15.

3.2.1.3.Elemental Analysis

The elemental analysis of carbon, hydrogen and nitrogen (C, O, N) was performed using a CHNS/O Analyzer 2400, Series II (*Perkin Elmer. USA*) This technique was used to determine the nitrogen groups that were effectively incorporated to the silica samples.

In order to do this, approximately 10 mg were used. This technique consists in the combustion of the sample under inert atmosphere, obtaining simple gases such as CO_2, H_2O and N_2, which can be analyzed by gas chromatography.

The density of amino groups, $ø_{\text{-}NH_2}$ [Amine molecules/nm^2], was calculated by means of the nitrogen concentration, using Equation 16:

$$\emptyset_{-NH_2} = \frac{Nc.N_A}{A_{BET}.10^{18}} \quad (9)$$

where Nc is the nitrogen concentration (mol g^{-1}), N_A the Avogadro number and A_{BET} is the specific surface area ($m^2\ g^{-1}$).

The literature[63,78,79] mentions the fact that, theoretically, two moles of N are required to capture one CO_2 mole to generate an ammonium carbamate. Therefore, the maximum theoretical adsorption capacity of CO_2 by chemisorption (MTAC) could be calculated.

3.2.1.4.[29]Si NMR Nuclear magnetic resonance

The nuclear magnetic resonance spectra of [29]Si for grafted the mesoporous silicas (MSG) and the pure sample (MSS) were obtained using a Bruker Avance II + 400, at room temperature. The measurements were made at a resonance frequency of 79.5 MHz, employing a spectra decoupling of protons with a pulse repetition time of 60 s and pulse angle of 90°. For the pure sample, this technique was used to determine the concentration of silanol groups on the surface available to react with APTES (Equation 17). For MSG samples, it represents the percentage of -OH groups that do not react after the grafting named ($\%_{-OH(Q)}$) as Si $_{\text{Q type}}$ from equation 10.[80] In addition, these values are used to calculate the APTES coverage percentage on the MSG surfaces using Equation 18, which illustrates the relation between the occupied silanol groups with the initial groups on the MSS sample.

$$\%_{-OH(Q)} = \frac{2Q^2 + Q^3}{Q^2 + Q^3 + Q^4} \quad (10)$$

where Q^2, Q^3 and Q^4 represent the different types of silicon bound to oxygen on solid silica in molar percentage (see Figure 11).

Figure 11 Chemical composition of silica surface

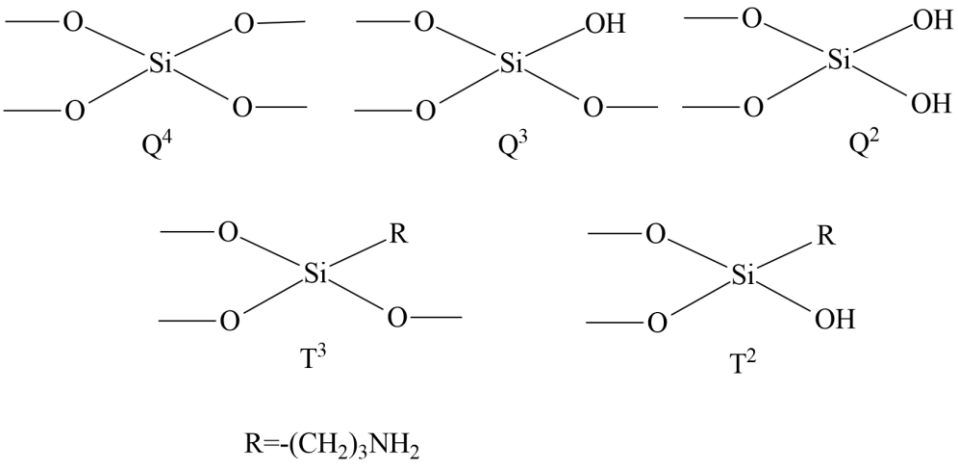

Source: Own authorship.

$$\%APTES\ surface\ coverage = \frac{\%_{-OH_{MSS(Q)}} - \%_{-OH_{MSG(Q)}}}{\%_{-OH_{MSS(Q)}}} \quad (11)$$

Equation 19 was used to compute the total of hydroxyl groups after the grafting process.

$$\%_{-OH(total)} = \frac{2Q^2 + Q^3 + T^2}{Q^2 + Q^3 + Q^4 + T^2 + T^3} \quad (12)$$

where T^2 and T^3 represent the different types of silicon bound to carbon in molar percentage, as well as oxygen on solid silica (see Figure 11).

Equation 20 calculates the density of the silanols group ($\emptyset_{-OH}$) in –OH molecules per nm^2. This property is very important because it provides an idea of distribution of these groups on the surface and how they interact with free and adsorbed CO_2.

$$\emptyset_{-OH} = \frac{\%_{-OH(total)} x N_A}{60.08 x A_{BET} x 10^{20}} \quad (13)$$

where 60.08 is the molecular mass of silica and 10^{20} is an unit conversion factor.

Equation 21 was used to compute the molar percentage of APTES after grafting process.

$$\%molarAPTES = \frac{T^2 + T^3}{Q^2 + Q^3 + Q^4 + T^2 + T^3} \quad (14)$$

3.2.1.5.Thermogravimetric analysis

In order to identify the volatile components of the material and analyze the mass loss events with increasing temperature, thermal analysis was performed for all samples. TGA-QMS equipment model STA 409 CD/403/5/G SKIMMER (Netzsch, Germany), coupled with a mass spectrometer was used. In these experiments, approximately 20 mg of material was weighted and the sample was heated to 800 °C with a heating rate of 10 °C min^{-1} under air flow (20 mL min^{-1}).

3.2.2. Adsorption Microcalorimetric experiments

For the adsorption microcalorimetric experiments, instrument Setaram C80, a Tian-Calvet microcalorimeter developed by *Setaram Inc. (France)* was used. It was coupled to a manometric system to measure simultaneously the CO_2 adsorption capacities and the amount of gas injected to the microcalorimeter under isothermal conditions. The microcalorimeter is internally composed of an array of thermocouples (9 rings of 19 thermocouples each, 19 inner and 19 outer ones, see Figure 12) that totally surround the sample and reference parts. The reference and sample cells have each volume of 12 cm^3 and are made of stainless steel. All heat that flows from the sample is captured and measured through a heat DSC sensor (3D) with 0.12 μW resolution. It also has a thermostat that allows for experiments ranging from ambient temperatures up to 300°C maintaining adiabatic conditions, if required. A power module receives command signals from a controller and provides the heating power for the thermostat and for the cooling fan command.[81]

The manometric system consists of seven valves forming a manifold, which is connected to the gas input. A pressure transducer P-30 model *(WIKA, Germany)* is also connected to the manifold with a precision of ≤ 0.1% and operating absolute pressure from 0 up to 1 bar. This is coupled to a digital multimeter of 6 ½ digits, 34401A model *(Agilent, USA)*, in order to measure the injection and equilibrium pressures.

Figure 12. Internal thermocouple configuration

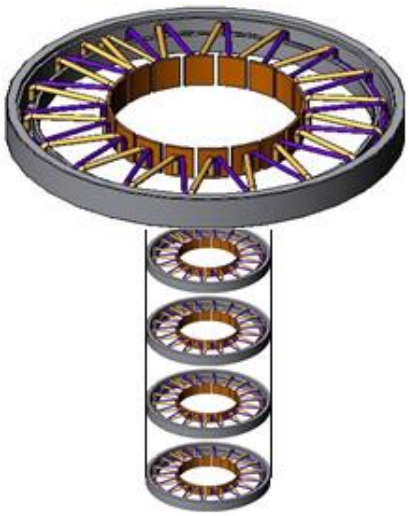

Source: Setaram C80, Commissioning.[81]

A vacuum pump model TC110 *(Pfeiffer, Germany)* is incorporated to the manifold to outgas the sample. Room temperature was monitored with a digital thermometer JProlab with operating range of -50°C up to 300°C and resolution of 0.1°C.

The complete system scheme is presented in Figure 13, valve 7 is the injection valve connected to the calorimeter and to the manometric system.

Figure 13 Microcalorimeter and Manometric system configuration

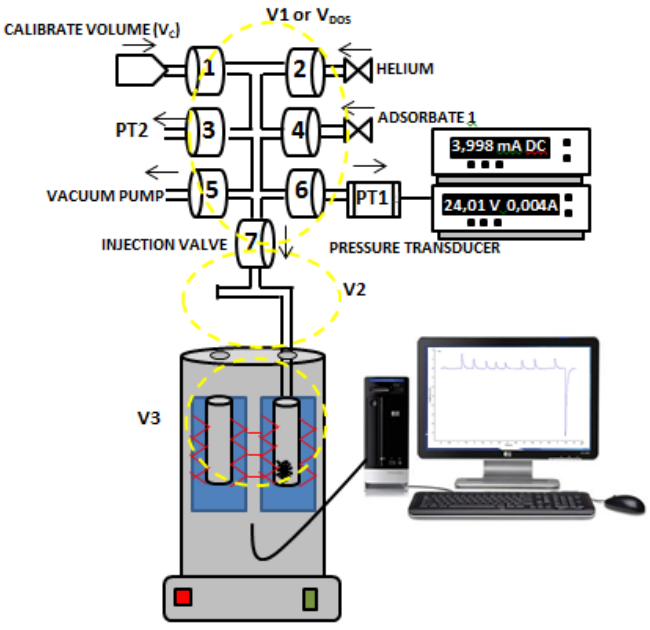

Source: Own authorship

Approximately 0.2 - 0.3 g of adsorbent was used for the experiments in this system. The silica samples were previously outgassed at 120 °C, for about 4 h under vacuum at pressures (10^{-6} bar) to ensure a clean surface required for the adsorption tests. The isotherms were measured up to 1 bar at 25 °C for all samples, plus 50°C for MSG60 and MSG20I30 with 3 regeneration cycles using vacuum and vacuum/temperature.

In order to calculate the adsorbed amount of gas, the initial moles injected in the cell and the equilibrium pressures are needed. Then, the following equations[82] was apply assuming ideal gas (low pressures).

$$n_{DOS} = \frac{p_i V_{DOS}}{R T_{DOS}} \tag{15}$$

$$n_e = \frac{p_{eq}(V_{DOS+} V_d)}{R T_{eq}} \tag{16}$$

$$n_i = \frac{p_{eq} V_d}{R T_{eq}} \tag{17}$$

where *pi* and p_{eq} represent the initial and equilibrium pressures, V_{DOS} the dosed volume, n_{DOS} the dosed moles, T_{DOS} and *Teq* the temperature of dosification and equilibrium, V_d the dead volume, *ni* and *ne* are the initial and equilibrium mole in the gas phase.

Then, equation 25 is used to compute the amount of gas that was adsorbed (n_{ads}), which is one of the points in the equilibrium adsorption isotherm.

$$n_{ads} = n_{DOS} + n_i - n_e \tag{18}$$

For the first data point, n_i is zero; for the next point, valve 7 (Figure 13) is closed and the last procedure is repeated for all points of the isotherm. An additional amount is then adsorbed, again according to equation 25. The complete isotherm representation n_{ads} per adsorbent mass vs p_{eq} is obtained with successive increments(i) from n_1 to n_i.[82]

3.2.2.1.Thermokinetic Parameter

The calorimetric signal (heat flow) decreases exponentially with the adsorption

time after the maximum of each adsorption peak, according to equation 26:

$$\mathrm{D} = D_m e^{-t/\tau} \tag{19}$$

where D and D_m are the deviation and the maximum deviation of the heat signal respectively. In equation 27, the thermokinetic parameter τ, or time constant, can be calculated as the inverse of the slope of the straight line obtained upon plotting *log D* as a function of time as shown by equation 33.[49] However, this thermokinetic parameter is not constant and varies as the adsorbent surface is filled.

$$\log D = logD_m - \frac{t}{\tau} \tag{20}$$

3.2.2.2.Differential Enthalpy of Adsorption

Before starting the calorimetric experiments, all samples were outgassed at 120°C for 4 h under vacuum (10^{-6} bar), in order to have a clean surface and eliminate impurities adsorbed from atmospheric air that could interfere with the equilibrium adsorbent-adsorbate.

Using the discontinuous method[13], currently the most common calorimetric procedure, it is possible to compute the differential adsorption enthalpy. The adsorptive is introduced in successive steps by means of the manometric system coupled with the Setaram C80 previosly described. This is done in order to determine the adsorbed amount for a given injection and use this value to calculate the adsorption enthalpy, as shown in equation 28:

$$\Delta h_{ads,T,n} = \left(\frac{dQ_{rev}}{dn^{\sigma}}\right)_{T,A} + V_d \left(\frac{dp}{dn^{\sigma}}\right)_{T,A} \tag{21}$$

The term dQ_{rev} of equation 21 is the result of the integration of the peak area detected by the calorimeter sensors, when dn moles are injected. The difference between the injection and equilibrium pressures is shown in the equation as dp. The microcalorimetric data is treated using the Calisto® Software (v1.043 AKTS-Setaram, *France*). The

experiments were carried out at 25°C for all samples, but both MSG20I30 and MSG60 samples were also tested at 50 °C in order to evaluate the material performance at higher temperatures (post-combustion) and their stability in adsorption cyclic processes.

It is important to note that each thermopile setup was factory calibrated by the supplier (Setaram) to convert automatically the voltage signal to power values. The system was considered to be in equilibrium, when the calorimetric signal remained constant for 10 minutes.

The dead volume V_d is calculated using the relation between the heat generated, measured directly from the thermopiles of the calorimeter and the differential pressure produced, when an inert gas (helium) is expanded through the cell that contains the sample (from a pressure close or higher than the atmospheric. The procedure is carried out because the gas is expanded in only one calorimetric cell. The sample was previously outgassed to guarantee a correct calculation of the dead volume.

3.2.2.3.Energy consumption between adsorption cycles

After the adsorption measurements, the gas was desorbed using high vacuum (approximately 10^{-6} bar). This process consumes heat which is sensed as a negative peak (endothermic), as shown in the thermogram of Figure 14. The desorption energy using only vacuum was computed by the integration of desorption peak area (Q_{desor}) subtracting the sum of power peaks detected for adsorption$\sum_{i=1}^{n} Q_{ads}$. For reversible samples, the result of this calculation is zero, while for irreversible samples the value obtained from the subtraction represents the energetic consumption necessary to complete the material desorption (equation 29). For complete desorption, it will be necessary to increase the temperature, simulating a hybrid adsorption process. Equation 30 is used to estimate the outgas temperature T_{reg} for the next adsorption cycle when the process is not completely reversible.

$$E_{regT} = |Q_{ads} - Q_{desor}| \tag{22}$$

$$T_{reg} = \frac{E_{regT}}{w_{ads} x C_{pads}} + T_{exp} \tag{23}$$

In equation 36, w_{ads} and C_{pads} are the adsorbent weight used and the specific heat (0.75 J g^{-1} °C^{-1}) of the solid, respectively, and T_{exp} is the experimental temperature (at which adsorption occurred).

Figure 14 Thermogram example of the adsorption-desorption process

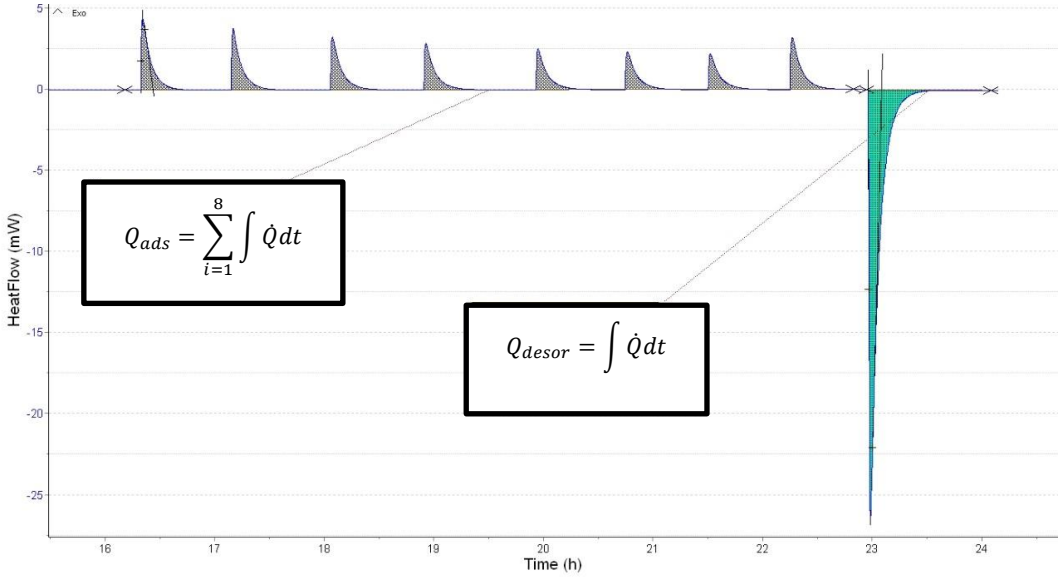

Source: Own authorship.

MSG60 and MSG20I30 samples were studied in 3 cycles of regeneration using only overnight vacuum at 25 and 50°C, in order to contrast the energy consumption required to reach complete desorption.

The samples were heated from T_{exp} up to the desired temperature in a rate of 2°Cmin^{-1}, outgassed at the final temperature for 3 hours and then submitted to vacuum overnight in order to measure the new adsorption capacity in isothermal condition.

3.2.2.4. Sites Energy Distribution

An important application of adsorption calorimetry is the determination of the site energy distribution in order to have a better understanding of the energetic surface sites and adsorption mechanisms.

Thus, the curve of the adsorption enthalpy vs the CO_2 adsorbed is fitted as a polynomial[51] as shown in equation 31.

$$\Delta h_{ads,T,n} = \frac{\Delta h_{int}}{dn} = \sum_{i=0}^{k} a_i n^i \quad (24)$$

where Δh_{int} is the integral heat of adsorption, *dn* is the adsorbed moles and a_i represent the polynomial coefficients.

Finally, the negative inverse of the polynomial derivative is related to the site energy distribution$f(q)$, as shown in equation 32.

$$f(q) = -\frac{dn}{d\Delta h_{ads,T,n}} = -\frac{1}{\sum_{i=1}^{k} i a_i n^{i-1}} \quad (25)$$

Depending on the attributes of the differential heat curve, one or more polynomials should be used to describe the entire range of heat.

The resulting graph $f(q)\ vs\ \Delta h_{ads,T,n}$ has peaks of accumulation of enthalpies. Each peak represents families where adsorption happens for example on different amounts of pores.

3.2.3. Adsorption equilibrium

3.2.3.1.Equilibrium isotherms of gas mixture at high pressures

Equilibrium isotherm measurements were carried out in a magnetic suspension balance (MSB) from Rubotherm *(Bochum, Germany)*, with a mass resolution of 0.01 mg and working pressure range from vacuum up to 15 MPa and working temperatures up to 500 °C. The experimental setup comprises the micro balance (Figure 15), the measuring cell, a data acquisition unit, a thermostat bath, an electric heater and a vacuum pump.

The samples were previously degassed under vacuum (0.01 bar) at 120°C for 4 hours. In this study, the gravimetric tests were carried out with pure gas (CO_2 and N_2) and gas mixture, simulating post combustion conditions (15% CO_2 and 85% N_2) at temperatures of 50 and 75 °C and pressure range of 0-10 bar.

Equation 33 is used to compute the excess amount of adsorbed gas. The microbalance senses the weight changes of the sample $\Delta m_{(P,T)}$. The second part of this equation represents the buoyancy correction from the calibration experiments, which is determined by the solid volume *(Vs)* and the volume of the balance components *(V_B)* ($cm^3\ g^-$

[1]). During these essays, helium was used as the inert gas, since it is assumed not to be adsorbed on the working conditions of pressure *(P)* and temperature *(T)*.

$$m_{ex(P,T)} = \Delta m_{(P,T)} + (V_B + V_S).\rho_{g(P,T)} \quad (26)$$

where, $\boldsymbol{m_{ex(P,T)}}$ is the excess adsorbed mass and $\boldsymbol{\rho_{g(P,T)}}$ is the gas density evaluated by means of an equation of state. Then, the specific adsorbed amount (per mass of adsorbent) is calculated by dividing $\boldsymbol{m_{ex(P,T)}}$ by the sample mass.

Figure 15 Magnetic suspension balance

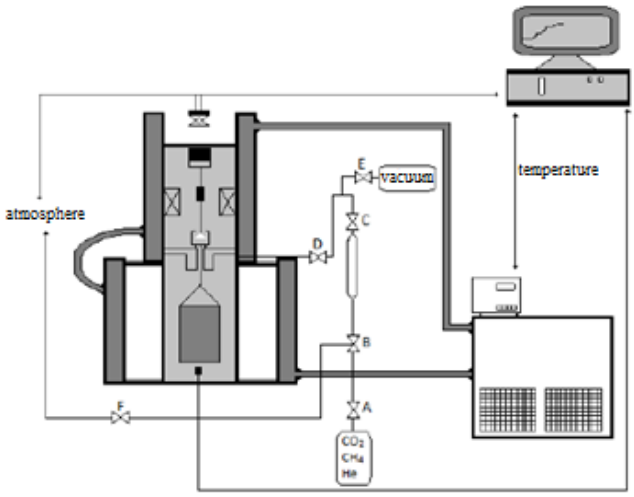

Source: Modified of Moura, 2017.[83]

3.2.4. Equilibrium models

The Langmuir model described in Equation 34 was used to fit the experimental data of N_2 and CO_2 isotherms on the MSS sample.

$$q = \frac{q_m.bp}{1 + bp} \quad (27)$$

This model is based on the Langmuir's theory[13,15], which considers that all adsorption sites to have the same energy. The parameter *b* (bar^{-1}) represents the affinity between adsorbate and adsorbent, and q_m $(mmol\ g^{-1})$ is the maximum adsorption capacity.

For CO_2 equilibrium, a similar concept was applied but considering that CO_2 is adsorbed in two different sites, one where chemisorption has an important contribution (site 1) and in another where physisorption is the predominant mechanism (site 2). With these concepts in mind, Equation 35 was used to model CO_2 equilibrium on functionalized samples.

$$q = \frac{q_{m1}.\, b_1 p_1}{1 + b_1 p_1} + \frac{q_{m2}.\, b_2 p_2}{1 + b_2 p_2} \tag{28}$$

The two parts of the equation represent the two active sites available (1,2) for adsorption in the MSG materials and MSG20I30 sample.

The Multi-Region Extended Langmuir was the model used for multicomponent equilibrium. This model also considers the existence of two different sites: one adsorbs both adsorbates (CO_2 and N_2) (Equations 38 and 39), assuming there is a competition between them, but the other one only adsorbs the component with more affinity (CO_2) considering chemisorption, as shown in equations 36 and 37.

$$q_{CO_2,1} = \frac{q_{m1CO_2}.\, b_{1CO_2} p_{CO_2}}{1 + b_{1CO_2} p_{CO_2}} \tag{29}$$

$$q_{N_2,1} = 0 \tag{30}$$

$$q_{CO_2,2} = \frac{q_{m2CO_2}.\, b_{2CO_2} p_{CO_2}}{1 + b_{2CO_2} p_{CO_2} + b_{2N_2} p_{N_2}} \tag{31}$$

$$q_{N_2,2} = \frac{q_{mN_2}.\, b_{N_2} p_{N_2}}{1 + b_{2CO_2} p_{CO_2} + b_{N_2} p_{N_2}} \tag{32}$$

The total amount of gas adsorbed q_T (g/g) is computed using equation 40, where q_{CO2} is the CO_2 amount on site 1 or site 2 and $q_{N2,2}$ is the nitrogen amount on site 2.

$$q_T = q_{CO_2,1} + q_{CO_2,2} + q_{N_2,2} \tag{33}$$

3.2.5. Selectivity

The selectivity is an important characteristic of an adsorbent in gas separation. It quantifies the adsorbent preference to adsorb a gas instead of another. The capacity to adsorb CO_2 preferentially in comparison to N_2 is important for industrial applications. For multicomponent experiments, the selectivity is calculated using Equation 41 from data of the binary model described by the equilibrium model that best fits the isotherm.

$$\alpha_{CO_2/N_2} = \frac{q_{CO_2}}{q_{N_2}} \frac{y_{N_2}}{y_{CO_2}} \tag{34}$$

where $\boldsymbol{q_{CO_2}}$ and $\boldsymbol{q_{N_2}}$are the CO_2 and N_2 uptakes, respectively. $\boldsymbol{y_{CO_2}}$ and $\boldsymbol{y_{N_2}}$ are the molar fractions in the gas mixture.

3.2.6. Working capacity

The working capacity (WC) is defined as the difference between the adsorption capacities at two specific working pressures. It is important to be considered in cyclic processes based on pressure swings to regenerate and reuse the adsorbent. For instance, if one assumes that the adsorption step is carried out at 1 bar (in mixture isotherm) and the desorption step at 0.02 bar, the working capacity is calculated as described in Equation 42.

$$WC_{(0.02-1\ bar)} = q_{1bar} - q_{0.02bar} \tag{35}$$

3.2.7. Adsorbent Performance Indicator – API

In order to compare adsorbents in a given gas separation/ purification process, a performance indicator has been suggested in the literature [84] , as observed in Equation 43.

$$API = \frac{\left(\alpha_{CO_2/N_2} - 1\right)^A WC_{CO_2}^B}{\left|\Delta H_{ads,CO_2}\right|^C} \tag{36}$$

Where A, B and C are empirical parameters, which may be chosen according to the desired separation/ purification process. α_{CO_2/N_2} is the CO_2/N_2 selectivity; WC is the working capacity of CO_2; and ΔH_{ads} is the CO_2 adsorption enthalpy.

4. RESULTS AND DISCUSSION

4.1. Thermogravimetric analysis

The thermal stability of the incorporated functional groups was studied using the TGA technique. The thermal profiles of the samples and their derivatives are shown in Figure 16 (A) and 16 (B) respectively. Mass loss events and respective temperature ranges for all samples are shown in Table 2. Figure 16A shows that the total weight loss increases with the progressive incorporation of amine on the sample, with MSG20I30 showing the highest weight loss, as expected.

Table 2 Mass loss of all samples with increasing temperature

Sample	Temperature Range (°C) Mass Loss %			Total mass loss
	30-170	170-500	500-800	
MSS	4.62	0.92	0.63	6.17
MSG10	4.97	7.30	2.04	14.31
MSG20	5.21	8.21	2.34	15.76
MSG40	5.66	8.17	2.43	16.26
MSG60	7.92	10.92	3.41	22.25
MSG20I30	28.10	23.25	5.37	56.72

For all samples, the initial weight loss around 100 °C is mainly due to the loss of physisorbed water, corresponding to 5%, for MSS, 10-14%, for MSG's samples and 25% for MSG20I30 (point 1 in Figure 16). The mass spectra analysis, Figure 17(A), presents the signals with m/z ratio of 17 and 18, which confirms the release of moisture. The difference between the weight loss in the samples can be explained with the additional m/z 44 found in the functionalized samples (MSG's samples and MSG20I30), that is attributed to the release of the atmospheric CO_2 adsorbed in the material due to the presence of amine groups. This result is in agreement with the increase in %C observed in elemental analysis.

Figure 16. Thermogravimetric curves (A) TGA (B) DTGA

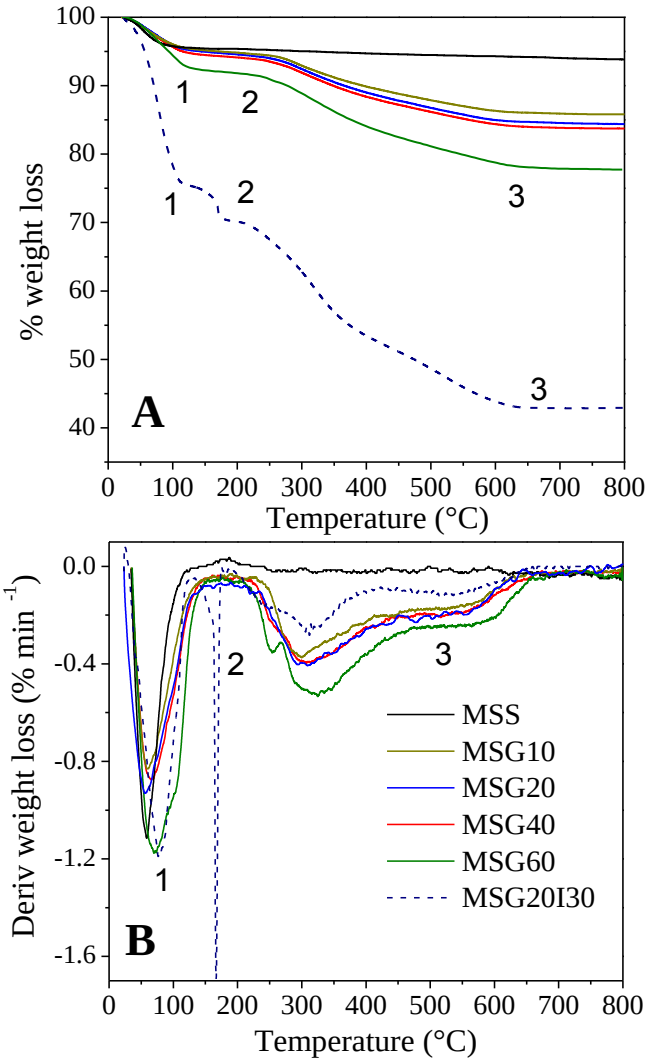

The second weight loss occurs in the range from 170 ˚C to 500 ˚C for MSG20I30 and 240 ˚C to 500 ˚C for MSG's samples, point 2 in the Figure 16. According to literature,[85] the mass loss in the temperature range is attributed to the decomposition of 3-aminopropyltriethoxysilane and Propyl Ethyl imine, used for the grafting (MSG's samples), and impregnation (MSG20I30), respectively. This is in agreement with mass spectra analysis Figure 17(B), where m/z 12, 13, 15, 27, 39, 43, 44 signals are relative to the release of the fragments of pending groups. The initial temperature in this range would be the maximum temperature of operation of the material. The last range occurs in the intervale of 500-800 ˚C, point 3 in Figure 16. It is attributed to the increase in the decomposition of the pending amines (in agreement with mass spectra analysis). The fragments and molecular ions, and their corresponding m/z, are presented in the Table 3.

Figure 17 Mass charge ratio distribution measured by TGA

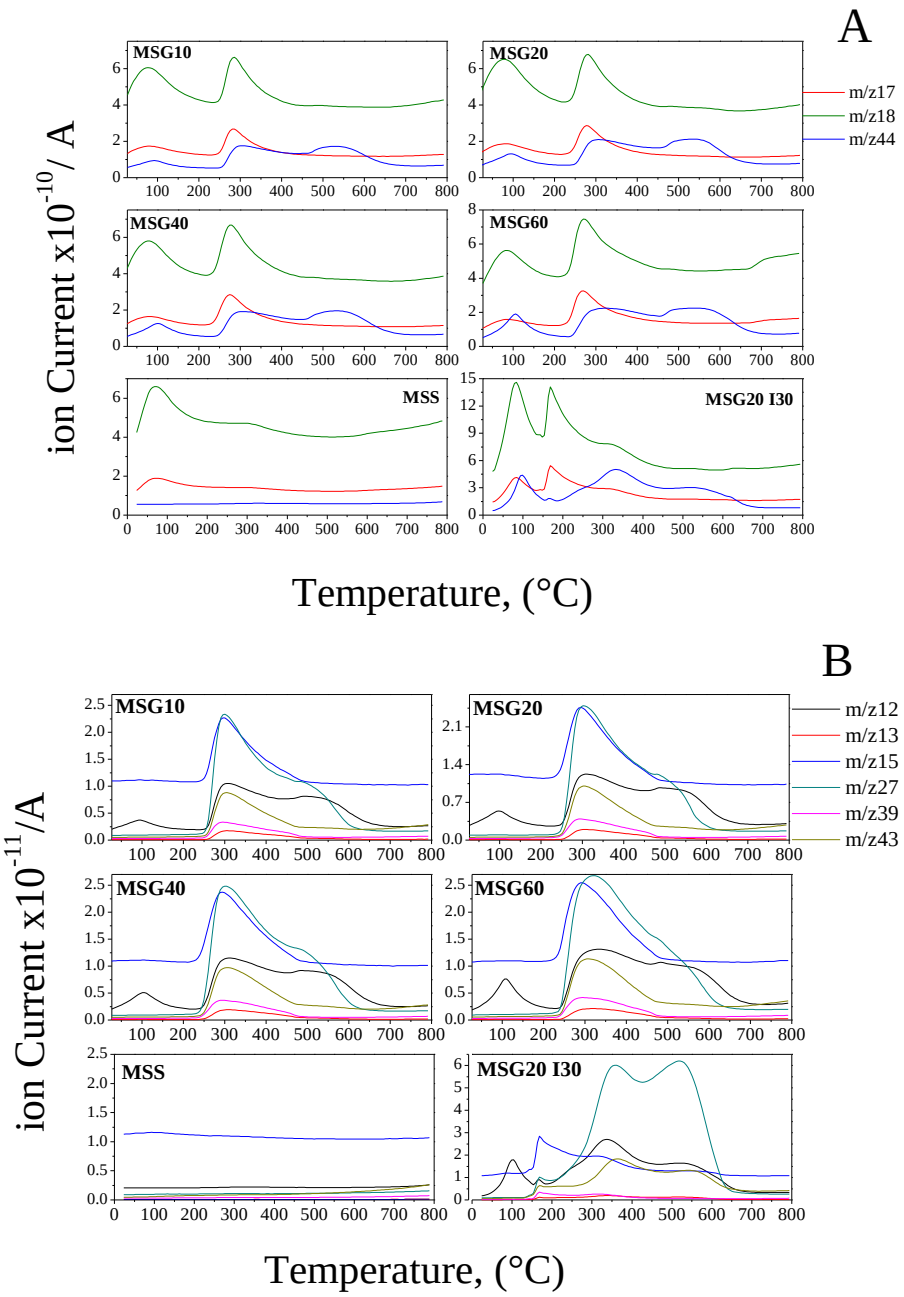

The thermal profile of MSG20I30 sample is different when compared with the other functionalized samples: a sharp weight loss appeared at 205 °C and when the temperature was increased above 220 °C, the rate of weight loss decreased, indicating that a different decomposition process took place. At 650 °C, the grafted amine was completely decomposed and removed as volatiles. The organic content in MSG20I30 was calculated to be about ~31 wt % (loss weight from 150 up to 750°C), in agreement with the designed PEI

loading. However, the starting sample (MSG20) has an organic content around 10%, indicating that there is loss of PEI during the impregnation process.

Table 3 Mass charge (m/z), fragments and their corresponding molecular ions

Mass Charge m/z	Fragments	Probable parent molecules
12	C+	CO_2, C_xH_y
13	CH+	C_xH_y
15	CH_3+, NH+	C_xH_y, NH_3
17	OH+	H_2O
18	H_2O+	H_2O
27	C_2H_3+	C_xH_y
39	C_3H_3+	C_xH_y
43	C_3H_7+	C_xH_y
44	CO_2+	CO_2

4.2.Textural Characterization

The nitrogen isotherms at -196 °C for the studied samples are presented in Figure 18 and their main textural characteristics are summarized in Table 4.

Figure 18 N_2 Isotherms at -196°C, open symbols represent desorption branch.

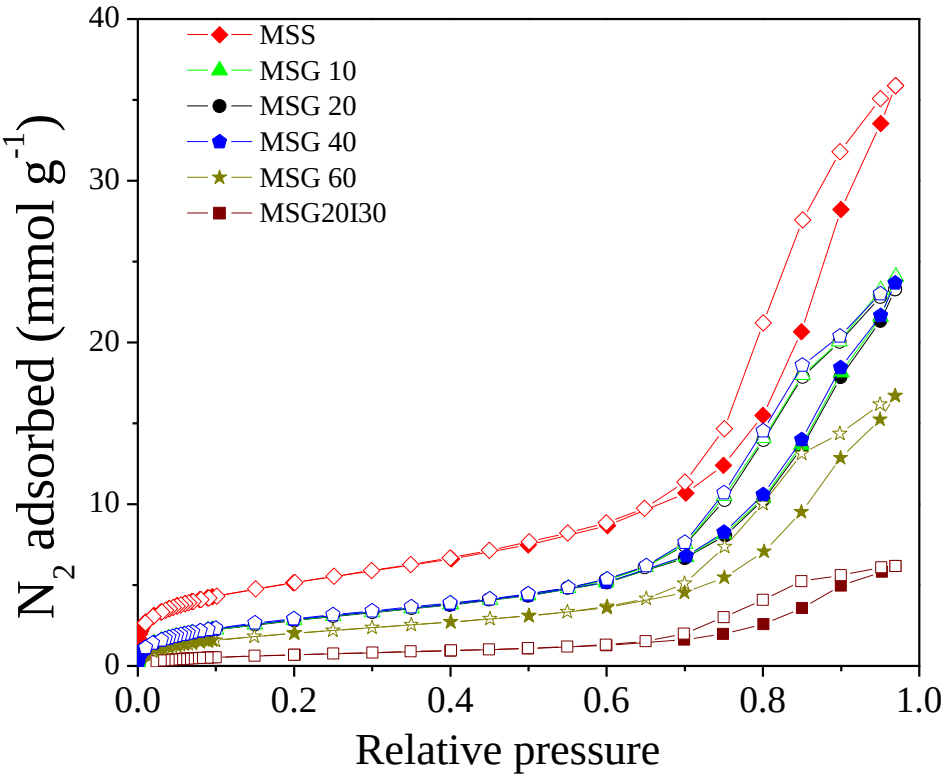

Table 4 Textural characteristic calculated from N_2 isotherms.

Sample	Surface area S_{BET} ($m^2 g^{-1}$)	Pore Volume $cm^3 g^{-1}$	Average pore size d_{DFT} (nm) desorption	Micropore volume[a] $cm^3 g^{-1}$	Microporosity, (%)
MSS	392	1.43	9.6	0.125	8.89
MSG10	213	1.02	7.8	0.057	5.61
MSG20	211	0.96	7.8	0.056	5.90
MSG40	215	0.98	7.8	0.056	5.73
MSG60	151	0.55	7.8	0.045	8.09
MSG20I30	52	0.06	7.8	0.014	26.09

[a]DR-equation

All samples show a reversible isotherm with type IVa behavior[14]. They are typical of mesoporous materials with a hysteresis loop due to condensation/evaporation effects. MSS presents a pore diameter and total pore volume similar to conventional SBA-15 (usually around 9 nm and 1 $cm^3 g^{-1}$respectively), as described in the literature.[86,87]

Contrary to the expectations, the loops were not H1 type, characteristic of the SBA-15 family, which indicate a narrow range of uniform mesopores. They rather look like a H2(b) hysteresis type which is associated to mesocellular silica foams (MSF), producing a shift to higher relative pressure as compared to hysteresis loops found for regular SBA-15.[14] The surface areas and pore volumes for functionalized materials (MSG) decrease in contrast with the MSS surface area. It is known that the average size of the APTES molecule varies between 0.6 and 1.0 nm[88,89]. Thus the APTES molecule is incorporated to a pure sample, a decrease of the available surface to adsorption and pore diameter is likely to happen. The PSD's for pure and grafted samples in logarithmic scale are presented in Figure 19 . The average pore size after the functionalization shows values of ~7.8 nm, confirming that the functionalize samples remain mesoporous.

For the two ways of functionalization (grafting and double functionalization), Table 5 summarize some reported data of specific surface area of pure and functionalized SBA-15, which have been synthesized by a similar methodology. Similar results in specific surface area reduction are observed for our samples, which decrease between 45 and 60% for grafted samples (depending of nitrogen content). For MSG20I30 the area decreases 75% in contrast with the MSG20 sample.

Figure 19 Pore Size Distributions (PSD's) to MSS and MSG materials.

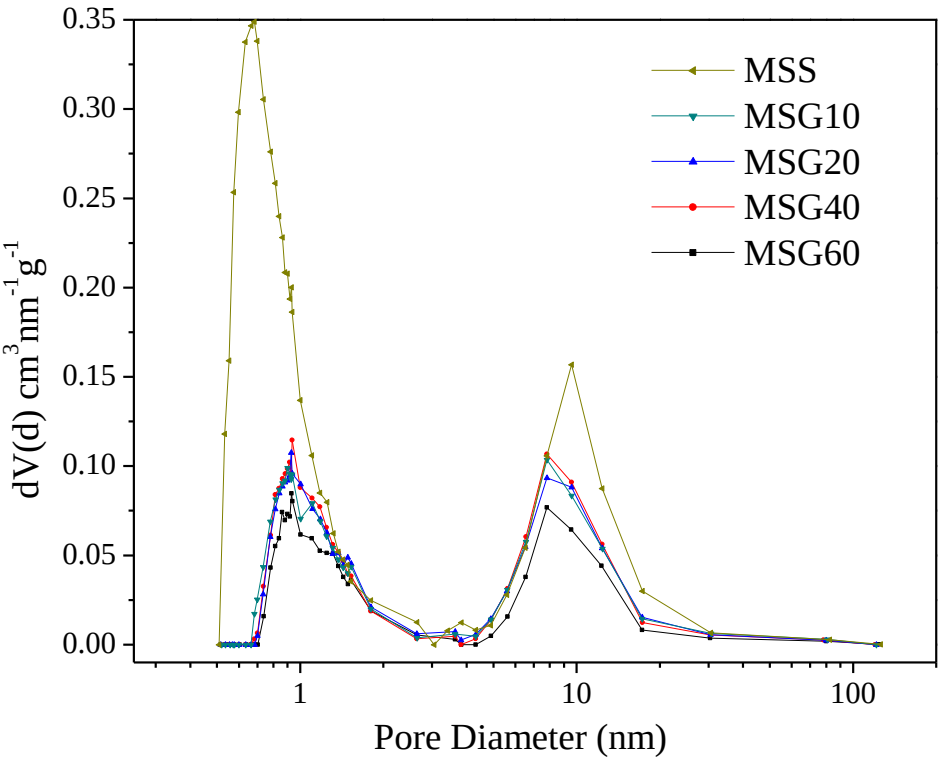

Table 5 Comparison between surface area results after and before functionalization of some mesoporous silica.

Functionalization type	S_{BET} ($m^2 g^{-1}$), before	Amine, N content (mmol/g)	S_{BET} ($m^2 g^{-1}$), after	Reference
GRAFTED SAMPLES	582	APTES, 1.99	372	Wang, L *et al.*[86]
	679	APTES, 2.46	207	Vilarrasa, G *et al.*[33]
	910	APTES, 2.57	364	Hiyoshi, N *et al.*[74]
GRAFTED / IMPREGNATED SAMPLES	228	APTES/ PEI, 7.64	38	Sanz, R *et al.*[63]
	258	APTES/ TEPA, 7.92	80	Sanz, R *et al.*[34]
	248	APTES/ PEI, 7.00	34	Sanz, R *et al.*[71]

MSG10, MSG20, MSG40 have a similar surface area, fact that could suggest that the variation of nitrogen incorporated is not enough to change significantly the textural properties of these samples.

After the immobilization of PEI on MSG20, the total pore volume was reduced from 0.96 to 0.06 cm^3 per gram of material (Table 4). The specific surface area was also reduced dramatically from 211 to 52 $m^2 g^{-1}$. These facts are expected since the incorporated

PEI fills the pores therefore the surface area and total pore volume should decrease. This may result in restricted access of nitrogen into the pores at liquid nitrogen temperature, although the average pore size calculated with BJH method (Figure 20) is still of 7 nm, confirming that the material remains mesoporous.

Figure 20 Pore size distributions (PSD's) to MSG20 and MSG20I30.

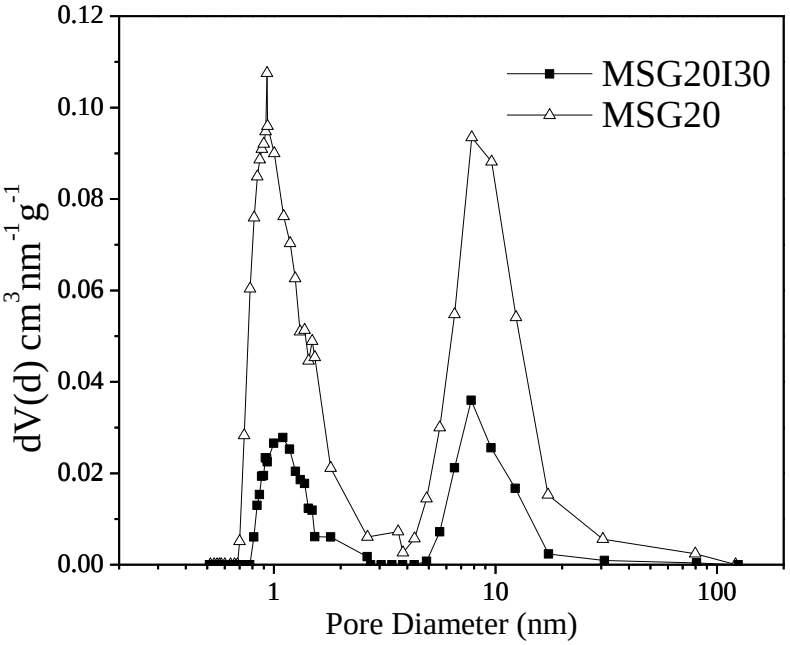

4.3.X-ray Diffraction (XRD)

Low-angle X-ray powder patterns of mesoporous silica MSS, MSG's samples and MSG20I30 are shown in Figure 21. The compiled diffractograms are contrasted with a conventional SBA-15.

Conventional hydrothermal SBA-15 shows a typical XRD pattern of an ordered network of mesopores with (100), (110) and (200) reflections which is typical of a hexagonal[56,90]symmetry. It can be seen that none of our samples presented the characteristic reflections of SBA-15. Vilarrasa *et al.*[85] and Liu *et al.*[92] showed similar behavior as characteristic of Mesocellular Foam Structure *(MSF)*. The presence of ammonium fluoride on the synthesis process could affect the hexagonal arrangement of the solid, limiting the growth of the mesochannels leading to shorter channels with low-range order. The reason of the use of fluoride is that it acts as a swelling agent. Many authors[93,94]attribute to this type of "*precursors*" the disruption of the ordered arrangement to a mesocellular structure, in which

an increase in the pore size is caused by NH_4F penetration into the hydrophobic core of the surfactant micelle, breaking up the typical honeycomb packing of the hydrothermal SBA-15. This is in agreement with the N_2 isotherm results (hysteresis type and isotherms shape) that were also characteristic for MSF materials.

Figure 21 XRD patterns of all silica mesoporous samples

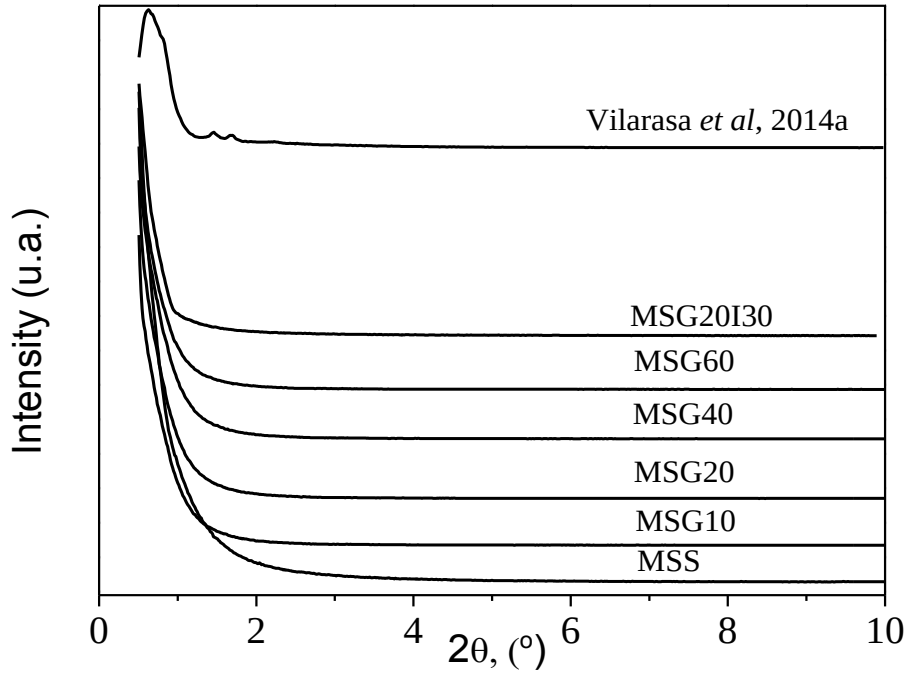

4.4.Elemental Analysis

The results of the elemental analysis are summarized in Table 6. It indicates that nitrogen has been effectively incorporated to the pure MSS sample. The amount of amine used in the grafting process increases proportionally to the nitrogen amount present on the solid.

In addition to nitrogen content, another important result that confirms the presence of primary amine on grafted samples (MSG) is the increase of the carbon amount. This increase is related to the incorporation of propyl groups of the APTES molecules in the grafting process.

Some amount of nitrogen is observed on the MSS sample; a possible explanation might be the NH_4F that remained on the material from the synthesis procedure. There is a difference between the C/N ratio measured (~3.3) and expected (3.0) for the MSG samples, possibly due to adsorbed atmospheric CO_2 that increases the carbon amount detected for the equipment as confirmed by ^{13}C-CP-MAS NMR experiments in other works[6,95].

Table 6 Elemental analysis of the samples studied

Sample	Carbon (%)	Hydrogen (%)	Nitrogen (%)	Carbon mmol.g^{-1}	Nitrogen mmol.g^{-1}	C/N
MSS	0.24	0.42	0.04	0.21	0.03	-
MSG10	6.39	1.44	2.20	5.32	1.57	3.38
MSG20	7.44	1.53	2.46	5.86	1.76	3.33
MSG40	7.76	1.74	2.73	6.46	1.95	3.31
MSG60	10.57	2.56	3.70	8.80	2.64	3.33
MSG20I30	21.08	5.39	10.62	17.57	7.59	-

The Maximum Theoretical Adsorption Capacity by chemisorption is summarized in Table 7 . The highest theoretical chemical adsorption is for MSG60 and MSG20I30, results that agree with the amine density per nm^2 of solid surface that will be shown in upcoming sections. This fact would probably improve the attractiveness of the solid for CO_2 adsorption.

Table 7 Amines density on functionalized samples and MTAC.

Sample	$Ø_{-NH2}$[a] , Amine molecule nm^{-2}	MTAC[b] mmol CO_2g^{-1}
MSG10	4.43	0.79
MSG20	5.02	0.88
MSG40	5.46	0.98
MSG60	10.53	1.32
MSG20I30	87.91	3.80

[a] Assuming a homogenous coverage.
[b] Maximum theoretical adsorption capacity by chemisorption.

4.5.Resonance Magnetic Nuclear ^{29}Si RMN

The spectra obtained for the MSS and MSG materials in this study are presented in Figure 22. All spectra of grafted samples show two peaks that are located approximately at -57 and -67 ppm, corresponding to T^2 and T^3 silanols[80,96,97] species, respectively. This suggests that the organic part Si–C (amine molecule) was covalently bonded to the silicon atoms of the pure sample (Si–O–Si, inorganic part).

Figure 22 ^{29}Si Chemical Shift to (a) MSG60 (b) MSG40 (c) MSG20 (d) MSG10 and (e) MSS samples.

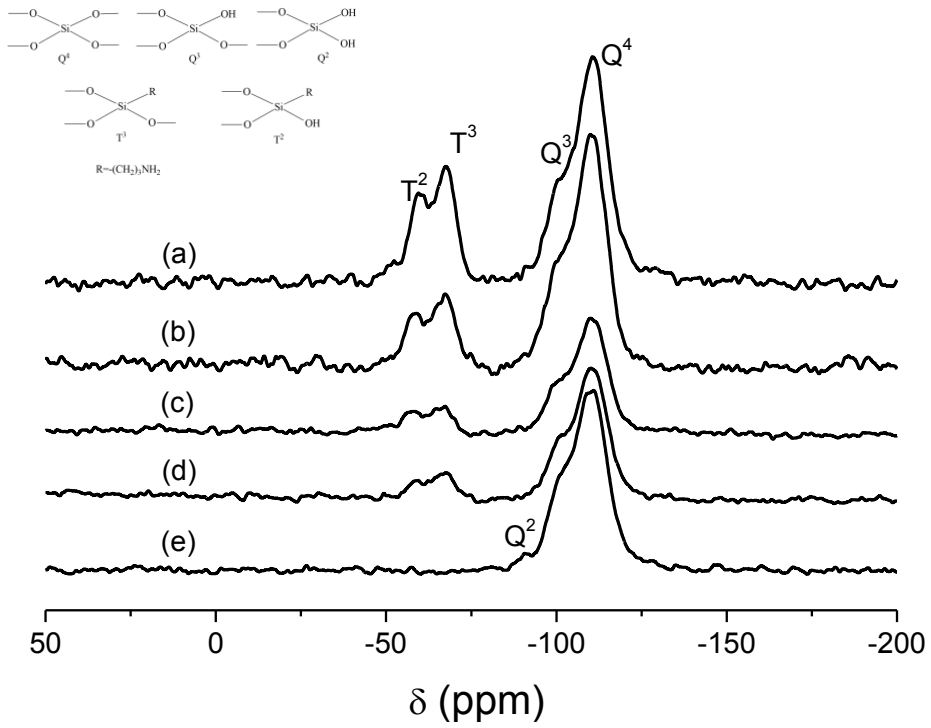

The progressive incorporation of APTES causes the increase of these peaks. Moreover the signals at -90 and -100 ppm, corresponding to Q^2 (germinal silanols), and Q^3 (free and vicinal silanols) silicon species[80]decrease (see Figure 11). These groups bonded with oxygen atoms represent the concentration of free silanol groups available to anchor the amine. Silicon species Q^4 (siloxane bridges) are present in all samples in a high percentage with a signal correspondent at -110 ppm. This result indicates that the majority of silanol groups have reacted during the synthesis process to form siloxane bonds, probably during the calcination stage[80,98]. These silicon species do not react with the amines, because they belong to the bulk inorganic structure. Therefore the amount of Q^4 is kept constant despite the increase in amine loading.

Figure 23 Deconvolution ^{29}Si chemical shift signal to mesoporous silica studied.

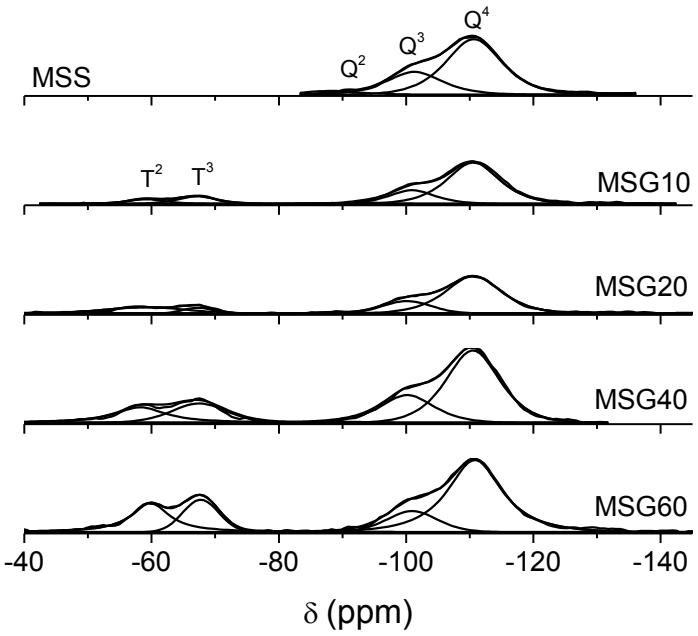

The T^2 and T^3 peaks confirm that the amine propyl group was incorporated on the pure mesoporous silica (MSS) as shown in the Figure 23. Table 8 summarizes the values obtained by the integration of these peaks. From these values, it is possible to calculate the silanol density and the percentage of APTES coverage as well as the silanols remaining after the functionalization. This table indicates the increase of Si T^2 and T^3 related to the APTES incorporation, and the decrease of Si Q^2 and Q^3, type as a result of the grafting.

Table 8 ^{29}Si MAS NMR peak integration for studied mesoporous silica

Sample	T^2 (int%)	T^3 (int%)	Q^2 (int%)	Q^3 (int%)	Q^4 (int%)
MSS	—	—	3.8	28.0	68.2
MSG10	5.4	8.8	1.8	18.9	65.1
MSG20	14.2	4.8	1.2	17.0	62.7
MSG40	11.2	12.5	0.9	11.7	63.7
MSG60	20.0	12.2	—	6.7	61.2

The molar amine percentage symbolized as "*R"* was calculated from the results of integration, as summarized in Table 9. The results also confirm that the anchored amine amount increases with the APTES incorporation by the grafting process.

Table 9 Molar percentages of silanols and R group contrast with the percentage of APTES coverage obtained from ^{29}Si NMR analysis

Sample	R content (%mol)	-OH (Q type) (%mol)	-OH (total) (%mol)	$\emptyset_{\text{-OH}}$ molec.nm^{-2}	% COVERAGE APTES
MSS	—	35.6	35.6	9.1	—
MSG10	14.2	26.2	27.9	10.6	26.4
MSG20	19.0	24.0	33.6	9.2	32.6
MSG40	23.6	18.1	24.7	6.2	49.2
MSG60	32.1	9.9	26.7	12.9	72.2

The silanols of Q type show that, as the APTES amount increases, it becomes more difficult to replace the -OH groups with the primary amine, phenomenon that could be caused by the decrease in surface area. A smaller surface hinders the contact between –OH and APTES to form the covalent bond. Several possible explanations are found in the literature for this phenomenon such is the pore blockage for the amine groups incorporated on the sample and the steric hindrance and inhomogeneous distribution of amino silanes[99]. The experiment result shows that the residual Q type silanols after grafting decreases as the amount of R in the sample increases, as expected. For MSG60, only 9.9 % of these groups are on the surface and this small amount explains the difficulty to attach the *R* group on this mesoporous material. About 72.2% of organosilane coverage on MSG60 corresponds to 10 amine molecules per nm^2, as calculated by elemental analysis and that will be in contact with 26.7% of –OH remaining after the APTES grafting. The total silanol percentage and the density of silanol groups do not increase with the grafted amine amount because the Si T^2 (that contains a molecule of –OH in its structure) is formed randomly and has no relation with the incorporation of amine groups on the sample. The distribution of silanols on the surface influences the mechanism of CO_2 adsorption being an important factor to be considered in a subsequent study of irreversible species formation.

4.6.Adsorption Microcalorimetric Experiments

The curves of the differential adsorption enthalpy as a function of CO_2 uptake are presented for all samples at 25°C up to 1 bar in Figure 24. All the samples show a stepwise decrease in the differential enthalpy with CO_2 uptake, which suggests initially that the solid adsorbent has a heterogeneous surface according to the classification described by Rouquerol *et al* [13].

This decrease is an indication of discrete heterogeneity. It means family of sites that decrease in energy as soon as they are occupied. The ΔH_{ads} for MSS sample starts from ~ -40 kJmol^{-1} up to one defined step in the curve, which points out to the presence of only physisorption sites. Many authors[100,101] attribute similar enthalpy values (~ -40 kJmol^{-1}) for $^{-}$OH/CO_2 interactions by hydrogen bonds.[102] These findings suggest that this value belongs to contributions of silanol groups present on the sample (35.5% calculated by ^{29}Si RMN/~9.1molec.nm^{-2}). For a better appreciation of the adsorption mechanism on MSS and MSG samples, Figure 25 shows the energy site distribution, -dn/dΔH_{ads}, as a function of -$\Delta H_{ads,}$ for all samples. For the MSS sample two peaks are presented with characteristic values of ~ -30 kJmol^{-1} and ~ -22 kJmol^{-1}. These energy peaks could perhaps be attributed to physisorbed carbon dioxide, as reported by the literature.[41,103]

Figure 24 Differential enthalpy of adsorption in function of CO_2 uptake for mesoporous silica samples

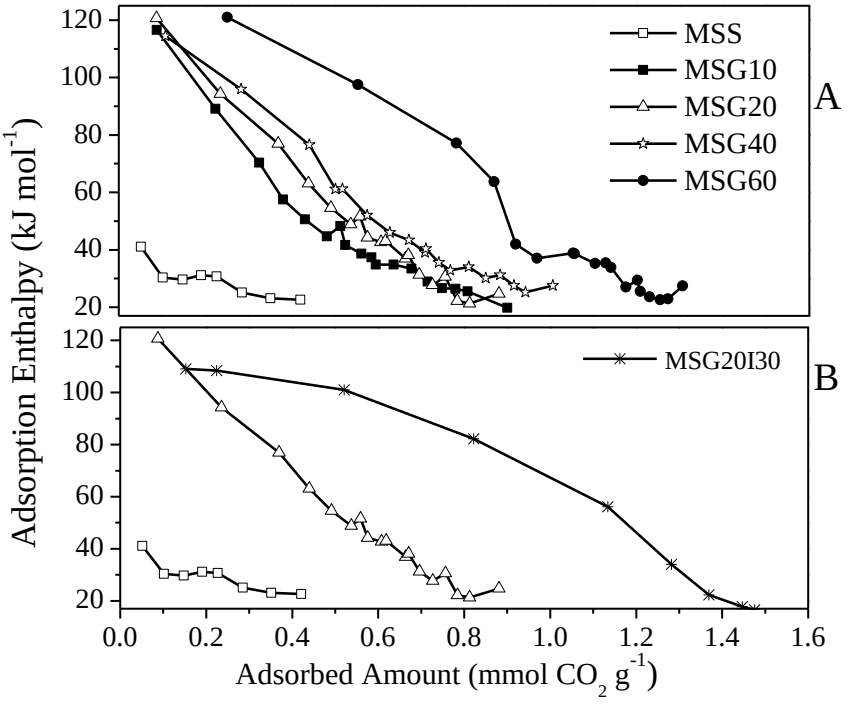

For the MSG series the values of initial enthalpies at low CO_2 coverage are higher than the value of MSS sample at low coverage, reaching ~ -110 kJmol^{-1}. This increase in the initial adsorption enthalpy is probably due to the chemisorption reaction between CO_2 and the amine pairs forming propyl ammonium carbamate species via intermolecular adsorption as reported by Alkhabbaz, *et al*[104]. They reported adsorption enthalpy values of -90kJmol^{-1} to the carbamate formation.

Another work found similar initial values when the nitrogen content is >1.2 mmol N g^{-1} [104], which is the case of our samples. The adsorption enthalpies of functionalized materials decrease when the concentration of adsorbed CO_2 increases up to enthalpies corresponding to CO_2 physisorption and for MSG20I30 sample up to ~-17 kJmol^{-1}(condensation enthalpy of CO_2). This decrease could be the result of a *steric hindrance effect*, when a high density of amine groups leads to generation of isolated amines surrounded by stabilized carbamates resulting in lower adsorption enthalpies. Potter *et al.*[87], using impregnated materials, mentioned the effect of increasing the CO_2 uptake on these materials. Their system had low amine density, suppressing the formation of amine pairs available for intermolecular carbamate formation obtaining low initial enthalpies. Four signals are present for the MSG 10, 20, 40, 60 in the energy site distribution: two at low enthalpy, that probably have relation with the bimodal distributions of the pore sizes and two at enthalpies higher or close to -40kJ mol^{-1}.

Figure 25 Energy site distribution plots for mesoporous silica samples.

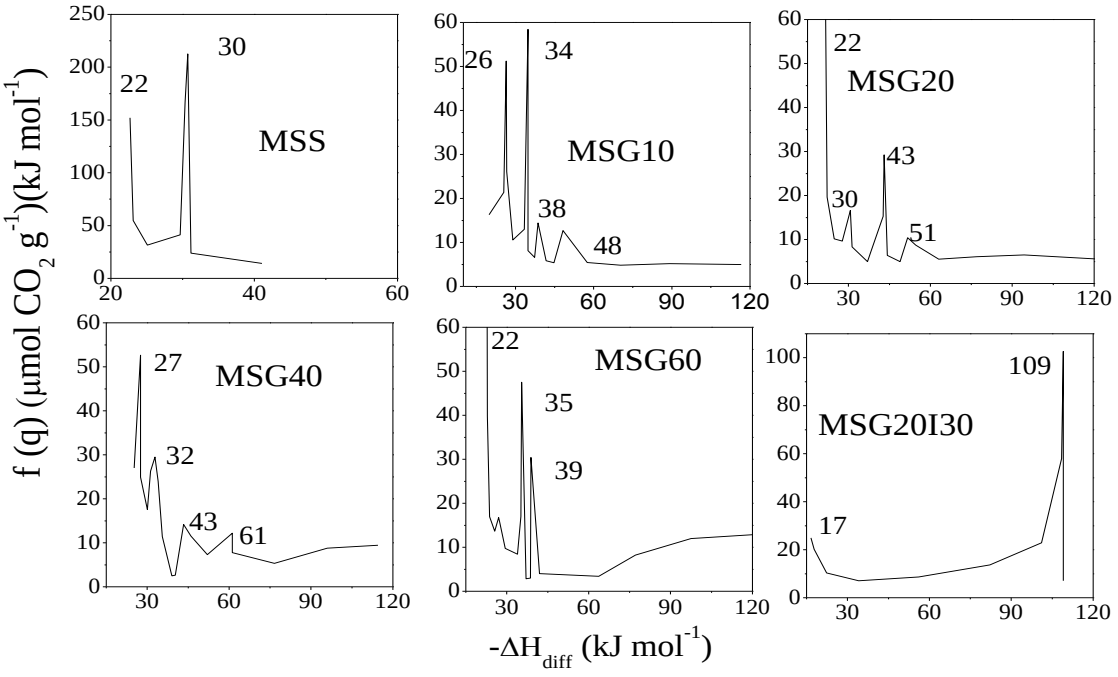

For the grafted samples, the products that could be probably formed by CO_2 chemisorption are: propyl ammonium carbamate – silyl propyl carbamate - carbamic acid, based on the analysis of the enthalpies in which the peak is formed as well as the RMN analysis and literature data. [105,106] Yoo *et al.*[107] mentioned in their work that the enthalpy value of -65 kJmol^{-1} could be associated to the combination of CO_2 adsorbed via intramolecular interactions with bound silanols (Q^2 and Q^3) and/or another amines (when the grafted groups are DI or TRI amines) to form carbamate on dry CO_2. Therefore, the peaks observed at the energy distribution curves in the range 50-65 kJ mol^{-1} could be attributed to the formation of silyl propyl carbamate (named surface bound carbamate) on material surface. When all the bound silanols are occupied, carbamic acid, with enthalpy formation ~40kJmol^{-1} [108] is stabilized by hydrogen bonding with free silanols.[107] Finally for pressures close to 1 bar, the samples present enthalpies corresponding to CO_2 physisorption. Thus the mechanism to adsorb CO_2 on functionalized samples depends on the amine density and their distribution across the surface, as well as the density of available silanols.[109]

Figure 26 Hypothetical representation of amine and silanols surface distribution on materials used in this study.

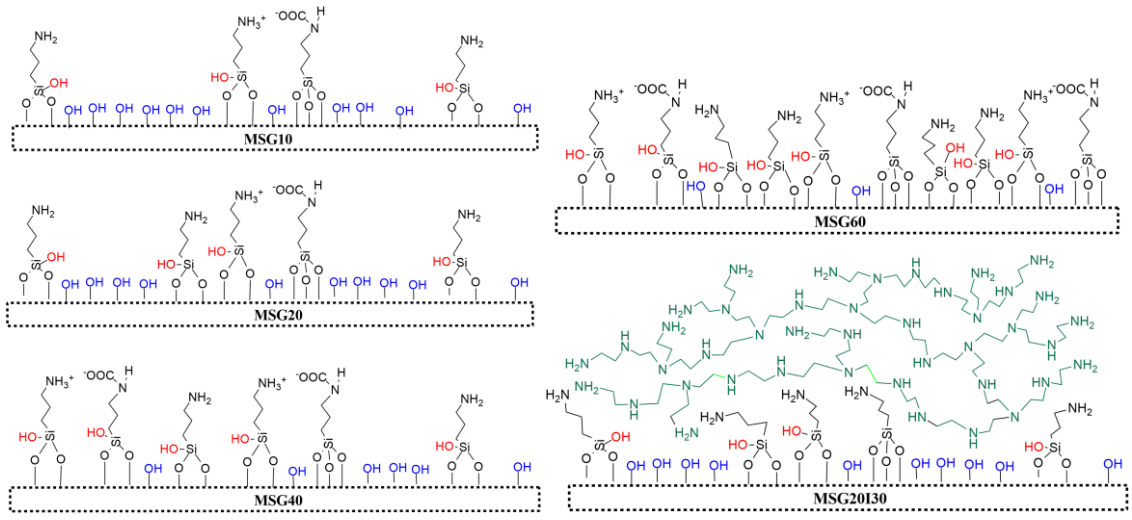

Source: Modified from Didas *et al.* 2014.[105]

A hypothetical surface group distribution of our materials is presented in Figure 26 based on the RMN results. For MSG10, CO_2 would easily interact with free –OH groups. Thus the peak at -38kJmol^{-1} in the energy distribution could perhaps correspond to this interaction. The peak at -48 kJmol^{-1} may suggests the interaction of amines/CO_2 with silanols groups may occur to stabilize carbamic acid or/and surface bound carbamate. MSG20 and MSG40 have peaks localized at -43kJmol^{-1}, maybe related to carbamic acid stabilization. The

peaks at -50-60kJmol^{-1} suggest the formation of silyl propyl carbamates, provided that these are not capped by chemisorbed species previously formed. MSG60 does not show any peak in its distribution at -60 kJmol^{-1}. This suggests that the –OH groups are capped by the formation of carbamate ion pair, limiting the formation bound carbamate, as mentioned by Danon *et al.*[110] The peak at -39kJmol^{-1} could be related to enthalpies corresponding to CO_2/OH^- interactions and/or stabilization of carbamic acid.

Sites energy distribution for MSG20I30 shows two signals, one at ~-100 kJmol^{-1} and another one at lower enthalpies, attributed to physisorption. This fact suggests the formation of propyl ammonium carbamate for high amine density (~88 molec.nm^{-2}). This density allows for the ideal conditions to form of carbamate pairs, thus suppressing the formation of other products due to a *steric hindrance effect*. The intensity of the physisorption peak is lower than for other samples, as an effect of the drastic reduction of surface area.

Figure 27 Schematic presentation of dry CO_2 chemisorption on mesoporous materials in function of amine density (1) propylammonium propylcarbamate, (2) H-bound carbamic acid to propylammonium propylcarbamate ion pair, (3) H-bound carbamic acid to surface silanols group (Q^2, Q^3), (4) H-bound carbamic acid to residual silanols group (T^2), (5) silyl propylcarbamate on propylamine modified silicas when subjected to dry CO_2, (6) CO_2/OH^- interaction.

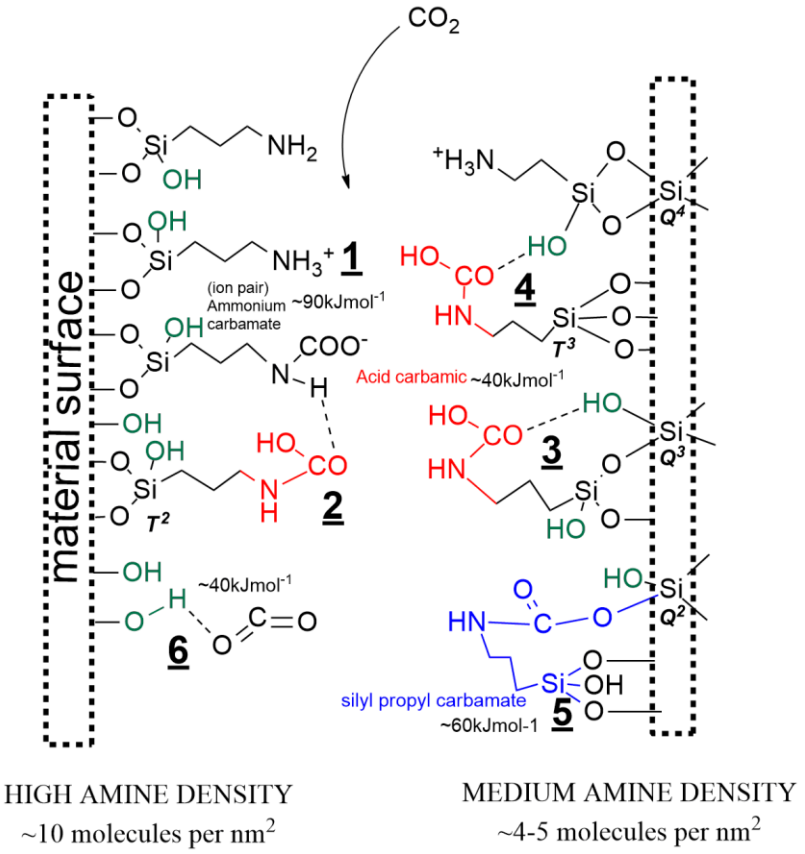

Source: Own authorship

The thermokinetic parameters (τ) as a function of CO_2 uptake is presented in Figure 28. In all cases, τ starts at low values, increasing up to a maximum and the decreasing to values close to the time constant of the microcalorimeter (200s). For the MSS sample, 471 seconds was the maximum value reached by thermokinetic parameter for a CO_2 uptake corresponding to an adsorption enthalpy of -30.7 $kJmol^{-1}$. This suggests that, for the pure sample, physisorption is the dominant mechanism. The τ_{max} for MSG20, MSG10 and MSG40 correspond to enthalpies ~-40 $kJmol^{-1}$ which suggests that CO_2 adsorption is kinetically governed by pure silanols interaction with the adsorbate or by carbamic acid stabilization, hydrogen bonding being possible in both interactions.

The different species probably produced by chemisorption of dry CO_2 on grafted samples are shown in Figure 27, for a better understanding of the explanation about the energy sites distribution. Bound carbamate formation is unlikely on materials with high amine density, whereas for materials with moderate amine density, the probability of forming carbamic acid and bound carbamate increases.

Although the possibility of bound carbamate formation is low on MSG60, we may assume that some was formed. The τ_{max} for MSG60 (613 seconds) corresponds to an enthalpy of ~-64 $kJmol^{-1}$ and bound carbamate though unlikely would probably be the dominant mechanism for this material.

Figure 28 Thermokinetic Parameter as a function of adsorbed CO_2

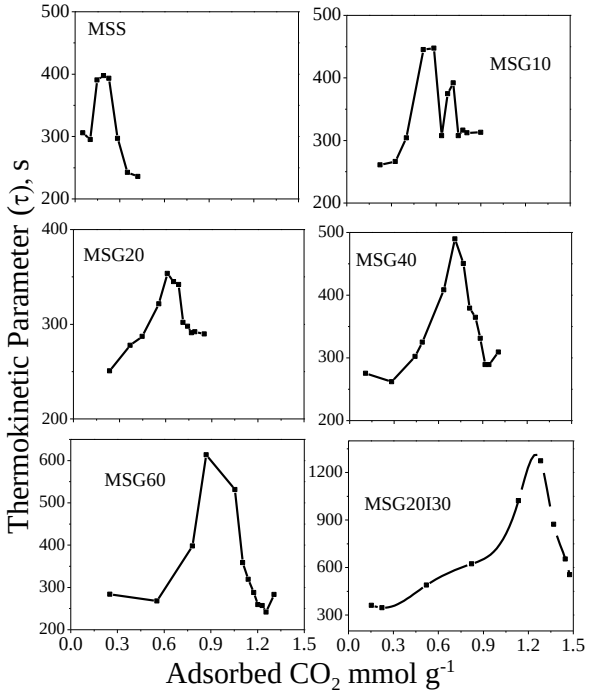

The results of the integration of the active sites curve for values of enthalpies of <-40kJmol^{-1} (considered as physisorption) and >-40kJmol^{-1} (considered as chemisorption) are summarized in Table 10 and represented graphically in Figure 29. Can be observed that the chemical sites have relation with the amine incorporation, against tendency is observed for physisorption sites where the amine mobility and random incorporation does not allow having variation of sites as amine functionalization increases as was shown in surface area results.

Figure 29 Energy sites distribution for all samples studied

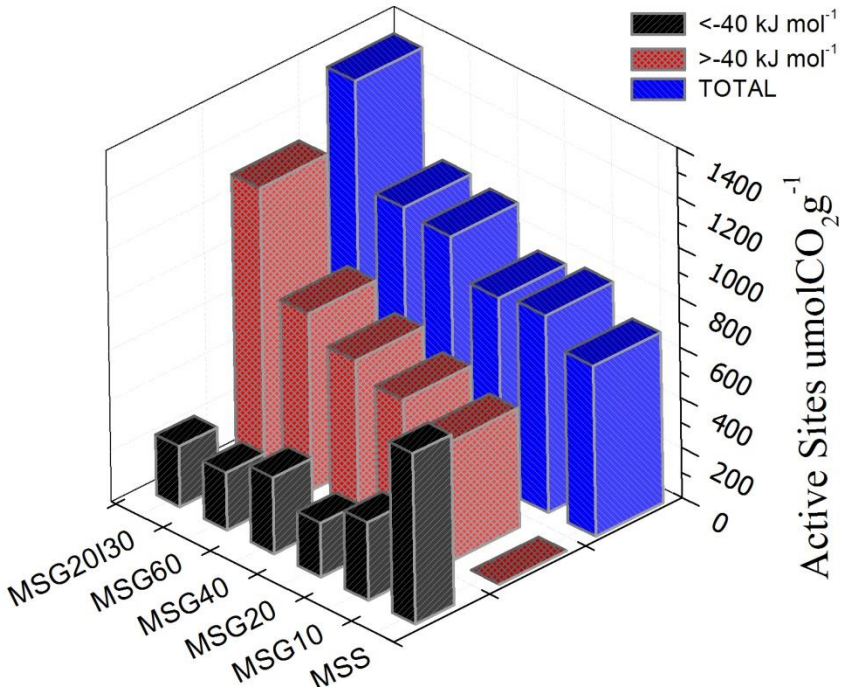

Source: Own authorship

It may be observed that the maximum kinetic parameter increases as the active sites for chemisorption increase. For MSG20I30, τ_{max} is 1274 seconds, the highest of all samples. It corresponds at -34 kJmol^{-1} and suggests diffusional resistances that have been observed for highly PEI loaded materials.[111] The enthalpy is lower than other functionalized samples because ammonium carbamate forms quickly and the formation of other subproducts is apparently suppressed, thus diffusion would perhaps be limiting kinetically the adsorption for MSG20I30 sample. Since the amine groups are randomly anchored, the active sites < -40 kJmol^{-1} do not decrease as the amine density increases, contrary to the behavior of chemisorption sites.

Table 10 Distribution of active sites and maximum thermokinetic parameter relate to percentage of APTES coverage.

Sample	$Ø^{-NH_2}$, Amine molecule. nm^{-2}	Distribution of active sites ($\mu molCO_2 g^{-1}$)		Maximum thermokinetic parameter (τ_{max})	
		<40kJmol^{-1}	>40kJmol^{-1}	τ_{max}, s	$\Delta H_{ads,}$ kJmol^{-1}
MSS	-	683	0	397	30
MSG10	4.43	311	476	447	43
MSG20	5.02	190	573	354	43
MSG40	5.46	303	612	489	40
MSG60	10.53	230	713	613	64
MSG20I30	87.91	240	1113	1274	34

Contrasting the result of integrating the adsorption peaks and the integration of the desorption peaks obtained only by vacuum (turbo molecular vacuum pump) for ~2.5 hours, all samples presented partial irreversibility, except the pure sample, in which case adsorption is reversible when vacuum is applied. The heat difference is summarized in Table 11. This value represents the additional energy that is required for complete degassing using heat. Assuming the specific heat for the samples as 0.75 $Jg^{-1}{\bullet}C^{-1}$ [112] , we can compute the degassing temperature in a hybrid process TGA/VSA.

Previous works have mentioned the irreversible character of adsorption in this class of functionalized materials. Bacsik *et al,* [113] concluded that the ammonium carbamate ion pairs and hydrogen-bound carbamic acid were weakly chemisorbed and could be outgassed by applying only vacuum. Danon *et al.*[110]mentioned that, after cell evacuation in the FTIR equipment, only the band associated with the bound carbamate was kept intact. On the other hand, the temperature required to desorb all CO_2 increases with the increase in the amine density. Tumuluri *et al.*[114] concluded that the adsorbed CO_2 binds weakly and desorbs at a higher rate on sorbents with a low amine density than the adsorbed CO_2 sorbents with a high amine density. The high amine density sorbents require higher temperatures to desorb CO_2 than those with low amine density, because of the nature of adsorbed CO_2 on sorbents with high amine density, which is stabilized via hydrogen bonding interactions with adjacent amine sites. Thus MSG60 and MSG20I30 had the highest calculated outgassing temperatures when desorption is carried out by dynamic vacuum.

Table 11 Outgassing heat requirement and required temperature with 2.5 hours of molecular vacuum at 25 ℃

Sample	Outgassing heat energy, (J $g_{material}^{-1}$)	Calculated outgassing temperature, (°C)
MSS	0	0
MSG10	10.71	40
MSG20	14.94	45
MSG40	22.66	55
MSG60	51.55	94
MSG20I30	89.2	114

4.6 Pure CO_2 isotherms at low pressures.

CO_2 adsorption isotherms of all materials at 25°C are compared in Figure 30. For all samples, except MSS, the isotherms showed a steep increase at pressure <0.1 bar and a gradual increase from 0.1 to 1.0 bar. The high capacity and steep nature of the CO_2 isotherm at low pressure on amine loaded silica are known as being caused by the chemical reaction between CO_2 and the primary amine groups (-NH_2), forming the products of adsorption previously discussed. The further gradual increase beyond the "knee" from 0.1 to 1.0 bar was attributed to the physical adsorption of CO_2 on MSG mesoporous materials, but is more notorious for MSS, which does not present the primary increase knee. As expected, the CO_2 adsorption at low pressures is more favorable for the samples that have higher percentage of grafted amines.

The elemental analysis showed that the amine densities are similar for MSG 10, 20, 40 samples. Therefore the chemical adsorption is similar in the first point of the isotherms for these samples. The MSG60 and MSG20I30 samples show higher CO_2 adsorption capacity in low pressures, since these materials with are highly nitrogen functionalized. In the next section both materials will be tested to evaluate the capacity at higher pressures and temperatures and their behavior in consecutive adsorption cycles.

Figure 30 CO_2 isotherms at 25 °C for mesoporous materials

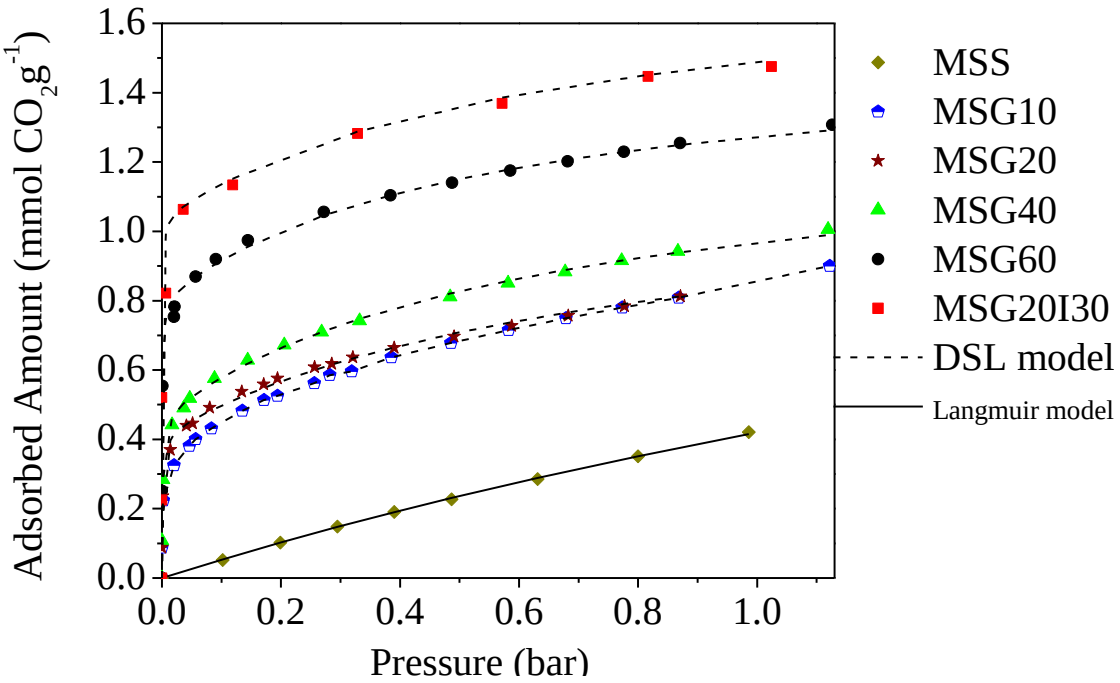

The model parameters for fits of experimental data to DSL equation are shown in Table 12.

Table 12 DSL fitting parameters to the experimental data at 25 ° C

Parameter	MSS	MSG10	MSG20	MSG40	MSG60	MSG20I30
qm_1	0	0.34	0.42	0.47	0.76	1.04
b_1	0	671.13	795.00	823.66	1705.74	2009.60
qm_2	1.84	0.93	0.76	0.81	0.68	0.68
b_2	0.29	1.17	1.24	1.50	2.64	1.70
q, 0.15bar	0.08	0.48	0.53	0.62	0.96	1.18
q, 1bar	0.42	0.85	0.84	0.97	1.27	1.48
R^2	0.99	0.99	0.99	0.99	0.97	0.86

qm_1 qm_2 and q in $mmolCO_2g^{-1}$, b_1 and b_2 in bar^{-1}.

For MSG60 the b_2 parameter shows that the interaction by physisorption is also important. Bourrelly *et al*,2005[100], explain the synergy between –OH groups and CO_2, at MSG60 presumably the peak in the energy distribution at -40kJmol^{-1} would be related to the –OH content. It explains the b_2 value since this sample has 12.9 –OH molecules per square nanometer in the surface of the material. MSG20I30 has the highest b_1, in contrast to other

samples, due to the strong interaction between the amine and the CO_2, forming products with high affinity. The correlation coefficient of the Dual-site Langmuir model with the experimental data shows that the model adjusts well the experimental data. It confirms the assumption of two types of adsorption for our functionalized samples.

4.7.Stability and energy consumption between adsorption cycles

For practical use, the adsorbent should not only possess a high adsorption capacity for pure CO_2, but also display a reversible adsorption–desorption pattern. Runs of CO_2 adsorption (isotherms, thermograms and differential enthalpies) on MSG60 and MSG20I30 previously degassed at 120 °C for 4 h are shown in Figure 31 and Figure 32, respectively, at 25 °C. The CO_2 adsorption isotherms for run 1 in contrast to run 2 at 25°C do not follow the same path in both adsorbents. The thermograms show a difference between adsorption and desorption enthalpies of 38.29 J per gram of solid for MSG60 and 39.01 for MSG20I30. This observation suggests that CO_2 is adsorbed in the first round cannot be completely desorbed even under overnight molecular vacuum. The enthalpies of adsorption at near-zero coverage do not differ distinctly for the first adsorption and the subsequent ones. This suggests that chemisorption is still happening on the free amine groups that remain after the first evacuation, in lower intensity for adsorption sites occupation. The first occupation of available sites may be due to the irreversible reaction between CO_2 and amine on these materials.[115] On the other hand, that irreversibility may also be attributed to diffusion limitations imposed by the high amine density of these materials [63,105]. This would result that after the first adsorption run not all CO_2 is released from the sample during the time under high vacuum. It is likely that both mechanisms (chemisorption and hindered diffusion) contribute to cause this irreversibility.

The calorimetric cycles at 50°C for MSG60 and MSG20I30 are shown in Figure 33 and Figure 34. The thermogram integration shows reversibility at this temperature for both cases. The three adsorption isotherms and thermograms overlap at this temperature. An increase of temperature eventually would enhance intraparticle mass transfer allowing for faster CO_2 evacuation and have the adsorption sites available again. The rupture of the strong bond formed between CO_2 and amino propyl groups may can be enhanced achieved with high temperature and molecular vacuum, as these results at 50 °C suggest. At this temperature, MSG20I30 achieves reversibility at 4 hours with vacuum, less time in comparison with MSG60, which reach reversibility at 9 hours. It is possible to consider that on grafted

samples, it is easier to form strong bonds that could lead to irreversibility (primary amines).

Figure 31(a) thermogram (at 25 °C) for CO_2 adsorption on MSG60 for four rounds.(b) Corresponding CO_2 adsorption isotherms and (c) Differential enthalpies of CO_2 adsorption (at 25 °C) for the four rounds of adsorption on the same MSG60 sample.

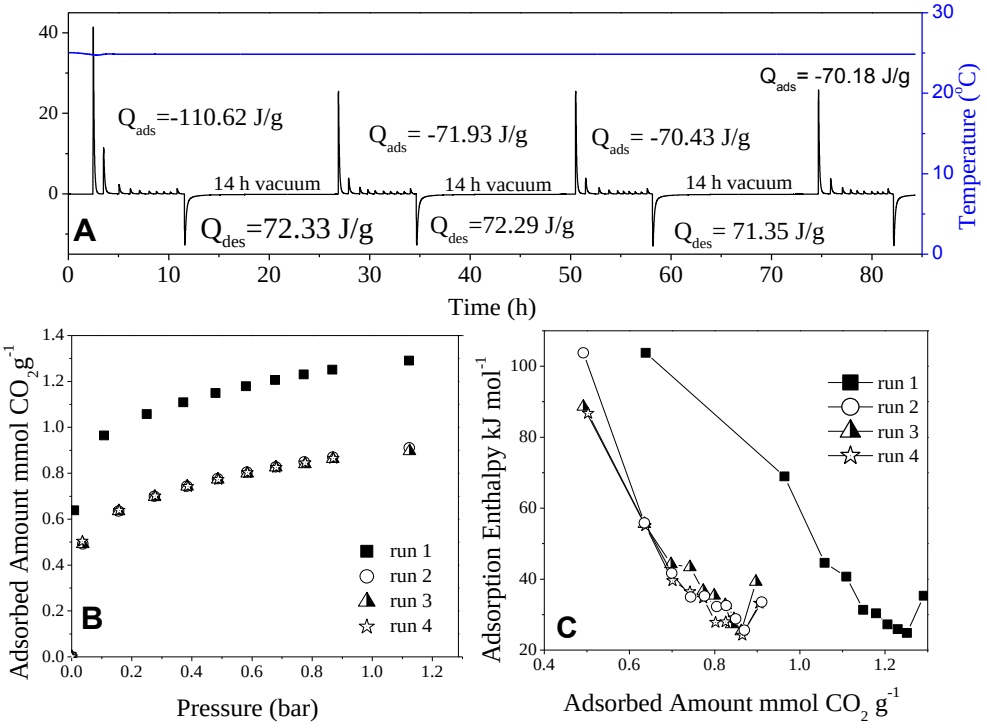

Figure 32 (a) thermogram (at 25 °C) for CO_2 adsorption on MSG20I30 for three rounds. (b) Corresponding CO_2 adsorption isotherms and (c) Differential enthalpies of CO_2 adsorption (at 25 °C) for the three rounds of adsorption on the same MSG20I30 sample.

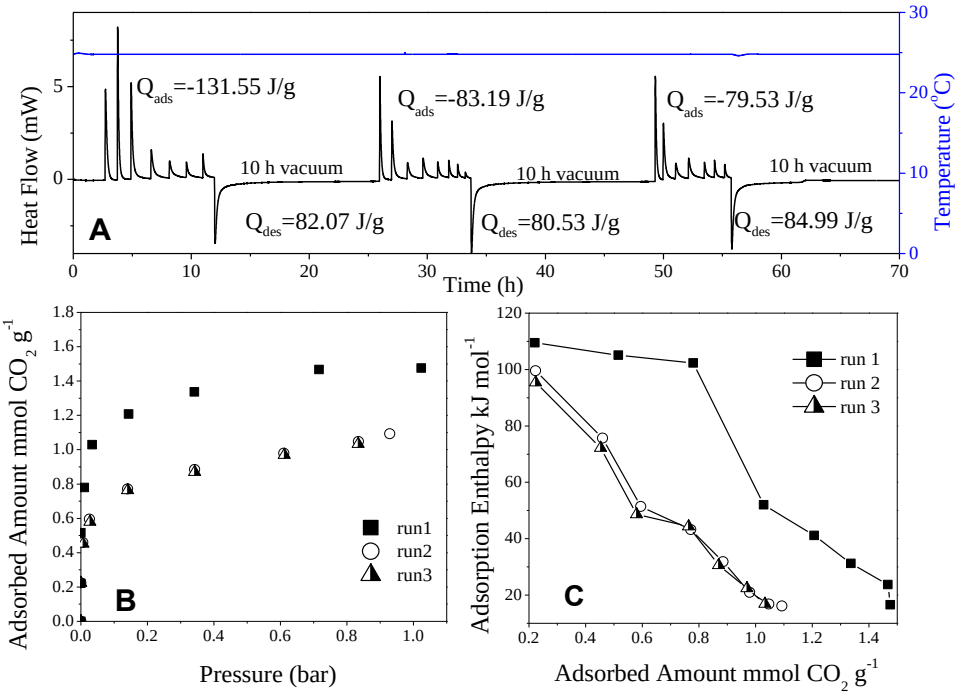

Figure 33 (a) thermogram (at 50 °C) for CO_2 adsorption on MSG60 for three rounds. (b) Corresponding CO_2 adsorption isotherms and (c) Differential enthalpies of CO_2 adsorption (at 50 °C) for the three rounds of adsorption on the same MSG60 sample

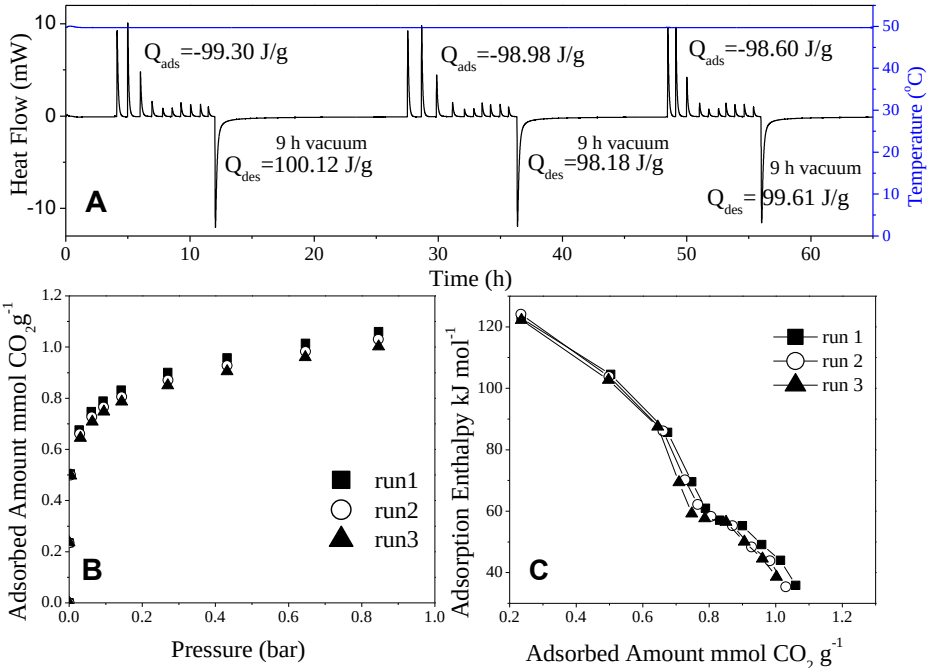

Figure 34 (a) thermogram (at 50 °C) for CO_2 adsorption on MSG20I30 for three rounds. (b) Corresponding CO_2 adsorption isotherms and (c) Differential enthalpies of CO_2 adsorption (at 50 °C) for the three rounds of adsorption on the same MSG20I30 sample.

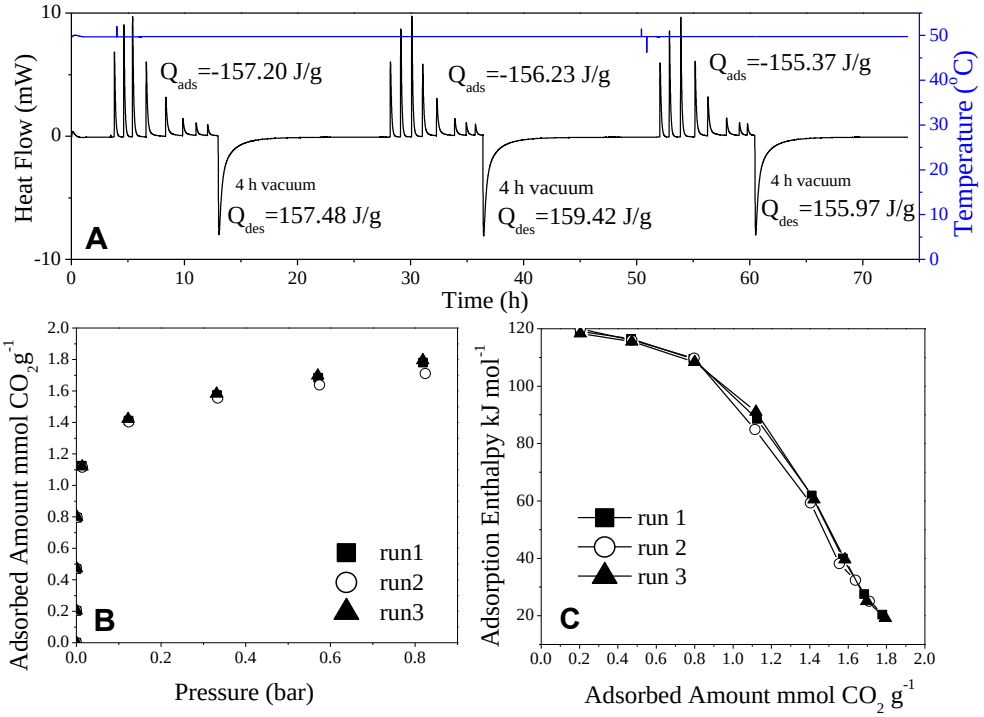

Based on the difference between the energies of adsorption and desorption (after vacuum application), the temperature necessary to get complete outgassing was calculated for experiments at 25°C, considering a caloric capacity of 0.75 J $g^{-1}°C^{-1}$ for both solids. These temperatures are in agreement with other works in our group,[116] where grafting materials were studied in a fixed bed calculating degassing temperatures around 90°C with partial pressure reduction. At 50°C the process for both samples is reversible, so this calculation was not computed. Enthalpy data for MSG60 and MSG20I30 are summarized in Table 13 in addition to the calculated temperatures for complete outgassing. MSG20I30 requires a higher temperature than MSG60. MSG20I30 adsorbs more CO_2 than MSG60, therefore it was expected that the calculated temperature would be higher for this sample.

Table 13 Adsorption/desorption energy (overnight) at 25°C and calculated temperature to outgassing of MSG60 and MSG20I30

Sample	Adsorption energy (J g^{-1})	Desorption energy (J g^{-1})	Q_{ads}-Q_{des} (J g^{-1})	Calculated temperature (°C)
MSG60	110.62	72.33	38.29	76
MSG20I30	131.55	82.08	49.47	91

Figure 35 CO_2 Adsorption Isotherms with regeneration temperature in addition to molecular vacuum, for MSG60 at 80°C and MSG20I30 at 92°C

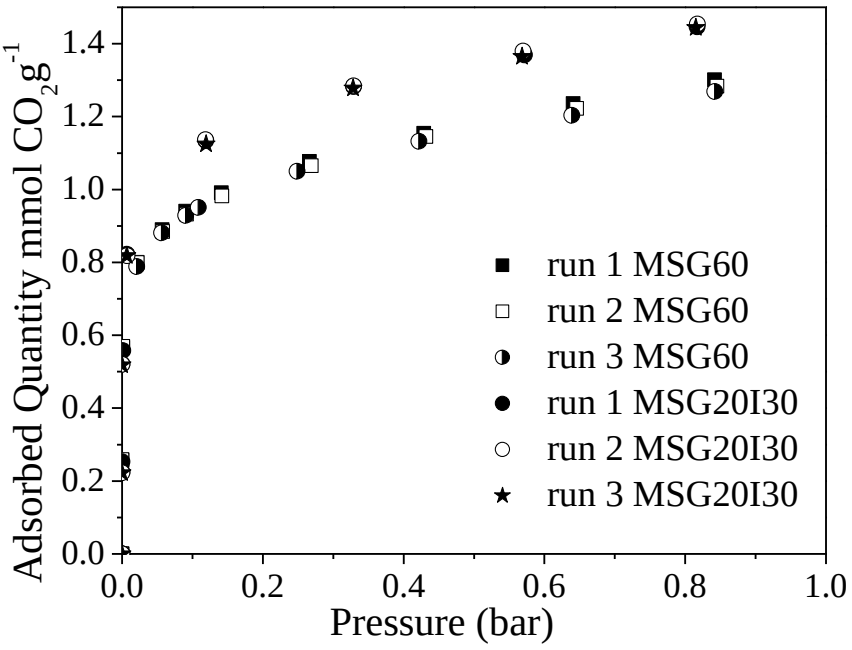

Three runs at 25°C for each sample under study are presented in Figure 35. Both heating up to the calculated temperature and molecular vacuum were used between the runs, with the purpose of testing if adsorption-desorption is truly reversible at these conditions. The results show that the solids have reversibility in the pressure range used (0-1 bar), confirming that an increase in temperature is required to completely desorb CO_2 from these samples.

4.8.CO_2 / N_2 and binary isotherms at high pressure

Single component equilibrium adsorption isotherms were measured for MSG60 and MSG20I30 at 50 and 75 °C for CO_2 and N_2, shown in Figure 36 and Figure 37.

The continuous lines represent the fittings using dual site Langmuir for CO_2 and Langmuir model for N_2. The isotherms were measured in the pressure range from 0 to 10 bar.

Figure 36 Single CO_2 and N_2 isotherms at 50 and 75 °C for MSG 60

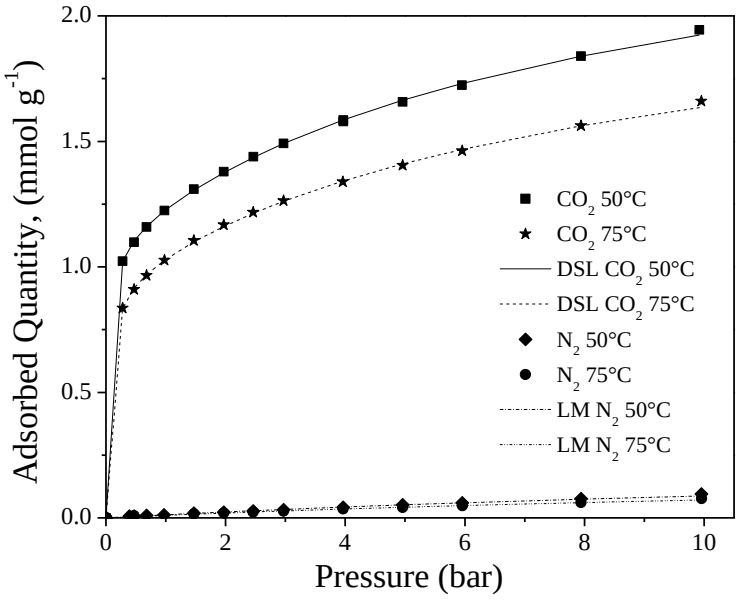

For MSG60, the adsorbed amount decreases with a rise in temperature for both gases as a typical behavior of physisorption, although it is known by calorimetry, that on these samples CO_2 is also chemisorbed. The parameters qm_1 and b_1 are in agreement with this behavior, so that at 50°C these values are higher than at 75°C. The opposite behavior is observed for MSG20I30 where CO_2 uptake is higher at 75°C. This is a typical behavior of chemisorption process so that the more functionalized sample MSG20I30 reaches at 75°C the higher adsorbed concentrations for CO_2. This behavior of PEI-impregnated on mesoporous materials, such as MCM-41 or KIT-6 was explained in other works[69] where the increase of

CO_2 adsorption capacity with temperature was attributed to an expansion of PEI aggregates within the pores when temperature is changed. Thus, at low temperature, PEI is disposed inside the channels, only the external active sites of PEI being accessible to CO_2 molecules. On the contrary, at higher temperatures PEI expands occupying all the available space in the pores, thus becoming more accessible to CO_2[75]. On the other hand, kinetic effects could be considered as an explication. When the temperature increases the kinetics and mobility of CO_2 is higher and it is easier to enter in the inaccessible regions at lower temperatures.[117]The result of this is the increase of CO_2 uptake with temperature and this reflects into the parameters of the model where for MSG20I30 qm_1 and b_1 are higher at 75°C than 50°C. Moreover N_2, uptakes decrease as temperature increases for this sample, fact expected by the physical interaction of this adsorbate with the material.

Figure 37 Single CO_2 and N_2 isotherms at 50 and 75 °C for MSG20I30

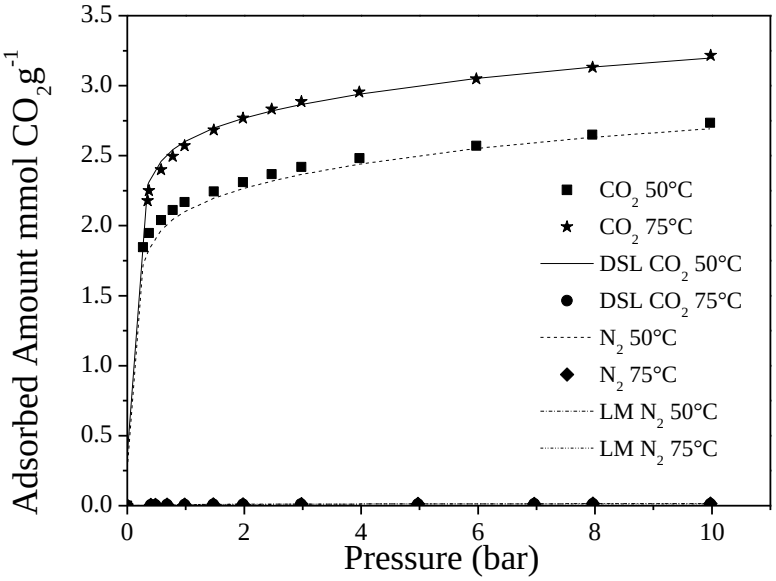

All parameters obtained from the fits of mono-component experiments are summarized on Table 14 and Table 15 for MSG60 and MSG20I30 at two temperatures. They will be used to predict binary gas adsorption.

Parameter b_2 are similar for both samples, which indicates that the difference in CO_2 uptakes between the two samples is the majority due to chemical functionalization.

Table 14 CO_2 Dual site Langmuir model parameters for MSG60 and MSG20I30

Parameter	MSG60		MSG20I30	
	50	**75**	**50**	**75**
qm_1	1.10±0.01	0.94±0.01	2.13±0.02	2.66±0.05
b_1	26.85±2.21	19.78±1.86	14.00±1.87	15.70±1.08
qm_2	1.50±0.05	1.29±0.06	1.02±0.05	1.06±0.08
b_2	0.12±0.01	0.12±0.01	0.13±0.03	0.11±0.04
R^2	0.9998	0.9996	0.9939	0.9970

qm_1, qm_2 in $mmolCO_2g^{-1}$, b_1 and b_2 in bar^{-1}.

Table 15 N_2 Langmuir model parameters for MSG60 and MSG20I30

Parameter	MSG60		MSG20I30	
	50	75	50	75
qm	0.27±0.06	0.22±0.07	0.016±3.92E-4	0.015±3.55E-4
b	0.048±0.01	0.047±0.01	0.940±0.11	0.910±0.10
R^2	0.9944	0.9915	0.9795	0.9825

qm in $mmolCO_2g^{-1}$and b_1 and b_2 in bar^{-1}.

For N_2, the behavior of both samples is typical of physisorption. When the temperature increases the adsorbed amount decreases, and this is visible in the affinity parameter of the model, slightly smaller at 75°C than 50°C. The correlation coefficients show that the model agreed well with the experimental data, with values above 0.9.

The results of adsorption capacities reported in the literature for SBA-15 functionalized with APTES and double functionalized with APTES/TEPA and APTES/PEI are summarized in Table 16. The adsorption capacities obtained in this work are in the same range as those found in the literature under similar conditions. The difference observed may be related to the fact that the mesoporous silica studied in this research does not present a same structure as a conventional SBA-15 reported in those works. Moreover our samples shows better adsorption capacities, except for the work published by Chang *et al.*[64]where the CO_2 capacity is calculated using a breakthrough measurements. For the double functionalized sample, CO_2 uptakes are in the range of other materials found in the literature.

Table 16 Comparison of adsorption capacity of MSG60 and MSG20I30 with others similar ones found in the literature

Sample	T (°C) / p_{CO2} (bar)	Amine, N content (mmol/g)	CO_2 uptake (mmol/g)	Reference
SBA-15	60 /0.15	APTES, 1.89	1.06	Chang *et al.*[64]
SBA-15	60 / 0.15	APTES, 2.70	0.52	Hiyoshi *et al.*[78]
SBA-15	60 /0.15	APTES, 2.61	0.66	Hiyoshi *et al.*[74]
MSG60	50, 75/0.15	APTES, 2.64	0.91 / 0.72	This work
SBA-15	45 / 1	APTES/ PEI, 7.64	2.52	Sanz, R *et al.*[63]
SBA-15	45 / 1	APTES/ TEPA, 7.92	3.16	Sanz, R *et al.*[34]
SBA-15	45 /1	APTES/ PEI, 7.00	1.88	Sanz, R *et al.*[71]
MSG20I30	50, 75/ 1	APTES/ PEI, 7.59	2.1 / 2.61	This work

Adsorption isotherms for binary mixtures of CO_2 with N_2 are shown in Figure 38 for MSG60 and MSG20I30. The binary mixture mole fraction was chosen to be representative of a post-combustion scenario: of flue gases (15% CO_2: 85% N_2) and at high temperatures (50-75°C). The points stand for experimental data and lines stand for predictions from the multi region extended Langmuir (MREL) model using parameters obtained from the single component isotherms.

Figure 38 Binary Isotherms (0.15 CO_2 and 0.85 N_2) at 50°C for MSG60 and MSG20I30, continuous lines is the fitting with the dual site Langmuir extended model.

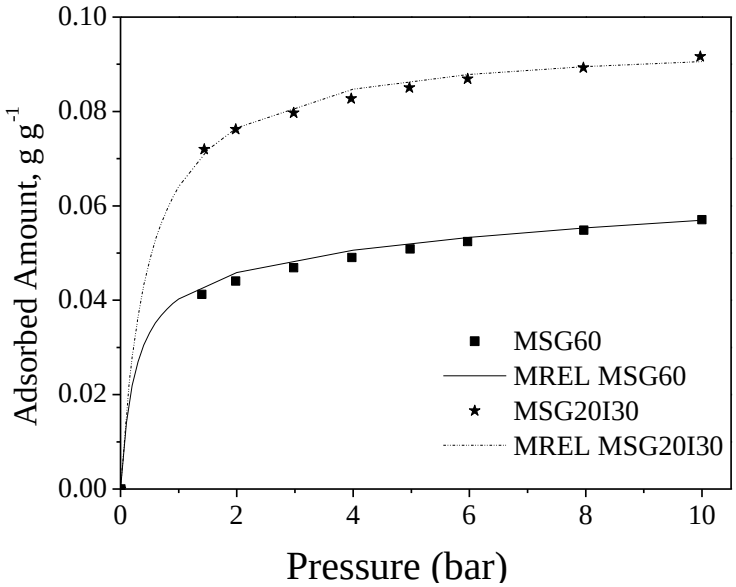

It can be observed that the gas uptakes for MSG20I30 are higher than for MSG60 at 50°C. This fact is probably due to its higher amine amount with respect to MSG60.

4.9.Selectivity

The MSG60 and MSG20I30 molar selectivity were estimated from binary isotherms using Extended Dual Site Langmuir (EDSL) to obtain the CO_2 adsorbed (Figure 39). The highest selectivity values are reached at low pressures. This is due to the strong interaction of CO_2 with the functionalized amine, which are mostly available at low pressures. N_2 at low pressures does not have strong interactions with either –OH or $–NH_2$ groups and the physisorption is weak. The highest values for selectivity, as expected, were obtained for MSG20I30 at both temperatures, stressing the advantage of this sample in contrast with the grafted one.

Figure 39 Selectivity from CO_2 and N_2 Mono Components Isotherms

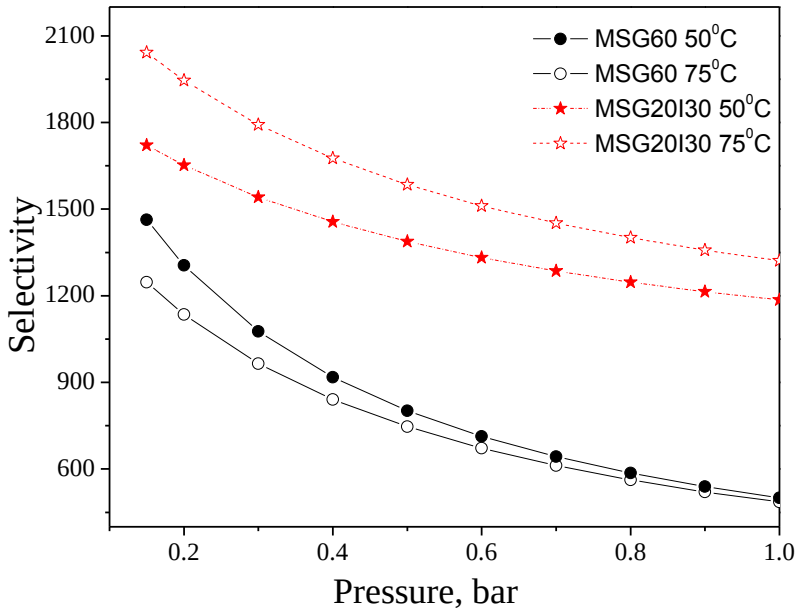

4.10. Working capacity

The working capacities in the pressure range between 0.02 and 1 bar are summarized in Table 17 for both samples. It is important to note that a powerful vacuum pump would be necessary to complete the desorption process. Atmospheric pressure ~1 bar would be the operation pressure for post-combustion scenario, so that it is not necessary a staged compressor, as well as temperature increase of (50-80°C).[118] We can see the highest working capacity for CO_2 was obtained for MSG20I30. The working capacity is higher as the

temperature increases, unlike for MSG60, which has an opposite trend.

Table 17 Adsorption Working Capacities (0.02—1 bar) for CO_2

Samples	Working capacity (mmol g^{-1})	
	50°C	75°C
MSG60	0.83	0.67
MSG20I30	1.37	1.41

4.11. Adsorbent Performance Indicator – API

The API was calculated for a working capacity in the pressure range from 0.02 bar to 1 bar at 50 and 75°C. The API values and parameters used to compute it are shown in Table 18. The exponents a, b and c were assumed as 1, following the procedure adopted to calculate the API for purification scenarios by Wiersum *et al.* [84]. The working capacity (WC) units have been converted to $cm^3.cm^{-3}$ (adsorbate volume per bed volume). This is a more physically meaningful parameter from an industrial point of view because the adsorbent will pack columns which will occupy a given volume (footprint). To convert the adsorbed concentration to volume units, the Ideal Gas Law was used (equation 44).

$$\rho = \frac{P.MM}{R.T} \qquad (37)$$

where, P is the gas pressure, MM the gas molecular weight, R is the Gas Ideal Constant and T is the gas temperature.

To convert the adsorbent mass to volume, a packing density of 0.4 g cm^{-3} was assumed. The packing density was roughly measured in the laboratory, by weighing the mass of adsorbent that can fill a given volume in a graduated cylinder.

The highest values of API are for MSG20I30. When the temperature increases the parameter increases too, indicating a good performance to purification on post combustion process. Moreover MSG60 presents high values of API in contrast with carbons[83,119] or MOF's [120]studied in other works so this porous solid also would be a good material to post combustion scenario.

Table 18 API values and parameters at 50 and 75 °C

Samples	Temperature (°C)	Working capacity (cm^3 cm^{-3}) 0.02-1 bar	Selectivity CO_2/N_2	Average Adsorption Enthalpy ($kJmol^{-1}$)	API
MSG60	50	9.75	972	68.8	138
	75	8.35	860		104
MSG20I30	50	15.60	1453	73.2	310
	75	17.39	1679		399

5. CONCLUSIONS

This study analyzes the characteristics and the behavior of mesoporous silica samples functionalized by grafting and by double functionalization, in order to evaluate in energetic terms their performance as CO_2 capture material in post combustion scenarios. The analysis of results leads to the following conclusions:

- The pure silica used in this study does not have the pore arrangement characteristic of SBA-15. The shape of the hystereris loop in the N_2 isotherms and mainly the X-Ray diffractogram suggest that this is rather a mesocellular foam. The functionalization process causes an increase in the CO_2 adsorption capacity at 25°C as amino groups were incorporated. A decrease of textural properties along with the elemental analysis, Si NMR, TGA and microcalorimetric experiments results suggest that this improvement in CO_2 adsorption capacity is due to the incorporation of amino groups.
- The TG analysis showed that the different functionalized materials have high thermal stability, being adequate to be used at high temperatures, up to 150°C for double functionalized material and 250°C for grafted materials.
- The maximum value of thermokinetic parameter calculated for pure silica was 471 seconds at 30.7kJmol^{-1} which suggests that physisorption is the dominant CO_2 binding mechanism. For the functionalized samples the maximum thermokinetic parameter found indicates that the dominant mechanism depends on the amine density. For the samples with medium amino groups density (4-5 molec.nm^{-2}) the carbamic acid /silyl carbamate formation would be the mechanism dominant. For the double functionalized sample (MSG20I30) CO_2 diffusion would be the limiting phenomenon. The calculated temperature for a complete desorption before molecular vacuum time of 2.5 h increases while the amine on the sample also increases. It has relation with the thermokinetic parameter calculated. It may be caused for possible formation of hydrogen bonds between species chemisorbed.
- The microcalorimetric studies confirm that new adsorption sites are generated by the functionalization step. Thus for the grafting method depending on the amine group density and silanols distribution, the adsorption mechanism changes from only physisorption to the formation of propyl carbamate, silyl propyl carbamate, carbamic acid and OH^-/CO_2 interactions as well as physisorption in a lesser extent. For materials

with higher amine density ~10molec.nm^{-2}, the proportion of Propyl carbamate/ Silyl carbamate formed is higher than for materials with low or medium amine density (≤~5molec.nm^{-2}). This is agreement with the distribution of sites found from the differential adsorption enthalpy of samples MSG60 and MSG20I30, those with the highest Nitrogen content. They do not present signal of silyl formation (stronger bonds that could cause irreversibility in cycles). This fact and the higher CO_2 adsorption capacity led us to choose these materials and study them under successive adsorption/desorption cycles and higher temperatures.

- A complete desorption of MSG20I30 and MSG60 at 25°C was not possible only by molecular vacuum. The differential adsorption enthalpy at zero coverage suggests that this irreversibility is attributed to the occupation of sites that are not restored after the first adsorption round, changing the sites distribution on the sample. This occupation of sites could be caused by either diffusional limitation or strong chemical bonds of adsorption products formed. At higher temperatures, these sites become free after the first outgassing process. MSG20I30 sample needs less time to show reversibility than MSG60, and this is an important fact for the application under dynamic process.
- CO_2 adsorption capacities increase with the temperature for MSG20I30 sample, an opposite behavior that MSG60 sample. This fact suggests a greater contribution of physisorption mechanism than CO_2 chemisorption on MSG60. As expected, N_2 adsorption on the two samples showed physisorption tendency with change of temperature. These properties derive in higher selectivity, higher working capacity and also higher API values for MSG20I30 than MSG60 sample at high temperatures (50 and 75°C). These data suggest that the double functionalization method would be a more efficient route to incorporate amino groups on the support with views to its application on post combustion scenarios under dry conditions.

REFERENCES

1. KIEHL, J. T.; TRENBERTH, K. E. Earth's annual global mean energy budget. ***Bulletin of the American Meteorological Society*** , v.78, p.197–208 ;1997.
2. **CO_2 Emissions from fuel combustion.** Paris (IEA Stadistical Review of world Energy, 2015).
3. HO, M. T.; ALLINSON, G. W.; WILEY, D. E. Reducing the Cost of CO_2 Capture from Flue Gases Using Membrane Technology. **Industrial & Engineering Chemistry Research** , v.47, p.1562–1568 ;2008.
4. BEZERRA, D. P.; OLIVEIRA, R. S.; VIEIRA, R. S.; CAVALCANTE, C. L.; AZEVEDO, D. C. S. Adsorption of CO_2 on nitrogen-enriched activated carbon and zeolite 13X**. Adsorption** , v.17, p.235–246 ;2011.
5. SUMIDA, K, et al. Carbon Dioxide Capture in Metal–Organic Frameworks. **Chemical Reviews** , v.112, p. 724–781 ;2012.
6. MOURA, K. O.; PASTORE, H. O. Physico-chemical of organo-functionalized magnesium phyllosilicate prepared by microwave heating. **Microporous and Mesoporous Materials** , v.190, p. 292–300 ;2014.
7. KIM, S.N.; SON. W.J.; CHOI, J.S.; AHN, W.S. CO_2 adsorption using amine-functionalized mesoporous silica prepared via anionic surfactant-mediated synthesis. **Microporous and Mesoporous Materials** , v.115, p. 497–503 ;2008.
8. CHOI, S.; DRESE, J. H.; JONES, C. W. Adsorbent Materials for Carbon Dioxide Capture from Large Anthropogenic Point Sources**. ChemSusChem** , v.2, p. 796–854 ;2009.
9. WU, D. et al. Direct Calorimetric Measurement of Enthalpy of Adsorption of Carbon Dioxide on CD-MOF-2, a Green Metal–Organic Framework**. Journal of the American Chemical Society** , v.135, p. 6790–6793 ;2013.

10. RADHA, S.; NAVROTSKY, A. Energetics of CO_2 Adsorption on Mg–Al Layered Double Hydroxides and Related Mixed Metal Oxides**. The Journal of Physical Chemistry** *C* , v.118, p. 29836–29844 ;2014.
11. GUERRERO-RUIZ, A.; GALLEGOS-SUÁREZ, E.; GONZALO-CHACÓN, L.; RODRÍGUEZ-RAMOS, I. Surface properties of Ru particles supported on carbon materials: A microcalorimetric study of the effects over the CO chemisorptions of residual anionic species. **Thermochimica Acta** , v.567, p. 112–117 ;2013.
12. BOMMINENI, S.; SKOGLUND, M. D.; MORRIS, A. R.; DOSKOCIL, E. J.; HOLLES, J. H. Characterization of selective oxidation catalysts from polyoxometalate precursors using ammonia adsorption microcalorimetry and methanol oxidation studies. **Applied Catalysis A**, v.467, p. 202–210 ;2013.
13. ROUQUEROL, François. **Adsorption by powders and porous solids: principles, methodology and applications.** Amsterdam (Elsevier/Academic Press, 2014), 626 p.
14. THOMMES, M. et al. Physisorption of gases, with special reference to the evaluation of surface area and pore size distribution (IUPAC Technical Report). **Pure and Applied Chemistry** , v.87, ;2015.
15. RUTHVEN, Douglas **Principles of adsorption and adsorption processes**. (John Wiley and sons, 1984), 453 p.
16. LAGE, F. et al. Preparation of a biocatalyst via physical adsorption of lipase from Thermomyces lanuginosus on hydrophobic support to catalyze biolubricant synthesis by esterification reaction in a solvent-free system**. Enzyme and Microbial Technology** , v.84, p. 56–67 ;2016.

17. SING, K., et al. **Reporting Physisorption Data for Gas/Solid Systems with Special Reference to the Determination of Surface Area and Porosity.** , v.57, p. 603–619 ;1985.

18. KELLER, Jürgen; STAUDT, Reiner. **Gas adsorption equilibria: experimental methods and adsorptive isotherms.** New York (Springer, 2005).

19. BASTOS-NETO, M.; TORRES, A. E. B.; AZEVEDO, D. C.; CAVALCANTE JR, C. L. Methane adsorption storage using microporous carbons obtained from coconut shells. **Adsorption** , v.11, p. 911–915 ;2005.

20. PRAUCHNER, M. J.; RODRÍGUEZ-REINOSO, F. Preparation of granular activated carbons for adsorption of natural gas. **Microporous and Mesoporous Materials** , v.109, p. 581–584 ;2008.

21. CASTRILLON, M. et al. CO_2 and H_2S Removal from CH_4-Rich Streams by Adsorption. **Energy & Fuels**, v.30, 9596–9604 ;2016.

22. DA SILVA, F. et al. Adsorption microcalorimetry applied to the characterisation of adsorbents for CO_2 capture. **The Canadian Journal of Chemical Engineering** , v.90, 1372–1380 ;2012.

23. AUROUX, Aline **Calorimetry and Thermal Methods in Catalysis.** Berlin, Heidelberg, v.154, (Springer Berlin Heidelberg, 2013), 561 p.

24. PATANOU, E.; TVETEN, E. Z.; CHEN, D.; HOLMEN, A.; BLEKKAN, E. A. Microcalorimetric studies of H_2 and CO on Co/γ-Al_2O_3 catalysts for Fischer–Tropsch synthesis**. Catalysis Today**, v.214, p. 19–24 ;2013.

25. GRAVELLE, P. C. Application of adsorption calorimetry to the study of heterogeneous catalysis reactions**. Thermochimica acta** , v.96, p. 365–376 ;1985.

26. BOLIS, V.; MAGNACCA, G.; CERRATO, G.; MORTERRA, C. Microcalorimetric characterization of structural and chemical heterogeneity of superacid SO_4/ZrO_2 systems**.** **Langmuir** , v.13, p. 888–894 ;1997.
27. PARRILLO, D. J.; GORTE, R. J. Design parameters for the construction and operation of heat-flow calorimeters. **Thermochimica acta**, v.312, p. 125–132 ;1998.
28. LLEWELLYN, P. Characterisation of microporous materials by adsorption microcalorimetry. **Recent Advances in Gas Separation by Microporous Ceramic Membranes** , v.6, 213–230 ;2000.
29. BROWN, Michael; GALLAGHER, Patrick Handbook of thermal analysis and calorimetry. **Applications to inorganic and miscellaneous materials.** *Vol. 5.* Amsterdam [u.a.]: Elsevier (2008), 755p.
30. GRAVELLE, P. C. in **Advances in Catalysis** , v.22, 191–263 (Elsevier, 1972).
31. GERVASINI, A.; BENNICI, S.; AUROUX, A.; GUIMON, C. Surface acidic properties of supported binary oxides containing CuO coupled with Ga_2O_3 and SnO_2 studied by complementary techniques. **Applied Catalysis A: General** , v.331, 129–137 ;2007.
32. BARRER, R., R. M. Specificity in physical sorption. **Journal of colloid and interfaoe science** , v.21, 415–434 ;1966.
33. LONDON, F. Zur theorie und systematik der molekularkräfte. **Zeitschrift für Physik** , v.63, p. 245–279 ;1930.
34. LUDWIG, S.; SCHMIDT, H.-D. Determination of heats of adsorption on graphite and on a microporous carbon black by gas—solid chromatography**.** **Journal of Chromatography** *A* , v.520,p 69–74 ;1990.

35. KISELEV, A. V. Non-specific and specific interactions of molecules of different electronic structures with solid surfaces. **Discussions of the Faraday Society** , v.40, p. 205–218 ;1965.

36. BELYAKOVA, L. D.; KISELEV, A. . V.; SOLOYAN, G. A. Specificity of Adsorption and Chromatographic Separation of some Cyclic Olefins and Aromatic Hydrocarbons on Barium Sulphate**. Chromatographia**, v.3, p. 254–259 ;1970.

37. FURLONG, D. N.; ROUQUEROL, F.; ROUQUEROL, J.; SING, K. S. Differential energies of adsorption of argon and nitrogen on rutile and silica. **Journal of the Chemical Society, Faraday Transactions 1: Physical Chemistry in Condensed Phases** , v.76, p. 774–781 ;1980.

38. GRILLET, Y.; ROUQUEROL, F.; ROUQUEROL, J. Two-dimensional freezing of nitrogen or argon on differently graphitized carbons**. Journal of Colloid and Interface Science** , v.70, p. 239–244 ;1979.

39. HILL, T. L. Statistical Mechanics of Adsorption. V. Thermodynamics and Heat of Adsorption. **The Journal of Chemical Physics** , v.17, p. 520–535 ;1949.

40. LLEWELLYN, P. L.; MAURIN, G. Gas adsorption microcalorimetry and modelling to characterise zeolites and related materials. **Comptes Rendus Chimie** , v.8, 283–302 ;2005.

41. DUNNE, J. A., et al. Calorimetric Heats of Adsorption and Adsorption Isotherms. 1. O_2, N_2, Ar, CO_2, CH_4, C_2H_6 and SF_6 on Silicate. **Langmuir**, v.12, 5888–5895 ;1996.

42. MITANI, Y.; TSUTSUMI, K; TAKAHASHI, H. Validity of energy distribution derived from heat of adsorption in an ammonia/cation-exchanged Y zeolite system. **Colloid and Polymer Science** , v.264, p. 445–448 ;1986.

43. BENNICI, S.; AUROUX, A.; GUIMON, C.; GERVASINI, A. Supported Binary Oxide Catalysts Containing CuO Coupled with Ga_2O_3 and SnO_2. **Chemistry of Materials ,** v.18, p. 3641–3650 ;2006.

44. AUROUX, A. in **Acidity and Basicity** Berlin, Heidelberg, v.6, p. 45–152 (Springer Berlin Heidelberg, 2006).

45. VILCHIZ, L. E.; PACHECO-VEGA, A.; HANDY, B. E. Heat-flow patterns in Tian–Calvet microcalorimeters: Conductive, convective, and radiative transport in gas dosing experiments**. Thermochimica Acta** , v.439, p. 110–118 ;2005.

46. CALVET, E; PRAT, H. **Recent progress in microcalorimetry**. Oxford (Elsevier, 1963).

47. OTT, H. **Noise reduction techniques in electronic systems.** New York (Wiley-Interscience, 1987).

48. GARCIA-CUELLO, V.; MORENO-PIRAJÁN, J. C.; GIRALDO-GUTIÉRREZ, L., SAPAG, K.; ZGRABLICH, G. **A new microcalorimeter of adsorption for the determination of differential enthalpies**. *Microporous and Mesoporous Materials* , v.120, p. 239–245 ;2009.

49. AUROUX, A.; HUANG, M; KALIAGUINE, S. Decrystallization process of HNaY zeolites upon mechanical milling: a microcalorimetric and thermokinetic study. **Langmuir** , v.12, p. 4803–4807 ;1996.

50. SOLINAS, V.; FERINO, I. Microcalorimetric characterisation of acid–basic catalysts. **Catalysis today** , v.41, p. 179–189 ;1998.

51. CARDONA-MARTINEZ, N.; DUMESIC, J. A. in **Advances in Catalysis** , v.38, p. 149–244 (Elsevier, 1992).

52. FERINO, I.; MONACI, R.; ROMBI, E.; SOLINAS, V. Microcalorimetric investigation of mordenite and Y zeolites for 1-methylnaphthalene isomerisation**. Journal of the Chemical Society, Faraday Transactions** , v.94, p. 2647–2652 ;1998.

53. BECK, J. et al. A new family of mesoporous molecular sieves prepared with liquid crystal templates. **Journal of the American Chemical Society** , v.114, p. 10834–10843 ;1992.

54. KRESGE, C. T.; LEONOWICZ, M. E.; ROTH, W. J.; VARTULI, J. C.; BECK, J. S. Ordered mesoporous molecular sieves synthesized by a liquid-cristal template mechanism. **Nature** , v.359, p. 710–712 ;1992.

55. ZHAO, D. et al. Triblock Copolymer Syntheses of Mesoporous Silica with Periodic 50 to 300 Angstrom Pores. **Science** , v.279, p. 548–552 ;1998.

56. ZHAO, D.; HUO, Q.; FENG, J.; CHMELKA, B. F.; STUCKY, G. D. Nonionic triblock and star diblock copolymer and oligomeric surfactant syntheses of highly ordered, hydrothermally stable, mesoporous silica structures. **Journal of the American Chemical Society** , v.120, p. 6024–6036 ;1998.

57. GALARNEAU, A.; CAMBON, H.; DI RENZO, F.; FAJULA, F. True Microporosity and Surface Area of Mesoporous SBA-15 Silicas as a Function of Synthesis Temperature**. Langmuir** , v.17, p. 8328–8335 ;2001.

58. GALARNEAU, A. et al. Microporosity and connections between pores in SBA-15 mesostructured silicas as a function of the temperature of synthesis. **New Journal of Chemistry** , v.27, p. 73–79 ;2003.

59. RYOO, R.; KO, C. H.; KRUK, M.; ANTOCHSHUK, V.; JARONIEC, M. Block-Copolymer-Templated Ordered Mesoporous Silica: Array of Uniform Mesopores or Mesopore−Micropore Network? **The Journal of Physical Chemistry B** , v.104, p. 11465–11471 ;2000.

60. SINDORF, D. W.; MACIEL, G. E. Silicon-29 CP/MAS NMR studies of methylchlorosilane reactions on silica gel**. Journal of the American Chemical Society** , v.103, p. 4263–4265 ;1981.

61. CAPLOW, M. Kinetics of carbamate formation and breakdown**. Journal of the American Chemical Society** , v.90, p. 6795–6803 ;1968.

62. BENAMOR, A.; ALI, B. S.; AROUA, M. K. Kinetic of CO_2 absorption and carbamate formation in aqueous solutions of diethanolamine. **Korean Journal of Chemical Engineering** , v.25, p. 451–460 ;2008.

63. SANZ, R.; CALLEJA, G.; ARENCIBIA, A.; SANZ-PÉREZ, E. S. Development of high efficiency adsorbents for CO_2 capture based on a double-functionalization method of grafting and impregnation**. Journal of Materials Chemistry A** , v.1, p. 1956–1962 ;2013.

64. CHANG, F.Y.; CHAO, K.J.; CHENG, H.H.; TAN, C.S. Adsorption of CO_2 onto amine-grafted mesoporous silicas**. Separation and Purification Technology** , v.70, p. 87–95 ;2009.

65. SÁNCHEZ-VICENTE, Y. et al. A new sustainable route in supercritical CO_2 to functionalize silica SBA-15 with 3-aminopropyltrimethoxysilane as material for carbon capture. **Chemical Engineering Journal** , v.264, p. 886–898 ;2015.

66. SANZ-PÉREZ, E. et al. Reuse and recycling of amine-functionalized silica materials for CO 2 adsorption. **Chemical Engineering Journal** , v.308, p. 1021–1033 ;2017.

67. CHOI, S.; GRAY, M. L.; JONES, C. W. Amine-Tethered Solid Adsorbents Coupling High Adsorption Capacity and Regenerability for CO_2 Capture From Ambient Air. **ChemSusChem** , v.4, p. 628–635 ;2011.

68. KO, Y.; SHIN, S.; CHOI, U. Primary, secondary, and tertiary amines for CO_2 capture: Designing for mesoporous CO_2 adsorbents. **Journal of Colloid and Interface Science** , v.361, p. 594–602 ;2011.

69. SON, W.; CHOI, J.; AHN, W. Adsorptive removal of carbon dioxide using polyethyleneimine-loaded mesoporous silica materials. **Microporous and Mesoporous Materials** , v.113, p. 31–40 ;2008.

70. OJEDA, M. et al. Novel Amine-impregnated Mesostructured Silica Materials for CO_2 Capture**. Energy Procedia** , v.114, p. 2252–2258 ;2017.

71. SANZ-PÉREZ, E.; ARENCIBIA, A.; SANZ, R.; CALLEJA, G. New developments on carbon dioxide capture using amine-impregnated silicas**. Adsorption** , v.22, p. 609–619 ;2016.

72. FULVIO, P.; PIKUS, S.; JARONIEC, M. Tailoring properties of SBA-15 materials by controlling conditions of hydrothermal synthesis. **Journal of Materials Chemistry** , v.15, p. 5049 ;2005.

73. VILARRASA-GARCÍA, E. et al. “Low Cost” Pore Expanded SBA-15 Functionalized with Amine Groups Applied to CO_2 Adsorption:. **Materials** , v.8, p. 2495–2513 ;2015.

74. HIYOSHI, N.; YOGO, K.; YASHIMA, T. Adsorption characteristics of carbon dioxide on organically functionalized SBA-15. **Microporous and Mesoporous Materials** , v.84, p. 357–365 ;2005.

75. XU, X.; SONG, C.; ANDRESEN, J. M.; MILLER, B. G.; SCARONI, A. W. Novel Polyethylenimine-Modified Mesoporous Molecular Sieve of MCM-41 Type as High-Capacity Adsorbent for CO_2 Capture. **Energy & Fuels** , v.16, p. 1463–1469 ;2002.

76. BRUNAUER, S.; EMMETT, P. H.; TELLER, E. Adsorption of gases in multimolecular layers. **J. Am. Chem. Soc** , v.60, p. 309–319 ;1938.

77. BARRETT, E. P.; JOYNER, L. G.; HALENDA, P. P. The determination of pore volume and area distributions in porous substances. I. Computations from nitrogen isotherms**. J. Am. chem. soc** , v.73, p. 373–380 ;1951.

78. HIYOSHI, N.; YOGO, K.; YASHIMA, T. Adsorption of carbon dioxide on modified mesoporous materials in the presence of water vapor. **Studies in Surface Science and Catalysis** , v.154, p. 2995–3002 ;2004.

79. SATYAPAL, S.; FILBURN, T.; TRELA, J.; STRANGE, J. Performance and Properties of a Solid Amine Sorbent for Carbon Dioxide Removal in Space Life Support Applications**. Energy & Fuels** , v.15, p. 250–255 ;2001.

80. OJEDA-LÓPEZ, R.; PÉREZ-HERMOSILLO, I. J.; MARCOS ESPARZA-SCHULZ, J., CERVANTES-URIBE, A.; DOMÍNGUEZ-ORTIZ, A. SBA-15 materials: calcination temperature influence on textural properties and total silanol ratio**. Adsorption** , v.21, p. 659–669 ;2015.

81. Setaram. **Commissioning Calorimeter C80**. ;2010.

82. CONDON, James **Surface area and porosity determinations by physisorption: measurements and theory.** (Elsevier, 2006).

83. MOURA, P. A. S. de. **Assessing the potential of activated carbons from polyethylene terephthalate (PET) as adsorbents to separate CO_2 from flue gas.** (2017). Master dissertation (Chemical Engineering) – Faculdade de Engenharia Química, Universidade Federal do Ceará, Fortaleza, 2017.

84. WIERSUM, A. D.; CHANG, J. S.; SERRE, C.; LLEWELLYN, P. L. An Adsorbent Performance Indicator as a First Step Evaluation of Novel Sorbents for Gas Separations: Application to Metal–Organic Frameworks. ***Langmuir*** , v.29, p. 3301–3309 ;2013.

85. VILARRASA-GARCIA, E. et al. CO_2 adsorption on amine modified mesoporous silicas: Effect of the progressive disorder of the honeycomb arrangement. **Microporous and Mesoporous Materials** , v.209, p. 172–183 ;2014b.

86. WANG, L.; MA, L.; WANG, A.; LIU, Q.; ZHANG, T. CO_2 Adsorption on SBA-15 Modiefied by Aminosilane**. Chinese Journal of Catalysis** , v.28, p. 805–810 ;2007.

87. POTTER, M. E.; PANG, S. H.; JONES, C. W. Adsorption Microcalorimetry of CO_2 in Confined Aminopolymers. **Langmuir** , v.33, p.117–124 ;2017.

88. MARIA CHONG, A.; ZHAO, X.; KUSTEDJO, A. T.; QIAO, S. Functionalization of large-pore mesoporous silicas with organosilanes by direct synthesis**. Microporous and Mesoporous Materials** , v.72, p. 33–42 ;2004.

89. SAVINO, R.; CASADONTE, F.; TERRACCIANO, R. In Mesopore Protein Digestion: A New Forthcoming Strategy in Proteomics. **Molecules** , v.16, p. 5938–5962 ;2011.

90. VILARRASA-GARCÍA, E, et al. CO_2 adsorption on APTES functionalized mesocellular foams obtained from mesoporous silicas. **Microporous and Mesoporous Materials** , v.187, p. 125–134 ;2014a.

91. SANZ, R.; CALLEJA, G.; ARENCIBIA, A.; SANZ-PÉREZ, E. S. CO_2 Uptake and Adsorption Kinetics of Pore-Expanded SBA-15 Double-Functionalized with Amino Groups. **Energy & Fuels**, v.27, p. 7637–7644 ;2013.

92. LIU, W.; WANG, Y.; WILCOX, W.; LI, S. A compact and high throughput reactor of monolithic-structured catalyst bed for conversion of syngas to liquid fuels. **AIChE Journal** , v.58, p. 2820–2829 ;2012.

93. LETTOW, J. S. et al. Hexagonal to mesocellular foam phase transition in polymer-templated mesoporous silicas. **Langmuir** , v.16, p. 8291–8295 ;2000.

94. SCHMIDT-WINKEL, P.et al. Microemulsion Templating of Siliceous Mesostructured Cellular Foams with Well-Defined Ultralarge Mesopores. **Chemistry of Materials** , v.12, p. 686–696 ;2000.

95. FERREIRA, R. B.; DA SILVA, C. R.; PASTORE, H. O. Aminopropyl-Modified Magnesium−Phyllosilicates: Layered Solids with Tailored Interlayer Access and Reactivity. **Langmuir** , v.24, p. 14215–14221 ;2008.

96. JUN, Y.S. et al. Adsorption of Pyruvic and Succinic Acid by Amine-Functionalized SBA-15 for the Purification of Succinic Acid from Fermentation Broth. **The Journal of Physical Chemistry C** , v.111, p. 13076–13086 ;2007.

97. LAGADIC, I. L. Schiff base chelate-functionalized organoclays**. Microporous and Mesoporous Materials** , v.95, p. 226–233 ;2006.

98. WANG, L.; YANG, R. T. Increasing Selective CO_2 Adsorption on Amine-Grafted SBA-15 by Increasing Silanol Density**. The Journal of Physical Chemistry C** , v.115, p. 21264–21272 ;2011.

99. HAN, Y.J.; STUCKY, G. D.; BUTLER, A. Mesoporous Silicate Sequestration and Release of Proteins. **Journal of the American Chemical Society** , v.121, p. 9897–9898 ;1999.

100. BOURRELLY, S. et al. Different Adsorption Behaviors of Methane and Carbon Dioxide in the Isotypic Nanoporous Metal Terephthalates MIL-53 and MIL-47. **Journal of the American Chemical Society** , v.127, p. 13519–13521 ;2005.

101. AUROUX, A.; VEDRINE, J. in **Studies in Surface Science and Catalysis** (eds. Imelik, B., Naccache, C., Coudurier, G., Been Taarit, Y. & Vedrine, J. C.) Amsterdam, v.20, 445 (Elsevier, 1985).

102. FLETCHER, A. J.; CUSSEN, E. J.; BRADSHAW, D.; ROSSEINSKY, M. J.; THOMAS, K. M. Adsorption of Gases and Vapors on Nanoporous Ni_2(4,4‘-Bipyridine)$_3$(NO_3)$_4$ Metal−Organic Framework Materials Templated with Methanol and Ethanol: Structural Effects in Adsorption Kinetics. **Journal of the American Chemical Society** , v.126, p. 9750–9759 ;2004.

103. KNÖFEL, C. et al. Functionalised micro-/mesoporous silica for the adsorption of carbon dioxide. **Microporous and Mesoporous Materials** , v.99, p. 79–85 ;2007.

104. ALKHABBAZ, M. A.; BOLLINI, P.; FOO, G. S.; SIEVERS, C.; JONES, C. W. Important Roles of Enthalpic and Entropic Contributions to CO_2 Capture from Simulated Flue Gas and Ambient Air Using Mesoporous Silica Grafted Amines. **Journal of the American Chemical Society** , v.136, p. 13170–13173 ;2014.

105. DIDAS, S. A.; SAKWA-NOVAK, M. A.; FOO, G. S.; SIEVERS, C.; JONES, C. W. Effect of Amine Surface Coverage on the Co-Adsorption of CO_2 and Water: Spectral Deconvolution of Adsorbed Species**. The Journal of Physical Chemistry Letters** , v.5, p. 4194–4200 ;2014.

106. DIDAS, S. A.; ZHU, R.; BRUNELLI, N. A.; SHOLL, D. S.; JONES, C. W. Thermal, Oxidative and CO_2 Induced Degradation of Primary Amines Used for CO $_2$ Capture: Effect of Alkyl Linker on Stability**. The Journal of Physical Chemistry C** , v.118, p. 12302–12311 ;2014.

107. YOO, C. J.; LEE, L. C; JONES, C. W. Probing Intramolecular versus Intermolecular CO_2 Adsorption on Amine-Grafted SBA-15. **Langmuir** , v.31, p. 13350–13360 ;2015.

108. HAHN, M. W. et al. Role of Amine Functionality for CO_2 Chemisorption on Silica. ***The Journal of Physical Chemistry B*** , v.120, p. 1988–1995 ;2016.

109. AZIZ, B.; HEDIN, N.; BACSIK, Z. Quantification of chemisorption and physisorption of carbon dioxide on porous silica modified by propylamines: Effect of amine density. ***Microporous and Mesoporous Materials*** , v.159, p. 42–49 ;2012.

110. DANON, A.; STAIR, P. C.; WEITZ, E. FTIR Study of CO_2 Adsorption on Amine-Grafted SBA-15: Elucidation of Adsorbed Species. ***The Journal of Physical Chemistry C*** , v.115, p. 11540–11549 ;2011.

111. BOLLINI, P.; BRUNELLI, N. A.; DIDAS, S. A.; JONES, C. W. Dynamics of CO_2 Adsorption on Amine Adsorbents. 2. Insights Into Adsorbent Design. ***Industrial & Engineering Chemistry Research*** , v.51, p. 15153–15162 ;2012.

112. KHATRI, R. A.; CHUANG, S. S. C.; SOONG, Y.; GRAY, M. Carbon Dioxide Capture by Diamine-Grafted SBA-15: A Combined Fourier Transform Infrared and Mass Spectrometry Study. **Industrial & Engineering Chemistry Research** , v.44, p. 3702–3708 ;2005.

113. BACSIK, Z. et al. Mechanisms and Kinetics for Sorption of CO_2 on Bicontinuous Mesoporous Silica Modified with *n* -Propylamine. **Langmuir**, v.27, p. 11118–11128 ;2011.

114. TUMULURI, U.; ISENBERG, M.; TAN, C. S.; CHUANG, S. S. C. ***In Situ*** Infrared Study of the Effect of Amine Density on the Nature of Adsorbed CO_2 on Amine-Functionalized Solid Sorbents. **Langmuir** , v.30, p. 7405–7413 ;2014.

115. SAYARI, A.; HEYDARI-GORJI, A.; YANG, Y. CO_2 -Induced Degradation of Amine-Containing Adsorbents: Reaction Products and Pathways. **Journal of the American Chemical Society** , v.134, p. 13834–13842 ;2012.

116. SANTIAGO, R. G. **Sílica mesoporosa funcionalizada com APTES para captura de CO_2 em cenários de pós-combustão: um estudo em leito fixo**. (2017). Master

dissertation (Chemical Engineering) – Faculdade de Engenharia Química, Universidade Federal do Ceará, Fortaleza, 2017.

117. SANZ, R.; CALLEJA, G.; ARENCIBIA, A.; SANZ-PÉREZ, E. S. CO_2 adsorption on branched polyethyleneimine-impregnated mesoporous silica SBA-15**. Applied Surface Science** , v.256, p. 5323–5328 ;2010.

118. ZHAO, L.; RIENSCHE, E.; MENZER, R.; BLUM, L.; STOLTEN, D. A parametric study of CO_2/N_2 gas separation membrane processes for post-combustion capture. **Journal of Membrane Science** , v.325, p. 284–294 ;2008.

119. ÁLVAREZ-GUTIÉRREZ, N. et al. Adsorption Performance Indicator to Screen Carbon Adsorbents for Post-combustion CO_2 Capture. **Energy Procedia** , v.114, p. 2362–2371 ;2017.

120. PILLAI, R. S. et al. Highly Selective CO_2 Capture by Small Pore Scandium-Based Metal–Organic Frameworks. **The Journal of Physical Chemistry C** , v.119, p. 23592–23598 ;2015.